ACTIVE COMBUSTION THROTTLE

by

Nathaniel Benjamen Black

B.S., Georgia Institute of Technology, 2005

Submitted to the Graduate Faculty of

the Swanson School of Engineering in partial fulfillment

of the requirements for the degree of

Master of Science

University of Pittsburgh

2008

UNIVERSITY OF PITTSBURGH

SWANSON SCHOOL OF ENGINEERING

This thesis was presented

by

Nathaniel Benjamen Black

It was defended on

April 2nd 2008

and approved by

Dr. Jeffrey S. Vipperman, Associate Professor

Dr. William W. Clark, Professor

Dr. Mark C. Miller, Associate Research Professor

Thesis Advisor: Dr. Jeffrey S. Vipperman, Associate Professor

ACTIVE COMBUSTION THROTTLE

Nathaniel Benjamen Black, M.S.

University of Pittsburgh, 2008

As environmental awareness increases, cleaner burning fuels are desired for use in power plants. Fuels such hydrogen, methane and syngas are cleaner and leaner burning, which causes combustion instabilities. The Active Combustion Throttle (ACT) project is sponsored by the Department of Energy's National Energy Technologies Laboratory (NETL) and aspires to create a valve capable of modulating the flow of fuel administered to gas turbines by $\pm 10\%$. Development of such a valve will require an integrated valve and actuator design that can withstand the harsh environment of a power plant as well have a closed loop feedback control system in order to avoid combustion instabilities.

In this thesis, an in-depth survey of current actuator and valve technologies revealed there are not any commercially available integrated valve assemblies capable of performing such a task. Two valve designs and one actuator design were devised to meet a list of specifications from NETL. Both valve designs as well as the actuator design underwent a rigorous battery of electromagnetic, stress, thermal, finite element analysis (FEA) and computational fluid dynamic (CFD) analyses using contemporary mechanical, electrical and physical theory and commercially available computer-aided design (CAD) programs.

Prototype valve designs were designed, machined, cold flow tested and approved for further prototype design and testing. Initial cold flow testing revealed that both valve designs had linear ranges, were quick opening and demonstrated adequate flow coefficients (C_v). Further testing will continue to refine the valve designs in preparation for creating integrated valve/actuator assemblies for more aggressive testing.

The primary contribution of this thesis are the two valve designs and actuator design that have thus far proven to be capable of fulfilling the requirements set forth by NETL for the ACT project. Further research and analyses of these designs will provide more robust prototype valve and actuator assemblies for eventual live testing at NETL. The framework provided by this thesis will allow those involved with the project to make changes to the current designs as needed since the same analyses can be more efficiently executed for subsequent changes throughout the remaining stages of development.

TABLE OF CONTENTS

LIST OF TABLES

LIST OF FIGURES

PREFACE

Thank you to my advisor Dr. Jeffrey Vipperman as well as all of the members of the Sounds, Structures and Systems Laboratory at the University of Pittsburgh. Your help at all hours of the day has been invaluable.

1.0 INTRODUCTION

The US Department of Energy has established very aggressive goals for pollution and performance standards for gas turbine engines of the future [1]. At the same time, engine operating conditions will become more variable, as they are converted to run on coal-derived syngas or hydrogen and are being combined into hybrid power plant configurations (e.g. fuel cell/gas turbines (FCGT), or gasification fluidized-bed combustion combined cycle systems, GFBCC). Combustion instabilities can easily arise in lean-burning engines, resulting in tremendous acoustic levels and damaging vibrations. The need for in-situ monitoring and fine control of the combustion process is needed to optimize performance and prevent turbine damage. Even modern natural gas combustors need finely controlled fuel/air mixtures, since they operate near the lean-extinction limit. There is currently no method to finely control combustion in a stationary gas-turbine engine. Rather, fuel is supplied from a manifold to multiple fuel injectors through fixed-orifice throttling valves. Poor manufacturing tolerances or engine wear over time can significantly compromise engine emissions performance. Furthermore, unexpected changes in fuel delivery or composition can affect flame anchoring. Thus, the flow to each engine injector must be closely monitored and carefully controlled (Figure 1) to provide the stable, low-emission, fuel-flexible operations to meet 21st century demands.

There are three components required for a closed-loop combustion system: sensor, actuator, and a control algorithm [2]. NETL has previously developed and patented an in-situ sensor probe based on flame-ionization called the Combustion Control and Diagnostics Sensor (CCADS) [3, 4]. The probe is capable of measuring dynamic heat release and has found use for monitoring (including flashback detection) and tuning of the combustor flame quality [5, 6, 7, 8, 9]. The device is currently under license and commercial development through

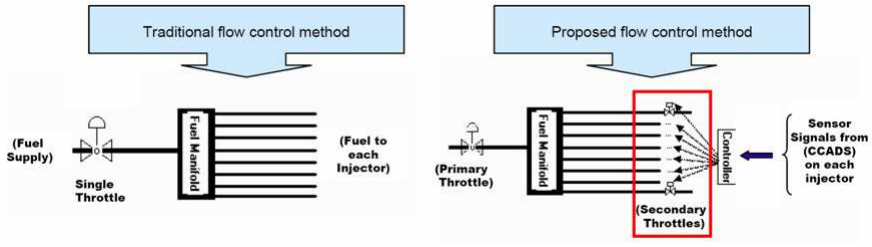

Figure 1: Comparison of conventional (left) and proposed (right) distributed fuel flow control for gas turbine engines. Note that the ACT devices will be within the red box (secondary throttles).

a Cooperative Research and Development Agreement (CRADA) with Woodward Governor Company. The proposed effort could leverage this prior NETL innovation by developing the Active Combustion Throttle (ACT) required to realize real-time stoichiometric control. With sufficient bandwidth, the throttle may also be suitable for implementing active control of combustion instabilities. Note that it is impractical to use conventional flow control valves on each fuel injector of a turbine, mainly because of dependability issues, not to mention prohibitive costs, size, and slow response time. The requirements for the ACT concept are given in Table 1.

Table 1: Requirements for active combustion throttle (ACT) valve.

1.	Amenable to retrofitting
2.	Target size: 1/2" diameter
3.	Fluid: natural gas, hydrogen, or syngas blends
4.	Nominal flow rate 3000 SCFH (for methane)
5.	Line pressure rating of 450 psi or greater
6.	10 psi pressure drop across valve
7.	650 degrees Fahrenheit temperature rating
8.	Controllability of +/- 10%
9.	Bandwidth of 1000 Hz
10.	Production costs less than $200 each
11.	Fail at a nominal flow rate (rather than open/closed)

2.0 LITERATURE SURVEY

2.1 OVERVIEW

Searches in the open literature have yielded no reports of a valve that simultaneously meets all of the stringent requirements set forth in this project. However, concepts from a number of different actuation technologies may prove useful if creatively combined to achieve the requirements in Table 1. Following is a survey of potential actuation technologies and valve types, which includes both conventional and non-conventional designs.

2.2 ACTUATION TECHNOLOGIES

Currently, there are quite a few means of actuation that are widely used throughout various industries. Table 2 includes all of the current actuation technologies investigated and detailed in this survey. Table 2 also lists the actuation technologies researched for the ACT valve. A brief description of their operation are included below while a comprehensive list of advantages and disadvantages are included in Table 20 in Appendix A.

2.2.1 Stepper Motors

Stepper motors are electromechanical devices that convert electrical pulses into mechanical movement, therefore producing a discrete motion versus a continuous one [10]. There are two basic components of a stepper motor: the stator and the rotor. As the coils on the stator are supplied with electrical impulses in a certain sequence, a "moving" (more accurately

Table 2: Actuation technologies explored for the ACT project.

1.	Stepper Motors
2.	Servo Motors
3.	Hydraulic Valves
4.	Pneumatic Valves
5.	Solenoids
6.	Piezoelectrics
7.	Electrochemical
8.	Electrostrictive
9.	Magnetostrictive

"rotating") magnetic field is produced that induces a current in the rotor. The conductive rotor in turn produces a magnetic field, causing the rotor's magnetic field to "chase" the moving magnetic field of the stator. This movement creates a torque in the rotor causing rotation. The speed, direction of travel, and length of rotation are all directly proportional to the input pulses, making stepper motors ideal for applications where controlled movement is needed. Such applications may require tight controllability of angle, speed, position and synchronism.

There are three classifications of stepper motors: variable-reluctance (VR), permanent-magnet (PM), and hybrid (HB). VR stepper motors are the oldest of the three types, while the PM and HB stepper motors are the most widely used. The HB type is considerably more expensive than the other types due to its increased controllability, so the other types should be fully investigated prior to resorting to an HB stepper motor [10]. Figure 2 depicts a hybrid stepper motor. In addition to the three classifications of stepper motors, there are two types: linear and rotational. Linear stepper motors tend to be expensive. Therefore, most stepper motors are rotational motors and use gearing when linear motion is required [10].

Stepper motors present several disadvantages relative to the ACT valve. Primarily, the current maximum operating temperature of around 300°C for stepper motors is not high

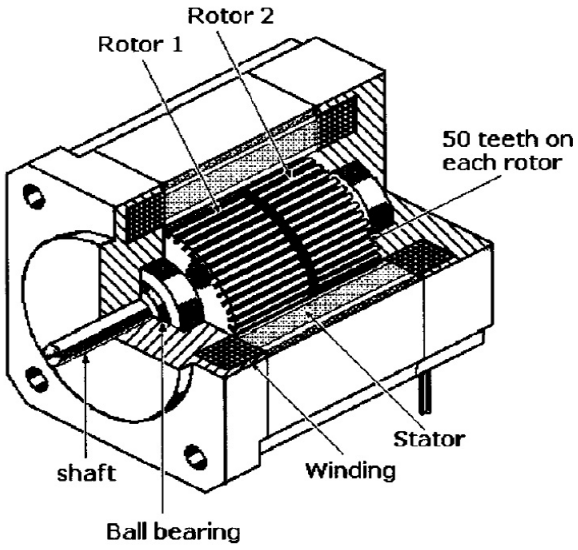

Figure 2: Cutaway view of a hybrid stepper motor [11].

enough [12]. New high temperature materials are being developed that may prove useful for such applications, but at this point they have not been sufficiently developed for commercial use. Also, a situation known as cogging may occur where the rotor and stator have difficultly aligning. Stepper motors are also more complex, requiring a controller for operation.

2.2.2 Servo Motors

Servo motors are similar to stepper motors: they also convert electrical impulses into mechanical movement. One type of servo motor can be seen in Figure 3. In its simplest form, a servomotor consists only of control circuitry and a potentiometer connected to a rotor. As electrical impulses are supplied to the servomotor, the rotor creates rotational motion proportional to the input pulse. The frequency and amount of time that a pulse is supplied determine the amount of rotation.

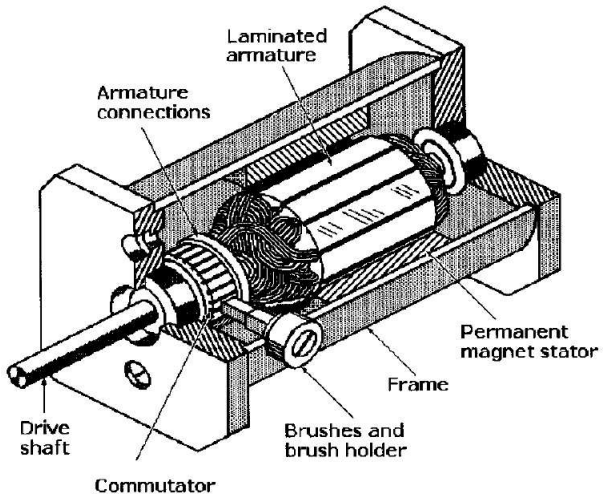

Figure 3: Cutaway view of a DC permanent magnet servo motor [11].

Servos are used in situations where precision, position and timing are of utmost importance [10]. They are low power devices and are currently primarily AC three-phase machines. Since the torque is linearly dependent on the armature current, the regulation and control via current is quite simple.

Unfortunately, servo motors are relatively expensive and are not good candidates when starting and stopping often, as is the case for the ACT valve. Also, since position is part of the control algorithm for servos, a closed loop control system is required.

2.2.3 Hydraulic Valves

Hydraulic valves utilize pressure differentials in the system to create mechanical motion [Figure 4]. Hydraulic systems consist of three main parts: the hydraulic pump, regulator and valve. The pump has an electrical input which drives the system. Hydraulic fluid (an oil of some sort) is pushed into the regulator where it is ensured that the pressure does not exceed the system's operating capability. The hydraulic fluid flow direction, pressure, and speed are controlled by the hydraulic valve.

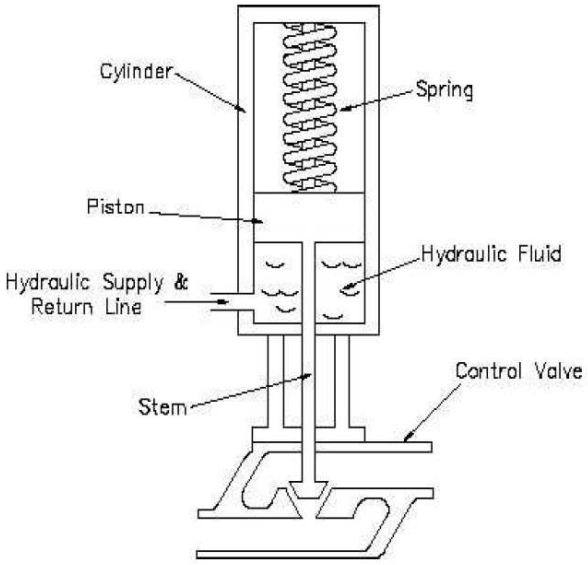

Figure 4: Cross section of a typical hydraulic actuator [13].

Hydraulic actuation is used when a large amount of force is needed in a relatively inexpensive and compact package. The typical pressure range of today's hydraulic systems is around 4350 to 7250 psi (320 to 500 bar). One reason for such high power density capabilities in hydraulic systems lies in the fact that the hydraulic fluid dissipates much of the heat generated in the system as the system operates [10]. This gives hydraulics an advantage over motors, where the heat cannot be carried away as easily.

In the ACT valve application, this type of actuator is ill-suited because hydraulic actuators tend to leak fluid. As it is unacceptable to have typically flammable hydraulic fluid mixing with the fuel that is being metered by the ACT valve, this technology is apparently not compatible unless a leak-free system can be devised. Also, the high temperature requirements for the valve prevent a hydraulic valve from any serious consideration as a viable solution because the fluid behaves differently at high temperatures and perhaps may even vaporize.

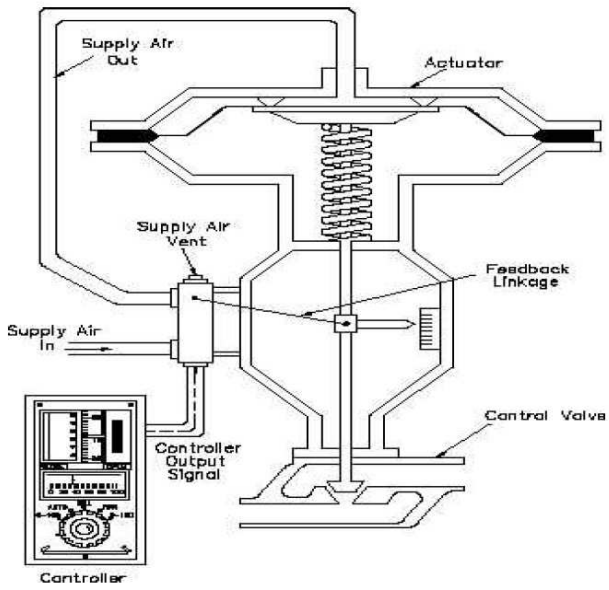

Figure 5: Cross section of atypical pneumatic actuator design [14].

2.2.4 Pneumatic Valves

Pneumatic valves are similar in operation to hydraulic actuators. They generally utilize compressed air or other gases to create a pressure differential within the housing that is used to attain mechanical motion. Pneumatic systems contain many of the same components present in hydraulic valves, often being of a piston design as shown in Figure 5. However, the force applied to the face of the piston must overcome the spring force opposing motion in order to actuate the system [10].

Similarly to hydraulic actuators, pneumatic actuators are relatively inexpensive. Pneumatic actuators, however, are not as power dense. The working fluid is air or an inert gas, however, which makes transportation of the fluid much easier than with hydraulics. An important difference between pneumatics and hydraulics, however, is the fact that the working

fluid is a compressible fluid, meaning that flows on the high- and low-pressure sides of the actuator may vary, giving the pressure-dependent flow characteristic an elliptic function [10]. Also, the compressibility of air creates a delay in operation, which is unfavorable for a device that requires a high bandwidth.

Again, like hydraulics, leaks are often an issue with pneumatic systems. In the ACT valve application, pneumatic actuators may not be able to withstand pressures as high as the criteria listed in Table 1 as most pneumatic devices operate at internal pressures between 30 and 120 psi [15].

2.2.5 Solenoids

Solenoids are similar to stepper motors (conversion of electricity into mechanical motion). Unlike a stepper motor, a solenoid is utilized for linear motion. They consist of a coil, armature, spring, and valve stem [Figure 6]. As electrical impulses are supplied to the coil, a magnetic field induces current into the armature [10]. This creates a magnetic field in the armature, and thus the magnetic fields cause an attractive force that pulls the armature upwards (into the core). In some instances, a spring is used to push the valve stem back to its original position when the force of the spring exceeds the coil.

Due to the nature of its electromagnetic operation, solenoid valves are typically either completely open or completely closed [10]. For use in the ACT application, it would be necessary to design a solenoid that could be operated in a proportional response mode.

2.2.6 Piezoelectric Materials

Piezoelectric materials are those that change their thickness when subjected to an electric voltage. The inverse piezoelectric effect, which is used in piezoelectric actuators, actually causes crystal lattice ions to change in thickness when subjected to an electric voltage. This type of material can be classified as natural crystals (such as quartz), polymers (such as polyvinyl fluoride, PVDF) or polycrystalline ceramics. Often used in piezoelectric actuator applications is PZT, lead-zirconate-titanate, which is based on ceramics [10].

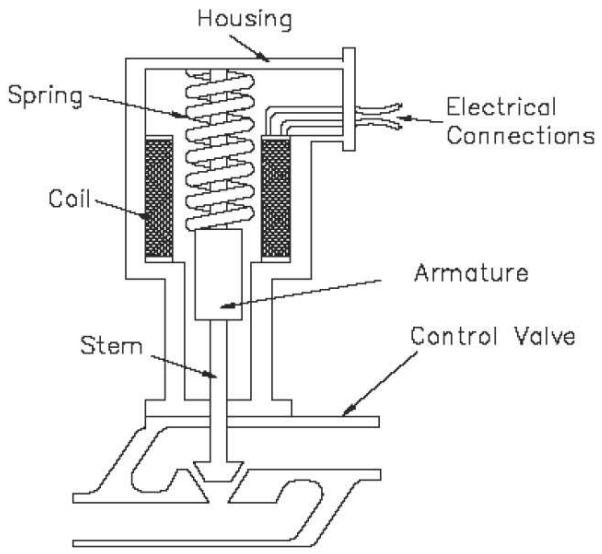

Figure 6: Cross section of a typical solenoid actuator design [16].

Piezoelectric actuators utilize the displacement change of a piezoelectric material and create mechanical motion. Most piezoelectric actuators are a type of stack actuator, as seen in Figure 7. Alternating discs are glued together in pairs of opposing polarity with metal electrodes and sealed with an insulator in stack type piezo actuators. The reason for using a stack structure in these actuators is that such a configuration increases the overall displacement while maintaining reasonable input voltages.

The resulting piezo actuators have an extremely fast response time and are capable of producing very large forces at an impressive electromechanical efficiency. However, piezoelectric materials are not well suited for use in extremely high temperature environments such as required by the ACT valve. The piezo effect can be altered when subjected to high temperatures. Also, over time, piezoelectric materials' characteristic properties may change, which is known as creep. There are higher-temperature piezoelectric materials under development, Thermiezo^{TM} [17] and aluminum nitride, but these are not yet commercially available and will potentially be quite expensive when they first arrive on the market. Also worth mentioning is that the piezo effect of both aforementioned new technologies still are not as large

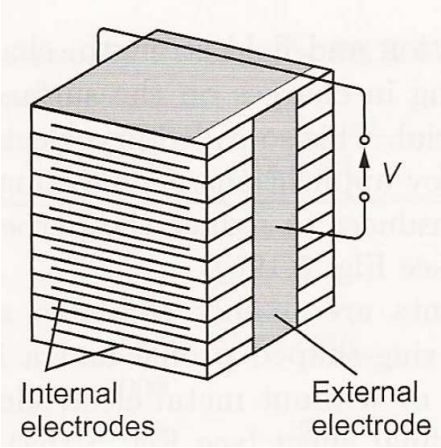

Figure 7: Basic structure of piezoelectric stack actuator [10].

in magnitude as PZT. Thermiezo^{TM}exhibits strains of 0.16% compared to PZTs 0.2%, but aluminum nitride's piezo effect is two orders of magnitude less. Also, it is extremely difficult to manufacture thick layers of aluminum nitride.

2.2.7 Electrochemical Actuators

Electrochemical actuators (ECAs) are devices which utilize small voltage inputs to evolve gas through chemical reactions within a closed system [10]. Since the system is closed, the pressure in the system increases and is then transformed into mechanical work. There are numerous chemical reactions that can be used in electrochemical actuators, but oxidation reduction reactions work the best.

Nickel-hydrogen and silver-hydrogen ECAs have been implemented since the 1990's, but they are still largely a custom-designed product. Currently, research and development in this field is focusing on raising actuation speeds by an order of magnitude (currently 0.1 mm/sec is a fairly fast-acting ECA), as well as making them more resilient to temperature (currently around -5 to 60°C can be accommodated by ECAs) and increasing durability. For this type of ECA, however, the temperature limitations and the relatively slow actuation time (on the order of seconds to tens of seconds) prevent use of such ECAs in the ACT valve.

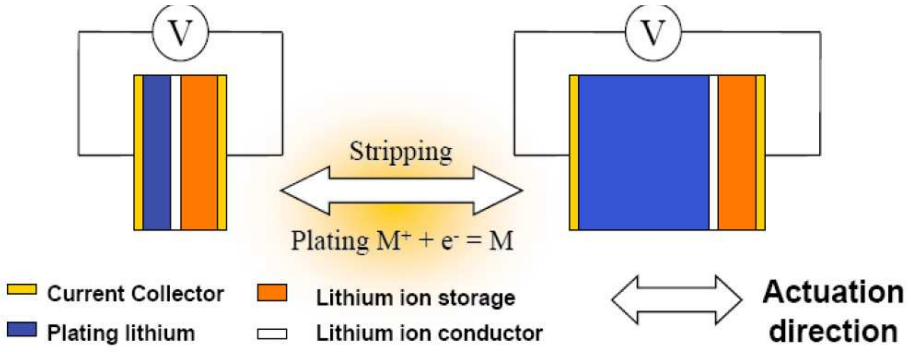

Figure 8: Li-ion/electroplating process schematic [18].

A more recent type of electrochemical actuator uses a lithium-ion (Li-ion) battery and electroplating to create a volume change capable of reversible work, as seen in Figure 8 [18, 19]. This new generation of ECAs suffers from the same issues as the old generation, however; they are ill suited for high temperature applications have and slow response time.

2.2.8 Electrosrictive Actuators

Electrostrictive actuators are similar to piezoelectric actuators in that they also exhibit a change in displacement due to an applied voltage, creating mechanical work from the displacement. The difference lies in the material itself. Piezoelectric actuators utilize PZT (lead-zirconate-titanate) typically while electrostrictive actuators use PMN (lead magnesium niobate) [20]. PMN inherently has substantially less creep and hysteresis than PZT making it more desirable for applications requiring more precision.

For all of the improvements of electrostrictive actuators over piezoelectric actuators, electrostrictive materials have several shortcomings relative to the ACT project. Electrostrictive materials require a very large voltage to induce a strain, are nonlinear in growth, produce lower strains than piezoelectric materials and the directional versions require a high bias voltage. Additionally, these materials are too temperature sensitive in the range required for the ACT valve.

2.2.9 Magnetostrictive Actuators

Magnetostrictive actuators are similar in operation electrostrictive and piezoelectric materials in that when excited, a shape change is experienced. However, here the shape change is induced by creating a magnetic field through the material. In the case of a magnetostrictive material (e.g. a ferromagnetic crystal), however, when magnetized the overall volume remains the same. This phenomenon is referred to as the Joule effect. In so called "giant" magnetostrictive actuators, a volume change does occur but it is negligible [10].

Magnetostrictive actuators and transducers are in many respects quite comparable in useful properties as piezoelectric actuators. Temperature still plays some role in properties of this type of material, but the most widely used magnetostrictive material, Terfenol-D®, is able to withstand temperatures of around 380°C [10]. An example of a magnetostrictive actuator utilizing Terfenol-D® can be seen in Figure 9. This material is difficult to create and is very expensive. At high temperatures, a preload is required for proper function. Other magnetostrictive materials are too strain limited, as the thermal strain experienced when heating from ambient to a high operating temperature is much greater than the magnetostrictive strain exhibited. Based on these facts, magnetostrictive actuators are not currently a wise choice for an ACT valve.

2.3 RHEOLOGICAL DAMPERS

In the most basic sense, rheology is the study of the deformation and flow of matter. More specifically, rheology deals with the behavior of complex, non-Newtonian, fluids. It should be noted that the yield stress of a rheological fluid is the threshold stress that stresses acting on the fluid must overcome before the fluid will flow. Certain fluids will climb a rod with a rotational speed. This is known as the Weissenberg effect. Fluids may also have what is known as fluid memory. This is the effect where a stress inside of viscoelastic fluid does not dissipate at the instant that stress is removed from the fluid. Rheological fluids are also susceptible to die swell which is a phenomena in which the fluid increases in diameter

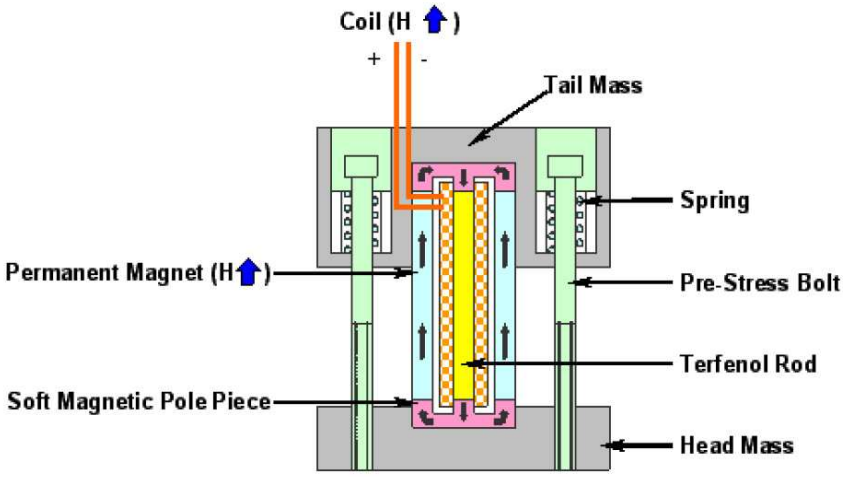

Figure 9: Terfenol magnetostrictive actuator cross section [21].

and swells when exiting a die. All of these peculiar characteristics of certain non-Newtonian fluids accentuate the fact that they are in fact not actuators, but rather actively controlled passive devices: we actively tailor the rheology to affect dissipation. Table 3 lists the types of rheological dampers considered for the ACT application while the advantages/disadvantages of rheological dampers are listed with the other actuation types in Table 20 in Appendix A.

Table 3: Actively controlled passive dissipation/dampers explored for ACT project.

1.	Magnetorheological
2.	Electrorheological

2.3.1 Electrorheological Dampers

Electrorheological (ER) dampers utilize an electrorheological fluid, which is a dielectric carrier fluid containing semiconducting particles and another polar fluid which is absorbed by the semiconducting particles [10]. The application of an electric field polarizes the particles allowing them to arrange in conductive chains. The electric field can be adjusted as to reg-

ulate the fluid viscosity from an easy flow to a solid condition. Without the presence of an electric field, the ER fluid behaves like a Newtonian viscous fluid.

Like so many of the actuation technologies reviewed thus far, properties of ER fluids are highly dependent upon temperature and have unpredictable and sometimes unrepeatable behavior at such high temperatures [10]. Age also affects the properties of ER fluids rather unpredictably.

2.3.2 Magnetorheological Dampers

Magnetorheological (MR) dampers are very similar to electrorheological dampers with the exception that MR fluids react to magnetic flux density instead of an electric field. MR fluid consists of a low-permeable base fluid with magnetizable particles suspended in the fluid. As magnetic flux increases, so does the fluid's resistance to flow [10]. Additionally, as the flux increases, the particles form magnetic dipoles which align with the magnetic field and form chains. The chains can be mechanically loaded thereby increasing flow resistance. Like ER fluids, when the method of excitation (in this case a magnetic field) is removed, the fluid returns to a Newtonian viscous fluid.

Similarly to ER fluids, age unpredictably affects the properties of MR fluids [10]. Other disadvantages that make an MR actuator a poor choice for the ACT valve include the fact that these fluids cannot do active work on a mechanical system and they are poorly understood. For example, there are no commercial measurement techniques, and compatibility with other materials for many MR fluids is still unknown.

An example of a practical application using MR fluids can be seen in Figure 10. This design is similar to eddy current brakes. When the current through the coil is increased, the MR fluid resists flow, therefore becoming more viscous and impeding rotation of the brake disc with relation to the housing.

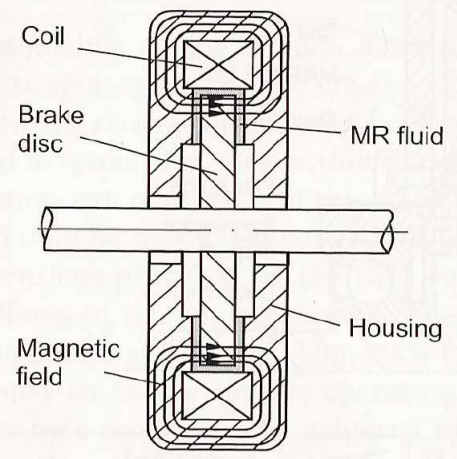

Figure 10: Basic construction of an MR fluid brake [10].

2.4 VALVE TYPES

Similarly to the available means of actuation, there are numerous designs of valves to be considered for this project. Some designs are standard, commercial designs, while others are original designs conceived for this project. Most of the latter resemble standard designs in one or more ways. Table 4 lists the valve types examined and evaluated. A brief description of each valve is included below, while a comprehensive list of advantages and disadvantages can be found in Table 21 in Appendix B.

2.4.1 Globe Valves

Globe valves are commonly used as control valves or as manual valves and can be found in many process industry applications. Conversely, this type of valve can be used as an on-off valve as well. Unlike other valves, a globe valve is not limited to inherent flow characteristics, as the flow characteristic can be designed into the shape of the plug. Features such as design simplicity, versatility of application, ease of maintenance and their ability to handle a wide range of pressures and temperatures make globe control valves the most commonly used in such processes [22].

Table 4: Valve technologies explored for ACT project.

1.	Globe Valve
2.	Needle Valve
3.	Gate Valve w/1 Gate
4.	Gate Valve w/2 Gates
5.	Butterfly Valve
6.	Ball Valve
7.	Single Orifice Valve
8.	Multi-Orifice Plate Valve (MOV)
9.	MOV Gate Valve (Linear Flow)
10.	MOV Gate Valve (Non-Linear Flow)
11.	Constricting Pinch Valve
12.	Thunder^{TM} Valve
13.	Linear Barrel Valve
14.	Barrel Valve w/2 DOF Motion
15.	DAHENV
16.	Turbine Throttles
17.	Football Valve

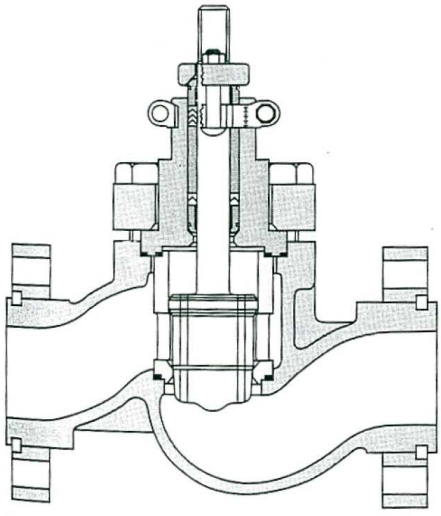

Figure 11: Cross section of a globe valve [22].

As seen in Figure 11, globe valves are characterized by a globe-styled body, and are linear-motion valves. They have a relatively long face-to-face dimension that allows the passageways within the valve to be smooth and to avoid sharp turns within the valve. The globe valve shown in Figure 11 is a single-seat design, which includes a single plug-seat arrangement. In this type of globe valve, the plug moves linearly relative to the seat to permit flow through the body. There are also double-seat arrangements, which utilize a pair of plug-seat interactions [22].

2.4.2 Needle Valves

Needle valves are very similar to globe valves, and can even be thought of as a subset of them used for extremely low flow conditions. Rather than having a larger, more obtuse plug, needle valves consist of a very narrowly-shaped plug head and a smaller diameter seat, as seen in Figure 12. Since flow coefficient and flow rate tend to vary drastically with diameter variations, it is imperative that the needle plug head be machined using special micromachining techniques. Such specialized machining processes can greatly increase the total cost of implementing such a valve in the application in question, however [22].

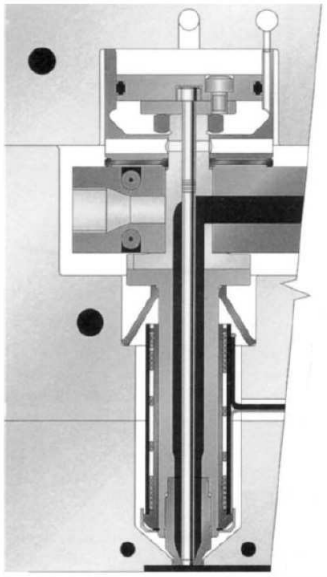

Figure 12: Cross section of a conventional needle valve [23].

Figure 13 depicts a non-conventional needle valve design considered for the ACT valve assembly. This design's distinguishing feature is its ability to maintain a nominal flow rate during a failure situation.

2.4.3 Gate Valve with One Gate

Typically, gate valves are linear-motion manual valves that are used for on-off block service. They feature a flat closure element perpendicular to the process flow which can be moved through the flow path to attain shutoff. While gate valves can be used for liquid or gas service, they are normally used for liquid service where entrained solids are present. When the valve is completely open, there is very little pressure drop due to the closure element as it completely out of the flow path. Traditionally, there are two types of gate valve classified on their gate shape: parallel-gate valves and wedge-shape gate valves. These classifications are quite self-explanatory: the parallel-gate valve uses a gate with parallel seats whereas the wedge-shape gate valve utilizes a wedge-shaped gate and angled seats [22].

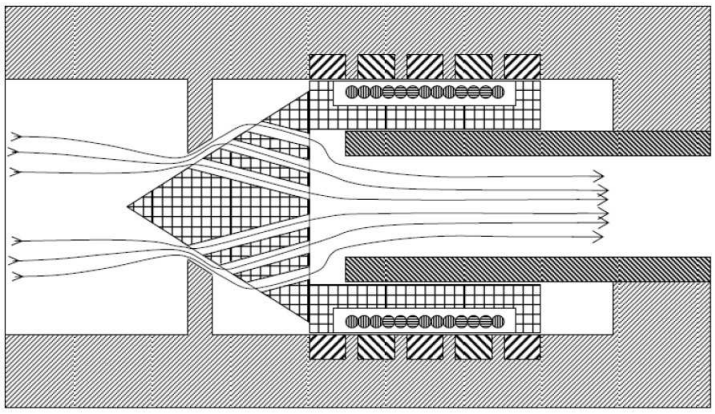

Figure 13: Cross section of a non-conventional needle valve [P. Hensel].

Gate valves tend to not be very efficient throttling valves as they produce inadequate control characteristics. Figure 14 depicts a modified gate valve design with a single gate actuated by means of a piezoelectric material without any seats or seals since the flow is never meant to be completely stopped [22].

2.4.4 Gate Valve with Two Gates

Similarly to the gate valve design with one gate, the two-gate design shown in Figure 15 has two gates perpendicular to the flow path within the valve body. Again, this design lacks any type of seats or sealing, since the flow is never desired to be totally impeded. Using two gates, a variety of orifice shapes can be created, as seen in Figure 15.

2.4.5 Butterfly Valves

Butterfly valves were invented in the 1930's and until the past 30 years, were mainly used as on-off valves. In a typical on-off block variation of the butterfly valve, a quarter turn (0° to 90°) of a manual actuator opens or closes the valve's concentric disc element, which can be seen in Figure 16. Over the past three decades, however, butterfly valves have increasingly been used in throttling and control applications. Butterfly valves used in control

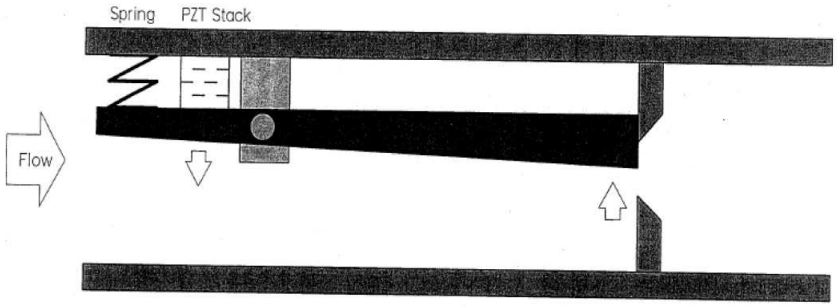

Figure 14: Cross section of an unconventional gate valve designed to work with a piezo stack actuator [B. T. Chorpening].

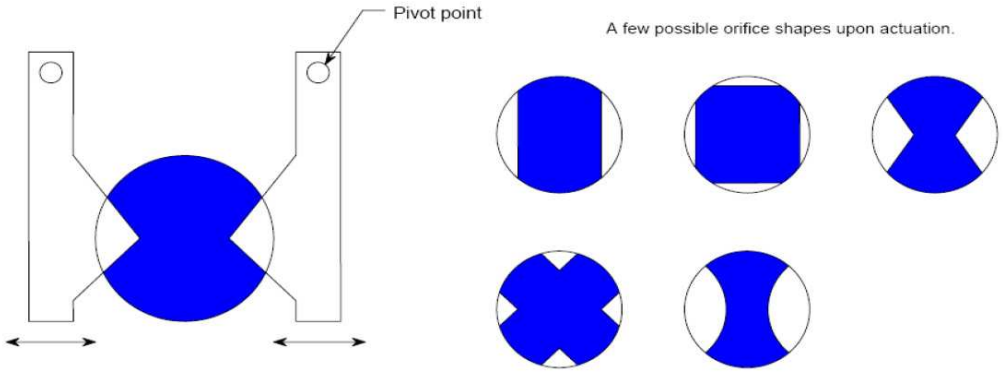

Figure 15: Cross section of a gate valve with two gates (left) and some of the possible orifice shapes possible depending on the shape of the gates used (right) [24].

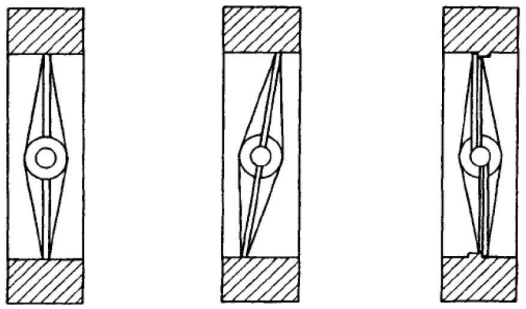

Figure 16: Simplified cross sections of three types of butterfly valves; left: swing-thru disc, center: angle-seated disc, right: step-seated disc [25].

applications are sometimes referred to as "high-performance butterfly valves," indicating use of an automatic actuator and control system to operate the valve. High-performance butterfly valves typically feature an eccentric disc element rather than a concentric one, giving them more efficient throttling control characteristics [22].

While not better than globe valves in high-pressure drop applications, butterfly valves do fair better in the realm of low-pressure drop applications. In high-pressure drop applications, butterfly valves tend to experience cavitation and choked flow more easily than globe valves, whereas in low-pressure drop applications, they excel due to a high pressure-recovery factor. Other areas in which butterfly valves excel over globe valves are actuator size (usually requires a smaller one), overall size and mass of the valve (typically 40 to 80% of the mass of a comparable globe valve) [22].

2.4.6 Ball Valves

Ball valves, much like butterfly valves, have been in existence for many years, but have just seen use as more than an on-off valve in just the past 30 years. Advances in sealing materials and design and machining techniques have allowed ball valves to create a tight shutoff as well as characterizable control. Ball valves truly excel in applications of high rangeability (e.g. 300 to 1), where a comparable butterfly valve of relatively high rangeability cannot provide the same values (e.g. 20 to 1) [22].

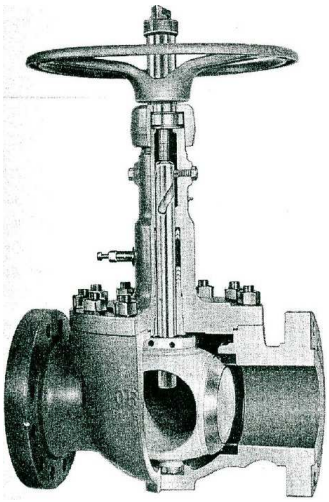

Figure 17: Cutaway of a manual ball valve [22].

As seen in Figure 17, one type of ball valve consists of a spherical or rounded regulating element (hence "ball" valve) to control flow. There are also matching rounded elastomeric seats that allow uniform sealing stress. There are a few different types of ball valve arrangements allowing the either the regulating element or the seat seals to "float" rather than be fixed. These arrangements utilize the pressure from the flow to maintain constant contact between the seals and the closure element. There are also two main types of regulating elements that dictate the overall type of ball valve: full-port ball valves and characterizable-ball valves. Figure 17 depicts a full-port ball valve, which is indicated by the spherical regulating element. In this type of valve, there is a hole that is bored through the regulating element that is the same inside diameter of the incoming pipe. When the valve is completely open, the bored hole is inline with the influent and effluent piping and the flow is completely unimpeded. Therefore, there is little to no pressure drop and turbulence when the valve is completely open. In contrast, the characterizable-ball valve uses a hollow segment of a sphere rather than a spherical regulating element. This hollow spherical segment has the flow characteristic cut into it with a V-notch or a parabolic curve. While this design causes more pressure drop and turbulence in contrast to the full-body valve that is best for on-off applications, it is more useful for throttling and control applications [22].

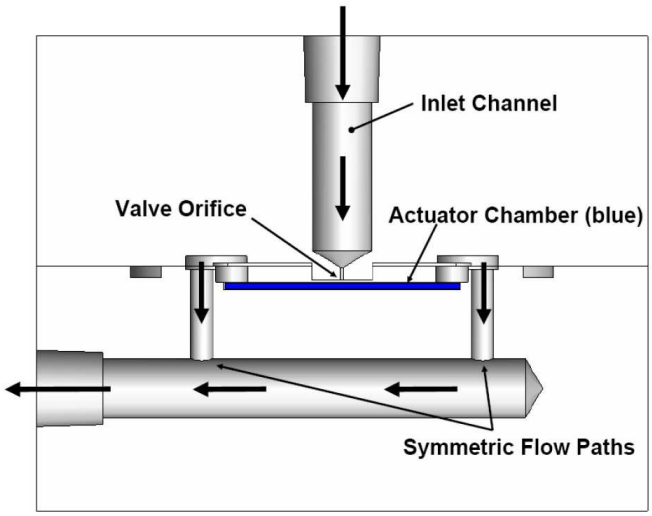

Figure 18: Cross section of a single-orifice valve [J. Vipperman].

2.4.7 Single Orifice Valve

Using a small orifice and a mating piezoelectric bender, a single orifice valve can control the fluid flow that flows out of the valve by varying the voltage applied to the bender material. Figure 18 depicts a cross section view of a single orifice valve that was designed, built and tested through a collaborative effort between NETL Morgantown and the University of Pittsburgh. It actually utilizes a piece of PZT (piezoelectric material) to control the flow through the outlet of valve and was developed for fuel cell flow control. This particular design only has one critical dimension for function as a control valve: the nominal distance between the top of the actuator and the bottom of the orifice surface. This dimension controls the non-actuated flow rate. Since tight tolerances are not an issue with this design, manufacture of this valve can be achieved on a commercial CNC machine which may reduce machining costs.

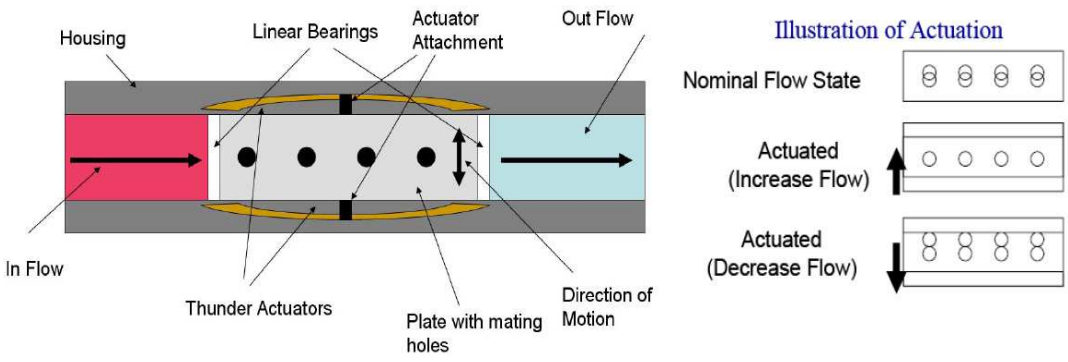

Figure 19: Cross section of a multi-orifice plate valve [J. Vipperman].

2.4.8 Multi-Orifice Plate Valve (MOV)

This non-conventional throttling valve consists of two sliding plates with identical hole patterns, as seen in Figure 19. These plates can be moved relative to one another in order to change the effective flow area and therefore change the flow. Vertical actuation is depicted and demonstrated in Figure 19; however, horizontal movement could also be used. The total flow capacity and the required stroke can be determined by the total number (and size) of the holes [24].

2.4.9 MOV Gate Valve (Linear Flow)

This type of valve was born out of optimization efforts for controlling large gas flow at high pressures. As seen in Figure 20a, this variation of the multi-orifice gate valve is supplied with fluid through a plate with respect to the outlet nozzles. The outlet nozzles are referred to as a seat valve nozzle. The resulting valve is a multiple-orifice arrangement with many miniature circular nozzles. This configuration results in a relatively small actuator stroke length, which could be well-suited to some of the actuator designs under consideration [26].

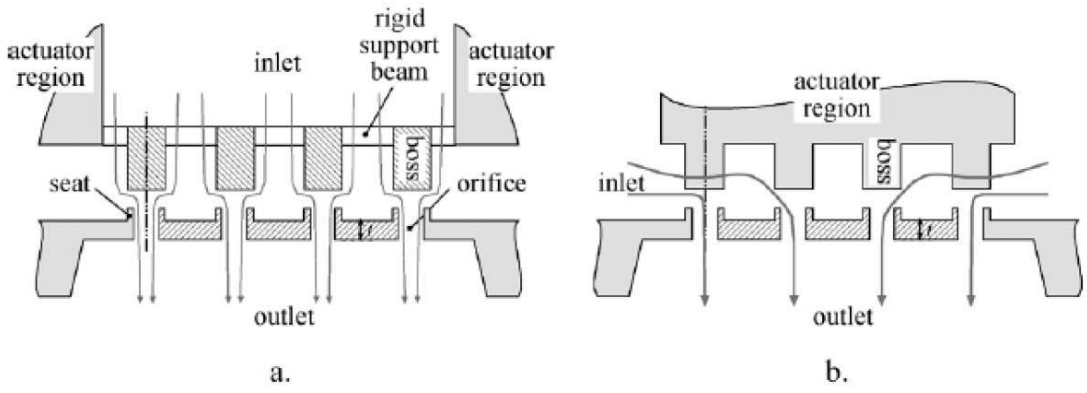

Figure 20: a. Cross section of an MOV gate valve with linear flow. b. Cross section of an MOV gate valve with non-linear flow [26].

2.4.10 MOV Gate Valve (Non-Linear Flow)

The only difference between the non-linear flow vs. linear flow versions of the multiple-orifice gate valve is the fact that the non-linear version gets its incoming fluid parallel to the plate with respect to the outlet nozzles. The difference is very apparent in Figure 20b. compared the linear flow in Figure 20a [26].

2.4.11 Constricting Pinch Valve

Traditionally, a pinch valve was a valve with a flexible elastomer body or liner that could be pushed together (hence, "pinch") through some mechanism or fluid pressure. This is a beneficial feature since there are no additional seals, gaskets or packing boxes of any type. As such, pinch valves are used where mixed liquid/solid phase fluids are transported (e.g. sewage). High-temperature applications, however, are ill-suited for this type of pinch valve since most liners are elastomeric [22].

From this concept, a valve utilizing braided sleeving rather than an elastomeric liner was conceived. Rather than a mechanism or means of actuation pushing together the sides of the valve liner, one end of the braided sleeving is held stationary while the other end is

stretched. This motion reduces the diameter of the braided sleeving and therefore reduces flow. Figure 21 depicts a test unit using braided sleeving.

Figure 21: Picture of a lab constructed constricting pinch valve using braided hosing.

2.4.12 Thunder^{TM} Valve

Similarly to the constricting pinch valve, the Thunder^{TM} valve is also based on the pinch valve concept [27]. This valve is actually closer to a traditional pinch valve, as a Thunder^{TM} piezoelectric actuator is used to reduce the cross sectional area of the valve, thus reducing flow. Figure 22 depicts this type of valve and indicates flow paths [28].

As a precursor to the ACT project, this valve was developed in conjunction with NETL during the VOAT project. Unfortunately, the Thunder^{TM} valve did not provide as much controllability of flow as anticipated.

2.4.13 Linear Barrel Valve

This valve is a cylindrical, multi-orifice valve that consists of a pair of concentric cylinders with identical hole patterns, as seen in Figure 23. In this specific design, an actuator moves one of the cylinders linearly relative to the other stationary cylinder to align (or misalign) the hole patterns, effectively increasing or decreasing the flow. As this is a linear design, it is possible that this valve could be actuated using a Thunder^{TM} actuator or other linear actuators [28].

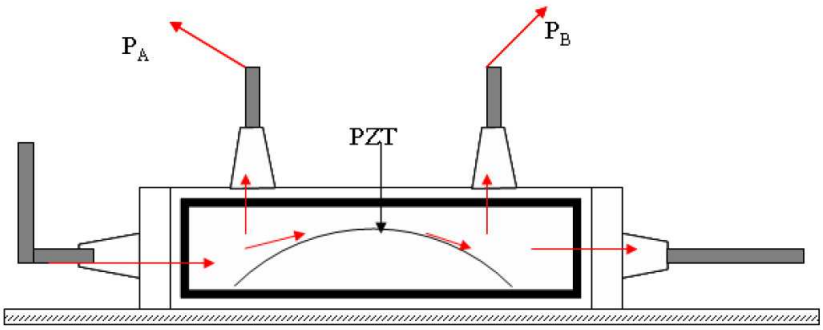

Figure 22: Cross section of a Thunder^{TM} valve design [28].

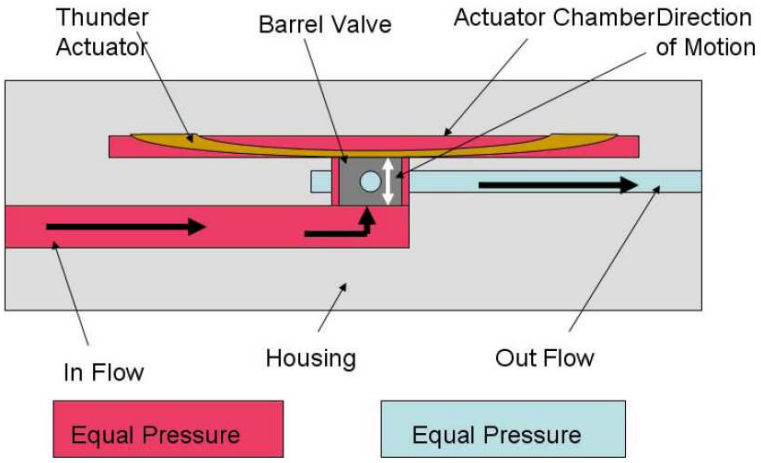

Figure 23: Cross section of a linear barrel valve [28].

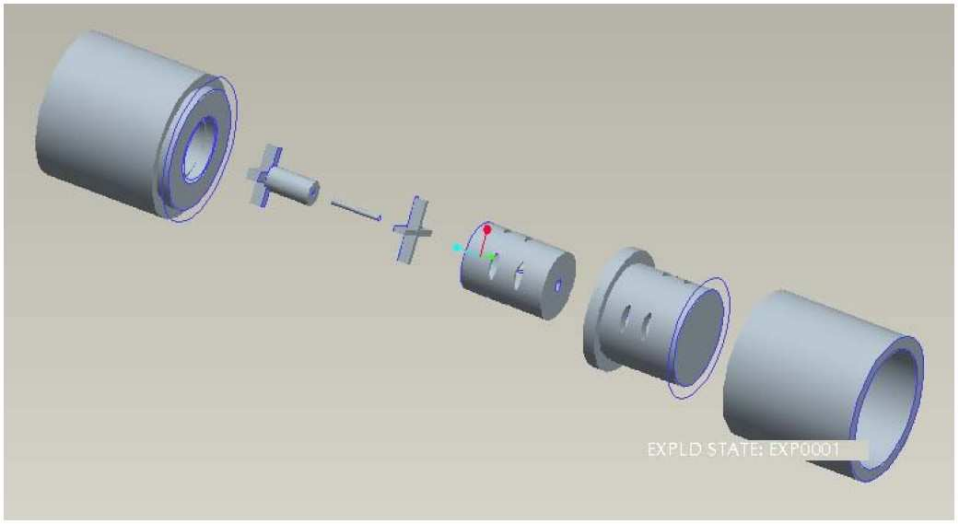

Figure 24: Exploded view of a 2 degree-of-freedom barrel valve [24].

2.4.14 Barrel Valve (w/ 2 DOF Motion)

This valve is similar to the linear barrel valve in that it is a cylindrical, multi-orifice valve and can be seen in Figure 24. With this design, however, the two inner cylinders translate and/or rotate with respect to each other to align (or misalign) the identical hole patterns, which will increase or decrease the flow, respectively. One implementation of this valve would use one degree-of-freedom for coarse-tuning adjustments while the other degree-of-freedom could be used for fine-tuning adjustments. Used in this way, it embodies the compact, axial flow characteristic that is desired and could possibly be actuated via internal rotational and/or linear electromagnetic transducers [24, 28].

2.4.15 DAHENV (Dual-Actuated Hybrid Enlarged Needle Valve)

The DAHENV is a hybridization of a needle and globe valve with axial flow characteristics where a chamfered plug (green) fits into a mating seat (translucent purple) as seen in Figure 25. Both surfaces could be actuated to double the effective motion, making stroke-

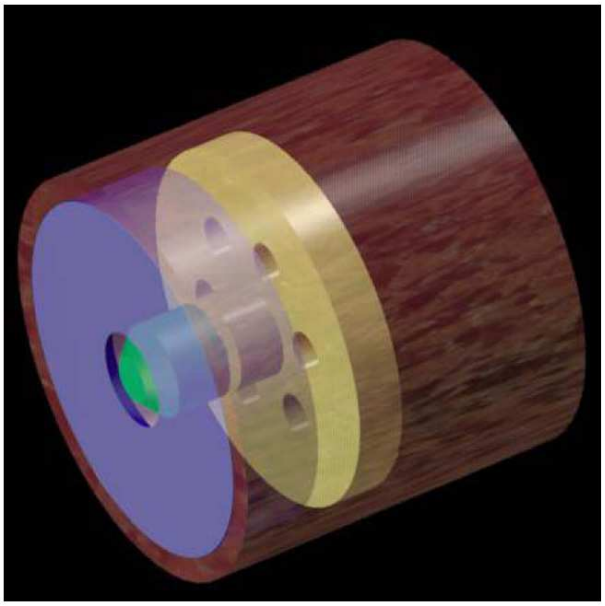

Figure 25: Dual-actuated hybrid enlarged needle valve [24].

limited materials such as piezoelectrics more practical. As seen in Figure 25, however, this valve is likely difficult and expensive to produce [24, 28].

2.4.16 Turbine Throttles

This valve is comprised of a turbine that introduces losses by removing momentum and decreasing flow through the valve. One possible method of controlling the turbine would use eddy-current damping on a magnetic turbine, resulting in possibly external actuation. A schematic of such a valve is shown in Figure 26.

2.4.17 Football Valve

The original design for this valve features an armature that moves relative to a football-shaped component to modulate flow, as can be seen in Figure 27. The valve characteristics can be modified by changing the shape of the middle part. Having a part shaped like a football, however, increases machining costs. It could be a fast-acting valve due to the

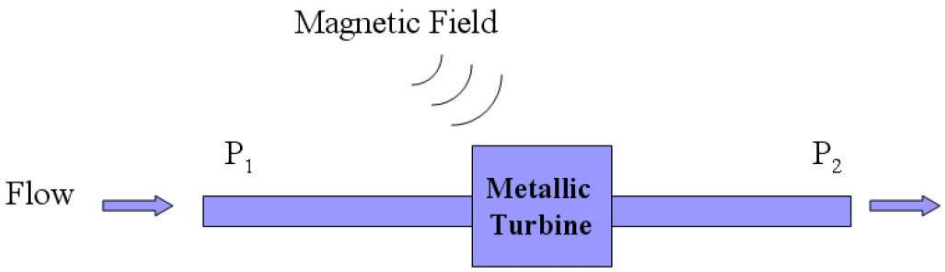

Figure 26: Schematic of turbine throttles in the flow path [29].

potentially light mass of the armature. Some variations of the football valve have been considered and will be further discussed in subsequent sections.

2.5 PATENT SEARCH

Exhaustive, periodic patent searches were conducted throughout the first phase of the ACT project. No patents were discovered during any of the searches that resembled the ACT valve assembly prospective designs. The main sources used include the United States Patent and Trademark Office website and the Google Patent website.

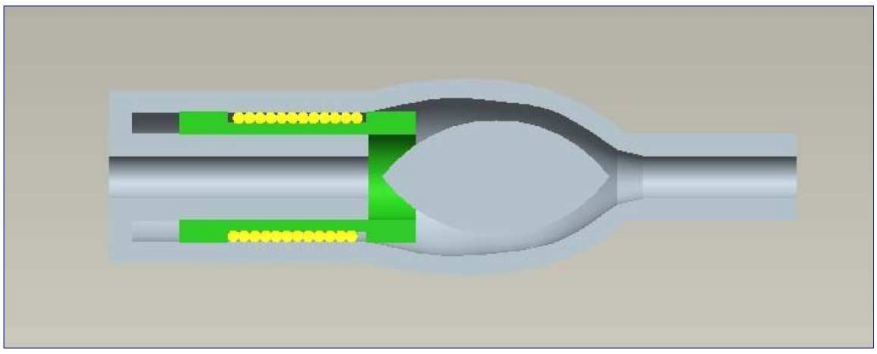

Figure 27: Cross section of the original "football" valve design [30].

3.0 THEORY

The ACT project is truly a multi-faceted project. Many mechanical topics must be considered to design and build the ACT valve assembly: electromagnetism must be considered for the development of the actuator; stress analysis indicates whether the design of the valve assembly can withstand the forces experienced by it; and thermal analysis determines the heat transfer and growth of the valve assembly due to temperature changes that will inevitably be present during operation. The basics of these topics that are fundamental to the design of the ACT valve assembly will be reviewed in subsequent sections.

3.1 ELECTROMAGNETISM

Electromagnetism is concerned with the effects of electricity on magnetic materials. In order to discuss a few basic principles of electromagnetism, it is important to first briefly mention the quantities associated with the subject. $\vec{B}$ is the magnetic flux density and is a vector field quantity that dictates the strength of a magnetic material. $\vec{H}$ is the magnetic vector field associated with a magnetic material. $\vec{M}$ is the magnetization intensity of a material, and in a sense indicates the extent to which the material is magnetized. It is important to note that a magnetic field can be caused by a magnetic material or electric current flowing through a wire.

3.1.1 Electromagnetic Force

The principle of electromagnetism that is primarily exploited in the ACT valve is the electromagnetic force equation, as seen in Equation 3.1.

$$\vec{F} = I\vec{L} \times \vec{B} \tag{3.1}$$

In Equation 3.1, $\vec{F}$ is the magnetic force vector, I is the coil current, $\vec{L}$ is a vector in the direction of the current and with the magnitude of the length of the coil, and $\vec{B}$ is the magnetic field vector. Therefore, the magnetic force produced by a device that operates according to this relationship can be altered by varying the magnitude and/or direction of the current. While other principles of electromagnetism are important to this project as well, Equation 3.1 dictates the amount of force produced to adjust the ACT valve.

3.1.2 Saturation

Another important aspect of electromagnetism is the concept of saturation. Saturation is a magnetic phenomenon that is characterized by very little increase in the $\vec{B}$-field (magnetic flux density) even with very large increases in the magnetic field, $\vec{H}$. In order to gain a better understanding of saturation, consider Equation 3.2.

$$\vec{B} = \vec{H} + 4\pi\vec{M} \tag{3.2}$$

Prior to a material becoming saturated, both $\vec{H}$ and $\vec{M}$ increase with the coil current, I. When saturation occurs, however, M is at a level called the saturation magnetization (M_s). Once M_s is reached, $\vec{M}$ will (practically) no longer increase with I. Therefore, $\vec{B}$ will only increase as $\vec{H}$ increases, yielding a much smaller increase in $\vec{B}$ with an increase in I [31].

Saturation occurs when a material is subjected to too much magnetic flux, which typically results in reduced performance and efficiency. A more specific discussion of detecting saturation relative to the electromagnetic actuator design will be presented in a later chapter.

3.2 STRESS ANALYSIS

The stress analysis methods used throughout the early stages of the ACT project revolve around manual and computer-aided analyses using the von Mises criterion, which is also known as the distortional energy density criterion [32]. Also vital in the stress analyses are the manual methods for finding the stress in threaded components. Both stress approaches will be summarized in the subsequent sections.

3.2.1 von Mises Criterion

Most components of the ACT valves are axisymmetric in design and are therefore conducive to working with in cylindrical coordinates. For the sake of the manual stress analyses, the components examined are approximated as thick-walled cylinders (i.e. the wall thickness of the cylinder is at least one-tenth of the radius). The stress components in cylindrical coordinates that required for the thick-walled cylinder equations are the radial stress (σ_{rr}), the tangential stress ($\sigma_{\theta\theta}$) and the longitudinal stress (σ_{zz}), which can be seen in Figure 28. To find the components of stress in cylindrical coordinates for thick-walled cylinders, Equations 3.3, 3.4, and 3.5 were utilized [32].

$$\sigma_{rr} = \frac{p_1 a^2 - p_2 b^2}{b^2 - a^2} - \frac{a^2 b^2}{r^2(b^2 - a^2)}(p_1 - p_2) \tag{3.3}$$

$$\sigma_{\theta\theta} = \frac{p_1 a^2 - p_2 b^2}{b^2 - a^2} + \frac{a^2 b^2}{r^2(b^2 - a^2)}(p_1 - p_2) \tag{3.4}$$

$$\sigma_{zz} = \frac{p_1 a^2 - p_2 b^2}{b^2 - a^2} - \frac{P}{\pi(b^2 - a^2)} \tag{3.5}$$

In the given equations, a is the inner radius, b is the outer radius, p_1 is the internal pressure, p_2 is the external pressure, P is an applied axial load (due to pressure or an external force of some kind), and r is the radial length at which the stress is to be found. After finding the components of stress, it is then possible to find the von Mises stress, or the effective stress,

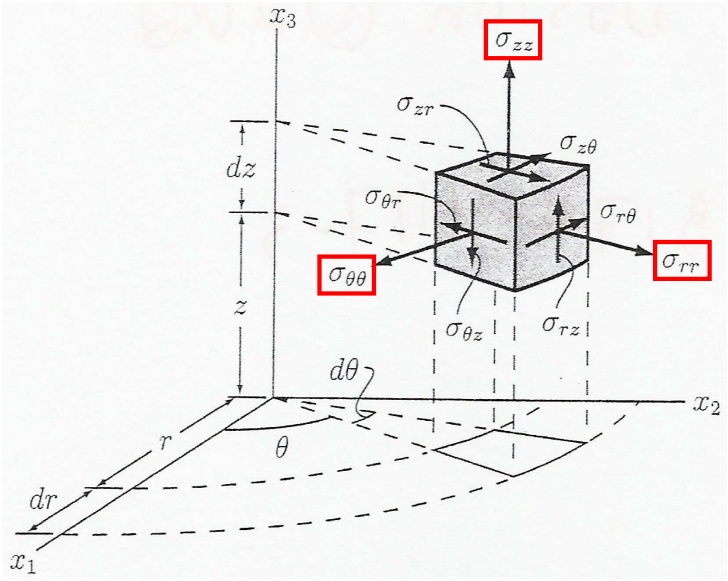

Figure 28: Stress components in cylindrical coordinates [33].

σ_e. Equation 3.6 shows how the components of stress in cylindrical components can be used to find the effective stress [32].

$$\sigma_e = \sqrt{\frac{1}{2}\left[(\sigma_{\theta\theta} - \sigma_{rr})^2 + (\sigma_{rr} - \sigma_{zz})^2 + (\sigma_{zz} - \sigma_{\theta\theta})^2\right]} \tag{3.6}$$

Once the effective stress is known for a given cylindrical component, this value can then be compared to the characteristic values of the material the component is made of, such as the yield strength.

3.2.2 Stress in Threaded Regions

As some components of the prototype valve designs include threaded sections, the shear stress in these threaded sections must be examined as well. Equations 3.7 and 3.8 indicate how the stripping-shear area was calculated for the threaded regions in question [34].

$$A_s = \pi d_r w_i p \tag{3.7}$$

$$A_s = \pi d w_o p \tag{3.8}$$

In the above equations, d_r is the minor diameter (corresponding to external threads, like on a bolt or screw), d is the major diameter (corresponding to internal threads, like in a nut), w_i is the area factor for thread-stripping shear area (corresponding to the minor diameter), w_o is the area factor for thread-stripping shear area (corresponding to the major diameter), and p is the thread pitch. It is important to note that Equations 3.7 and 3.8 result in units of area per thread. In order to find the total stripping-shear area, the number of engaged threads must also be determined. After finding the area over which the shear stress is applied, Equation 3.9 is used to find the shear stress for thread stripping [34].

$$\tau_s = \frac{F}{A_s} \tag{3.9}$$

In Equation 3.9, F is the axial force shearing the threads. The key to finding accurate values of the thread stripping shear stress lies in finding the amount of axial force applied to the threads. Once a value of this stress is determined, it is again compared to characteristic strength values of the material used to make the component in question.

3.2.3 Saint-Venant's Principle

Saint-Venant's principle implies that at an appreciable distance from the restrained end of the body in question, the stress distribution should closely resemble the manual hand calculations from the von Mises equation examined earlier. In other words, regardless of the conditions of the constrained end of any of the cylindrical components analyzed, the stress distribution away from the constrained end will be a straightforward case that can easily be calculated using the simple equations highlighted earlier in this section. Throughout the stress analyses conducted in the ACT project, Saint-Venant's principle was always considered and was in fact used as a method of validating finite element analyses (FEA) used extensively throughout the design phase.

3.3 HEAT TRANSFER

According to the specifications set forth by NETL in Table 1, the ACT valve must be able to operate at 650°F. In order to assure proper operation, it is necessary to to consider the heat transfer rate within the valve assembly during operation. With the temperature gradient known, the dimensional changes due to temperture (be it expansion or in some cases retraction) can be determined. Therefore, the thermal analysis of the ACT valve will first include determining the heat transfer.

3.3.1 General Equation of Heat Transfer

To find the heat transfer, first consider the general equation of heat transfer seen in Equation 3.10.

$$Q = \frac{\Delta T}{R} \tag{3.10}$$

In Equation 3.10, Q is the heat transfer (typically in watts, W), ΔT is the change in temperature, and R is the thermal resistance. Often, R is in fact an equivalent thermal resistance based on the thermal circuit of the object(s) in question. In practical terms, thermal resistance can be thought of as the resistance of material to change in temperature [35]. For a given body or configuration, a so-called thermal circuit can be constructed. All individual components' thermal resistances must be calculated, then total effective thermal resistance can be determined similar the determination of equivalent electrical resistance of an electrical circuit. To find the total thermal resistance in a given body, three separate modes of heat transfer must be addressed: conduction, convection and radiation. In the case of the ACT valve, all three modes of heat transfer will be considered.

Once the resultant equivalent thermal resistance has been determined, Equation 3.10 can be solved for the heat transfer, Q. Finding the heat transfer of the valve assembly allows the thermal expansion to be calculated since the change in temperature drives the growth. Using Equation 3.10 and the heat transfer value determined from the method described above,

temperatures can be calculated for each discrete piece. These temperatures can ultimately be used to determine the thermal expansion of individual components. A subsequent section explains in more detail how the thermal expansion of an object is determined.

3.3.2 Conductive Thermal Resistance

Conduction occurs between two bodies in contact as well as within a body. It also occurs between gasses and liquids, though in a negligible quantity relative to the conduction between two solids. The ACT valve will be comprised of solid components in contact with one another and will therefore be subject to heat transfer via conduction. For cylindrical bodies, Equation 3.11 yields the calculation of thermal resistance due to conduction [35].

$$R_{cond} = \frac{\ln\left(\frac{R_o}{R_i}\right)}{2\pi l k} \tag{3.11}$$

In Equation 3.11, R_o is the outer radius of the solid, R_i is the inner radius of the solid, l is the length of the solid, and k is the thermal conductivity of the solid.

3.3.3 Convective Thermal Resistance

Convection, on the other hand, is the transfer of energy in the form of heat by fluid flow [35]. This mode of heat transfer occurs in moving gasses and fluids only. As the ACT valve will have a fuel traveling through the center of the valve, convection will play an important role in the overall heat transfer of the valve assembly. Equation 3.12 yields the convective thermal resistances [35].

$$R_{conv} = (hA)^{-1} \tag{3.12}$$

In Equation 3.12, A is the area in contact with the fluid and h is the convective heat transfer coefficient.

The convective heat transfer coefficient varies greatly with the temperature gradient of the fluid in question and is quite difficult to accurately estimate without extensive knowledge of the conditions present in the fluid and its environment. There are several dimensionless parameters that must be considered in order to determine the convective heat transfer coefficient: Reynolds number (ratio of the inertial to viscous forces; Re), Grashof number (ratio

of buoyancy to viscous forces; Gr), Prandtl number (ratio of the momentum and thermal diffusivities; Pr), and Nusselt number (dimensionless temperature gradient at the surface; Nu) [35]. It it also important to consider that there are two different types of convection that play a role in the case of the ACT valve: forced convection and free convection.

3.3.3.1 Convective Heat Transfer Coefficient for Forced Convection Forced convection occurs when a fluid is being pushed by an external means, be it a pump, a fan or some other device [35]. Gaseous fuels will move through the ACT valve and therefore there is forced convection. In order to find the convective heat transfer coefficient due to forced convection, one first determines the Reynolds number [35]:

$$Re = \frac{v_m D}{\upsilon} \tag{3.13}$$

In Equation 3.13, v_m is the mean flow velocity, D is the diameter of the flow, and υ is the kinematic viscosity, which is typically published in a tabular form for various temperatures. To determine v_m:

$$v_m = \frac{\dot{m}}{\rho A_c} \tag{3.14}$$

In Equation 3.14, $\dot{m}$ is the mass flow rate of the fluid, ρ is the density of the fluid and A_c is the cross sectional area of the flow path (or tube).

Once the Reynolds number is calculated, one can then be determine whether the forced convective flow is turbulent. The lowest threshold for the onset of turbulence is typically observed to be $\approx$ 2,300, although this does not indicate that the flow is necessarily well developed and turbulent [35]. Therefore, if the Reynolds number is greater than 2,300 (as it will be later shown is the case in the ACT valve), the flow is turbulent and a certain set of empirically determined equations must be used to find the forced convection heat transfer coefficient. Otherwise, the flow is laminar and a different set of equations must be utilized. As previously stated, the flow through the ACT valve was determined to be turbulent at the operating pressure and flows specified in Table 1.

Table 5: Results of Ar calculation.

Condition	Indication
$Ar \ll 1$	Free convection is negligible
$Ar \gg 1$	Forced convection is negligible
$Ar \approx 1$	Neither forced nor free convection is negligible

Assuming the flow is found to be turbulent, the Grashof number is calculated via Equation 3.15 [35].

$$Gr = \frac{g\beta(T_s - T_\infty)L^3}{\upsilon^2} \tag{3.15}$$

In Equation 3.15, g is the acceleration due to gravity, β is the volumetric thermal expansion coefficient, T_s is the source temperature, T_∞ is the quiescent temperature, L is the length of flow, and υ is again the kinematic viscosity. Recall that for an ideal gas, β is the inverse of the absolute temperature of the fluid.

The Grashof number determines whether free convection is negligible. To determine its importance, the Archimedes number is calculated [35]:

$$Ar = \frac{Gr}{Re^2} \tag{3.16}$$

Table 5 summarizes how the Archimedes number indicates whether forced and/or free convection are negligible [35]. As will be shown in subsequent chapters, the ACT valve falls into the first condition from Table 5.

Assuming the free convection is negligible for the fuel flow through the valve, the Prandtl number is retrieved from published tables for the specific fuel being used. Based on the values of the Reynolds number, the Prandtl number and the ratio of L/D, the Nusselt number (Nu) is then calculated. For the specific case of the ACT valve, the following is used [35]:

$$Nu = \frac{\frac{f}{8}(Re - 1000)Pr}{1 + 12.7(\frac{f}{8})^{\frac{1}{2}}(Pr^{\frac{2}{3}} - 1)} \tag{3.17}$$

where f is the friction factor. Various equations for the friction factor are used based on turbulence and values of other dimensionless parameters [35]. For the case of the ACT valve designs, f was found using the following equation:

$$f = 0.316Re^{-\frac{1}{4}} \tag{3.18}$$

Having determined the Nusselt number, the convective heat transfer coefficient for the forced convection case can be found by solving an alternate equation for the Nusselt number [35]:

$$Nu = \frac{hD}{k_f} \tag{3.19}$$

In Equation 3.19, h is the convective heat transfer coefficient, D is the diameter of the flow, and k_f is thermal conductivity of the fluid (again, often a published, tabulated value based on temperature). Using the value of h, the convective thermal resistance can then be calculated using Equation 3.12 from earlier in the chapter.

3.3.3.2 Convective Heat Transfer Coefficient for Free Convection Similarly to the method of finding the convective heat transfer coefficient for the forced convection case, the free convection case uses many of the same dimensionless parameters. For instance, the free convection analysis begins with calculation of the Reynolds number [35]:

$$Re = \frac{u_\infty D}{\upsilon} \tag{3.20}$$

In Equation 3.20, u_∞ is the velocity of the fluid (air in this case) flowing over the object in question, D is the diameter of the object in question and υ is again the kinematic viscosity of the fluid. As this is free convection, a relatively small Reynolds number should be obtained.

Again, the Nusselt number must be calculated, this time using Equation 3.21 below, which is for laminar flow [35].

$$Nu = 0.664Re^{\frac{1}{2}}Pr^{\frac{1}{3}} \tag{3.21}$$

Once a value for the Nusselt number has been calculated, Equation 3.22 is used with the results to solve for the convective heat transfer coefficient [35].

$$Nu = \frac{hL}{k_f} \tag{3.22}$$

In this Nusselt number equation, L is the characteristic length over which the free convection is considered (in the case of the ACT valve, L is the outer diameter of the valve) while k_f is again the thermal conductivity of the fluid.

For a visual representation of the method outlined above for finding both the free and forced convective heat transfer coefficients, refer to the flowchart in Figure 69 in Appendix C. Note that the flowchart was designed specifically for the ACT project and therefore does not dictate an exhaustive process for finding the convective heat transfer coefficient. For such a process, refer to Chapters 7, 8 and 9 in [35].

3.3.4 Radiative Thermal Resistance

Radiation is defined as energy emitted by matter at a finite temperature. Such energy emission can occur from solid surfaces, liquids and gases. Due to changes in the electron configurations of the molecules within the emitting entity, the energy transported by electromagnetic waves. Radiation differs from the other modes of heat transport in that no material medium is required. As a result, radiation occurs most efficiently in a vacuum. An important note about radiation: it occurs in parallel with convection at the surface of a body.

For an emitting body separated from other bodies by a gaseous medium, the thermal resistance for radiation can be found [35]:

$$R_{rad} = (h_r A)^{-1} \tag{3.23}$$

In Equation 3.11, h_r is the radiative heat transfer coefficient and A is the area in contact with the surroundings. The radiative heat transfer coefficient can be found:

$$h_r = \varepsilon\sigma(T_s + T_{sur})(T_s^2 + T_{sur}^2) \tag{3.24}$$

In Equation 3.24, ε is called the emissivity of a surface (a constant between 0 and 1), σ is the Stefan-Boltzmann constant ($5.67 \times 10^{-8} W/m^2 \cdot K^4$), T_s is the temperature of the body in question in Kelvin, and T_{sur} is the temperature of the surroundings in Kelvin.

3.4 THERMAL EXPANSION

After using the equations and procedure mentioned in the previous section, the temperature difference can then be used to determine how much a given body will expand or contract due to thermal effects. As the ACT valve will be subjected to extreme temperatures and perhaps extreme temperature gradients as well, it is important to determine the thermal expansion of the components. In order to determine the expansion:

$$X = X_o(1 + \alpha \cdot \Delta T) \tag{3.25}$$

In Equation 3.25, X is the final length (or any other linear dimension, such as diameter or radius), X_o is the initial length (or other linear dimension), α is the coefficient of thermal expansion, and ΔT is the change in temperature. Using Equation 3.25, the approximate dimensional increase of each component in an assembly can be determined. This allows in depth stress analysis to determine if an assembly's components have considerate thermal change.

4.0 METHODS

The following sections spanning the methods utilized to design both the actuator and the valve design are presented separately, and as such tend to suggest that the actuator and valve designs were developed independently of one another. This is not the case, as the designs chosen for each part of the ACT valve complement one another by design.

4.1 ACTUATOR DESIGN

4.1.1 Actuator Design Down-Selection

To determine an actuator design that simultaneously fulfills all of the requirements of the ACT valve set forth in Table 1, a subjective evaluation decision matrix was formed using input from the members of the ACT project team. The decision matrix compared all of the actuation technologies researched throughout the literature review by numerically assigning values to several metrics, many of which were dictated at the onset of the ACT project by Table 1. Such metrics as temperature, bandwidth, and cost were assigned numbers between 0 and 3 (lowest to highest) by each member of the ACT project team. For each of the 14 valve types considered, the total of all 9 metrics were calculated. The actuation technologies with the highest total values were considered to be worth further examination. Subsequent meetings of the ACT project team used the results from this decision matrix to guide the direction of the actuator design. A summary of the decision matrix will be reviewed in a following chapter.

4.1.2 Electromagnetic Design

Throughout the literature review, it became increasingly apparent that certain requirements listed in Table 1 were going to be harder to satisfy than others. For instance, the maximum operating temperature of 650°F (≈ 343°C) tended to be one such requirement that very few actuation technologies could accommodate while remaining in the neighborhood of the budget of $200 per valve assembly. While not directly a consequence of this single requirement, the relatively high temperature eliminated most all of the currently available actuation technologies, save for electromagnetic devices. After further exploring electromagnetic actuators and devices, it was determined that such an actuator is the primary candidate for the ACT valve. Essentially, this decision was driven by the fact that a particular high-temperature magnetic material was found (a type of samarium cobalt: Sm_2Co_{17}) that can withstand such temperatures.

While some of the actuation technologies are types of electromagnetic devices (e.g. solenoids and motors), a new design was required to meet the ACT valve specifications. An actuator design was developed in conjunction with Lambeth Systems [36] that in principle resembles a hard drive actuator (essentially a pancake motor) with linear motion rather than rotational motion. In construction, the design is quite similar to a solenoid, which in turn is similar to a voice coil actuator (seen in audio speakers).

The basic design of the actuator can be seen in Figure 29. The key difference is that the magnetic field runs radially outward through the coil instead of through the center of the coil along the axis. Consequently, each permanent magnet ring is poled radially with a direction that alternates with each layer (given by yellow or cyan in the figure). Inner and outer keepers (gray) prevent leakage of the magnetic field from the magnetic "circuit". By alternating the poling direction, each layer becomes a separate magnetic circuit, preventing the entire magnetic flux from flowing through the keepers and therefore reducing saturation. The lightweight armature (magenta) contains a separate coil for each magnet layer, which is wound in alternating directions corresponding to the alternately poled magnet rings (shown as red or green). Current is passed through the copper wire in the armature and a force is exerted on the armature according to Equation 3.1. Thus, by varying the amount and/or

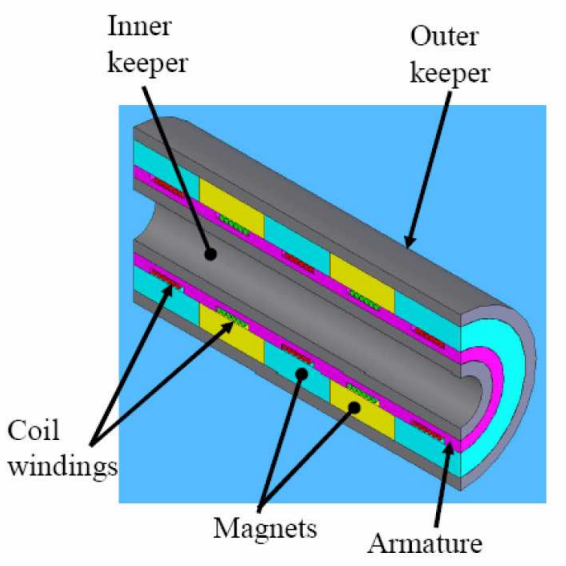

Figure 29: Solid model of magnetic actuator design.

direction of the current, the force acting on the armature can be changed, which in turn will move the armature. Figure 30 indicates the alternating polarity of the magnets and coils on a two-dimensional, axisymmetric cross section of the actuator design to further clarify the actuator concept.

While the overall design has been chosen, the dimensions of each component have yet to be finalized. In particular, the thickness of the magnets, keepers, and copper wire need to be specified. These dimensions will be dictated by the amount of force needed to be produced by the actuator, which was originally to be determined by the computational fluid dynamics (CFD) analysis. However, manual experiments at the University of Pittsburgh will be used to estimate the force needed to move the actuator. Some preliminary parametric analysis has been conducted, however, in order to better understand how changing various dimensions affects the performance of the actuator and to provide guidelines for finalizing dimensions when required.

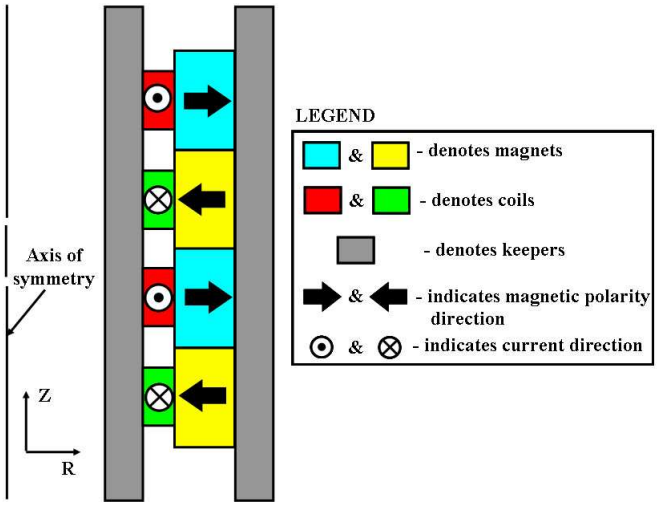

Figure 30: Two-dimensional, axisymmetric cross section of the magnetic actuator design demonstrating alternating coil wraps and magnet polarities.

4.1.3 Electromagnetic Benchmark Modeling

In order to validate the electromagnetic FEA (discussed later) of the chosen actuator design, benchmark electromagnetic modeling and testing is in order. Although shaped differently, the magnetic design in the conceived electromagnetic solenoid in Figure 29 is similar to the pancake motor design used in computer hard drives. The only potential obstacle to this design is finding the magnet rings with radial poling (which was resolved through custom manufacturing). Given the similarities, along with the abundance of old hard drives, a model validation program was established by performing FEA modeling on the hard drives. A companion test program was conducted to perform the model validation. This ensured that the modeling techniques and methods are correct. In particular, an appreciation for the need for three-dimensional modeling was established.

4.1.3.1 Hard Drive Solid Model and Simulation Numerical models of the hard drive were created by disassembling and measuring the geometry of the hard drive. The models were first created in SolidWorks® and then exported to an IGES file to be imported

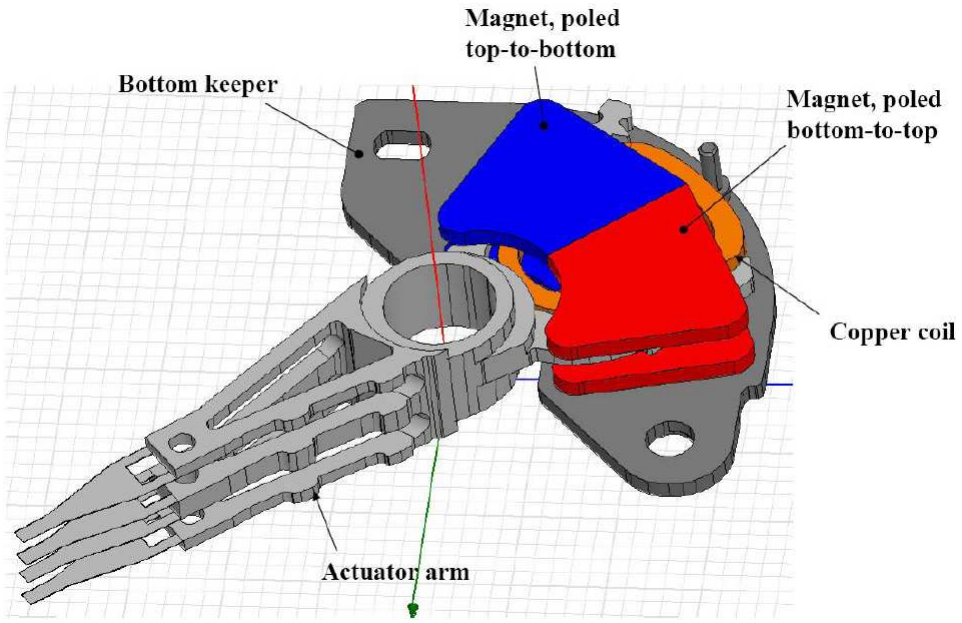

Figure 31: Ansoft Maxwell® 3D hard drive model.

into Ansoft Maxwell® 3D modeling software [37]. A three-dimensional modeling program was required since the motion is actually rotational rather than linear. A two-dimensional, axisymmetric model would require that the plane cross section of the actuator have motion within the specified plane, and further that the cross section be revolved around a specified axis to give the three-dimensional version of the model. In the case of the hard drive actuator, the motion is into and out of the plane of the cross section, indicating that only a three-dimensional model will suffice.

Figure 31 depicts the hard drive solid model imported into Maxwell® 3D. In this figure, the top keeper has been removed to expose the internal components of the hard drive. The red halves of the top and bottom magnets are poled top-to-bottom while the blue halves of the top and bottom magnets are poled bottom-to-top. This creates forces in the same direction on opposite sides of the coil (which have opposite current directions). The dark gray object is the bottom keeper (note that the top keeper is identical), while the lighter gray object is the actuator arm. The orange object represents the copper coil. As current is

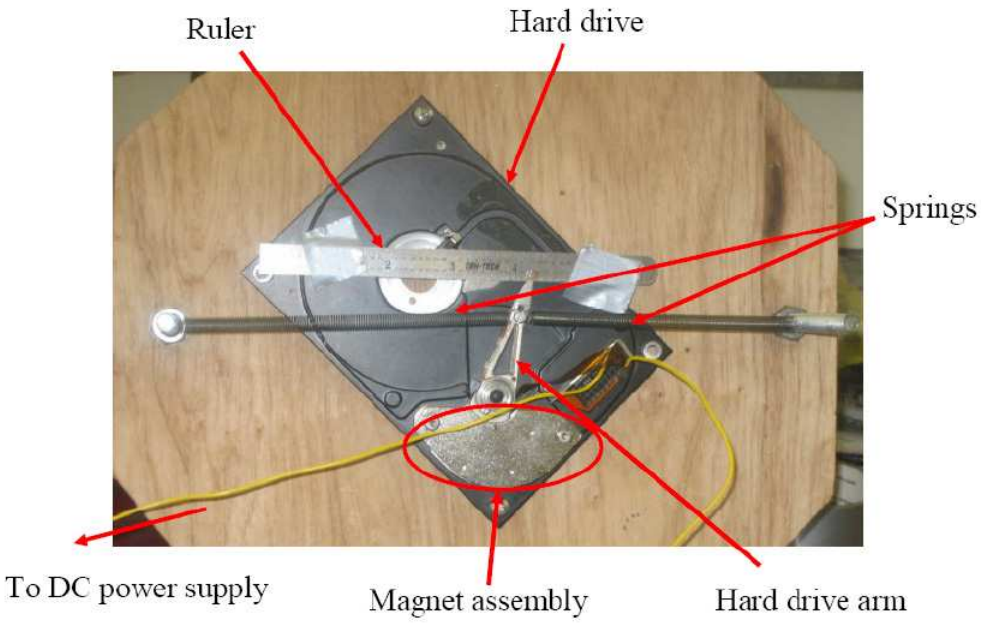

Figure 32: Hard drive experiment setup overview.

passed through the coil, a force is produced in accordance with Equation 3.1. In Maxwell® 3D, the current was varied while the corresponding forces were recorded for a single position (the position shown is the position of maximum force) of the arm and coil.

4.1.3.2 Hard Drive Experiment For comparison of the hard drive FEA model, experiments were conducted using a hard drive from a personal computer. As seen in Figure 32, a the hard drive was disassembled and mounted such that two springs are in constant tension with the actuator arm held at a nominal position. A DC power supply was used to supply current to the device and the displacement of the actuator arm was measured for varying values of current. From the displacement of the actuator arm, the force exerted by the actuator was determined for each current applied according to:

$$F_{actuator} = 2kx \tag{4.1}$$

In this equation, k is the spring constant given by the manufacturer and x is the displacement of the actuator arm relative to the nominal position seen in Figure 32. The springs were

assumed to be linear per the manufacturers specifications within the range of stretched lengths observed throughout the experiments. The purpose of this experiment was to produce a comparable data set of current versus force for the simulated hard drive model and the hard drive tested.

4.1.4 Electromagnetic Analyses of Valve Actuator Design

In order to perform electromagnetic analyses of the valve actuator deign depicted in Figure 31, a model was required in an appropriate electromagnetic FEA software. Once the model was completed, analyses concerned with the force the actuator produces as well as the level of saturation present in components of the valve actuator design were conducted.

4.1.4.1 Modeling of Valve Actuator The electromagnetic actuator design was modeled in Ansoft Maxwell® 2D. As discussed in a previous section, a two-dimensional, axisymmetric representation of the actuator is possible this time, since the conditions mentioned in the previous section are met. Specifically, the model seen in Figure 33 can be rotated around the axis of symmetry to provide the three-dimensional model while the motion of the actuator is within the 2D plane shown. Within Maxwell® 2D, materials were created for the inner and outer keeper materials (a non-linear iron material) as well as for the magnet material (Sm_2Co_{17}) using the values shown in Table 6. "Non-linear" in this sense simply refers to the relationship of $\vec{B}$ and $\vec{H}$ for a material. Non-linear iron material is susceptible to saturation as discussed in a previous chapter. Maxwell® 2D comes preloaded with a linear iron material, but this is a non-realistic approach since it can never reach saturation. If a linear keeper material was used throughout the electromagnetic analysis, no useful results would be produced since it would appear that any amount of magnetic flux ($\vec{B}$-field) could be supplied to an actuator with very thin keepers and never reach saturation.

4.1.4.2 Saturation Analysis The goal of the saturation analysis was to determine the threshold of saturation based on magnet strength (which supplies the $\vec{B}$-field present), current (which essentially supplies $\vec{H}$, or magnetic field), keeper size and magnet size. As

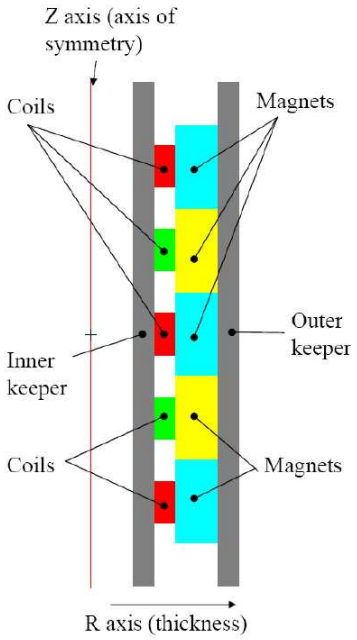

Figure 33: 2D, axisymmetric model of actuator design in Ansoft Maxwell® 2D.

Table 6: Properties of Sm_2Co_{17} (grade S3/245) used in Ansoft Maxwell® FEA.

Symbol	**Description**	**Sm_2Co_{17}**	**Iron**
μ_r	relative permeability	1.12	101
H_c [kA/m]	coercivity	-811.68	N/A
B_r [T]	retentivity	1.145	N/A
M_s [T]	saturation magnetization	N/A	1.0

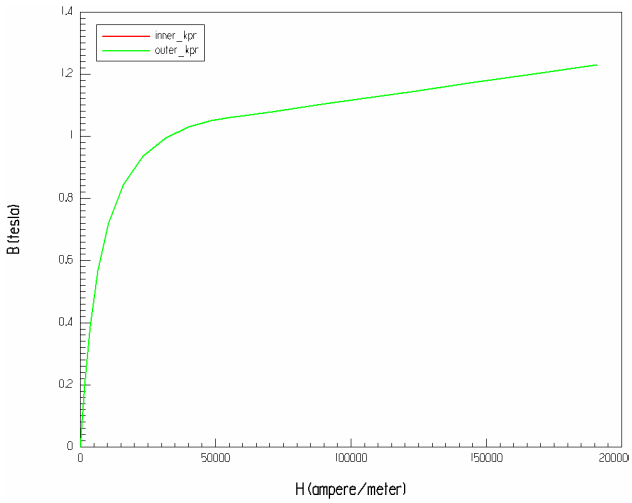

Figure 34: Example of a B-H curve for a non-linear material.

previously stated, saturation is undesirable since it results in magnetic flux leaking out of the keepers and air gap (which is where the coil is located), therefore wasting magnetic flux that could otherwise be used for actuation. This leakage reduces the performance and efficiency of the actuator.

To check for saturation with a given set of material parameters and component geometry, Ansoft Maxwell® 2D was used to perform an electromagnetic FEA which returns the value of $\vec{B}$-field present throughout the model (as well as other electromagnetic results, such $\vec{H}$ and electromagnetic force produced). The resulting $\vec{B}$-field concentration can be compared to the B-H curve for the material of the component in question. For instance, the non-linear iron material created for the valve actuator model has a B-H curve associated with it. See Figure 34 for an example B-H curve. Such a curve can then be compared to the results given by Ansoft Maxwell® 2D to determine the level of saturation present in the iron keeper under scrutiny. If any part of the component in question is higher than approximately the "knee" of its B-H curve (non-linear region), that component could be considered saturated. This process was repeated for various values of magnet strength, current and component size to determine realistic ranges of these values that result in saturation-free keepers.

4.1.4.3 Force Analysis Having determined various realistic magnet and keeper dimensions during the saturation analysis phase, the force produced by varying amounts of current and number of magnet rings could be determined using Ansoft Maxwell®. Therefore, the force analysis phase of the electromagnetic analyses included recording the force results indicated by Ansoft Maxwell® for various combinations of magnet and keeper sizes along with the number of magnet rings and current.

4.2 VALVE DESIGN

4.2.1 Valve Design Down-Selection

Similarly to choosing the actuator design, a subjective evaluation decision matrix was completed by each member of the ACT project team for the various valve designs examined in the literature review as well. Again, each design was ranked over a range of metrics. Of the metrics, complexity, speed of actuation and the ability to fail nominally ranked among the most critical. Each of the 14 metrics were assigned numerical values from 0 to 3 (lowest to highest) for each of the 17 valve designs considered. The total numerical value for each valve designed helped guide the team as to which designs seemed most promising in the sense of accommodating all of the requirements set forth in Table 1.

4.2.1.1 Braided Sleeving Valve Concept Early in the conceptual stages of the ACT valve design, one possible valve design was conceived that appeared to be promising but far too complex to model using traditional computer-aided design (CAD) in a timely manner. The valve is essentially a section of braided sleeving that can be stretched or compressed in order to reduce or increase flow, respectively. Practically in parallel to creating the subjective evaluation decision matrices for both actuator and valve design, simple experiments were conducted in order to determine the viability of this valve design.

Figure 35 depicts the braided sleeving valve in a nominal position. It was conceived that one end of the braided sleeving would be held stationary while a linear actuator would move

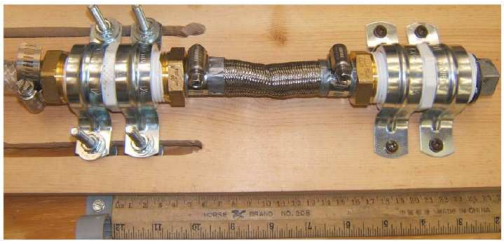

Figure 35: Braided sleeving valve in nominal state.

the other end. This configuration was desirable since the chosen electromagnetic actuator is linear. To determine whether the valve would alter the fluid flow, the experiment seen in Figure 36 was implemented. A compressed air source was used to pass air through the sleeving while a rotameter flow meter was used to monitor the amount of leakage that escaped from the sleeving at various positions. This process was repeated for several inlet pressures, which were indicated by the pressure transducer seen in Figure 36. The resulting data were reviewed to determine whether the flow rate was altered an appreciable amount by compressing and stretching the braided sleeving.

4.2.2 Preliminary Valve Designs

As required for the ACT project, two preliminary valve designs were selected to further pursue. They are in fact hybrid designs that incorporate concepts from various valve designs researched. One of the original valve designs examined for the subjective evaluation decision matrix is shown in Figure 37. This design incorporates an armature that moves linearly to mate with the football-shaped center component of the valve. Making this design more realistic to machine and assemble led to the valve design seen in Figure 38. This valve design has a very similar operation to the "football" valve with the main exception being that the flow splitting plug is cone-shaped rather than football-shaped. This was chosen due to the impracticalities that arise with machining a football-shaped valve component.

The second preliminary valve design is essentially a linear barrel valve, as seen in the literature review in Figure 23. Modifications to this valve design produced the second prelim-

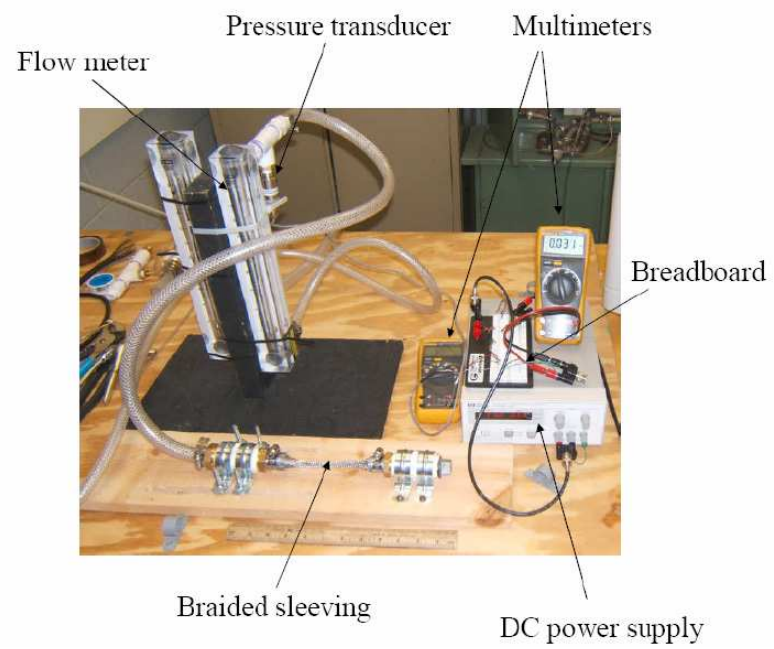

Figure 36: Braided sleeving experimental setup.

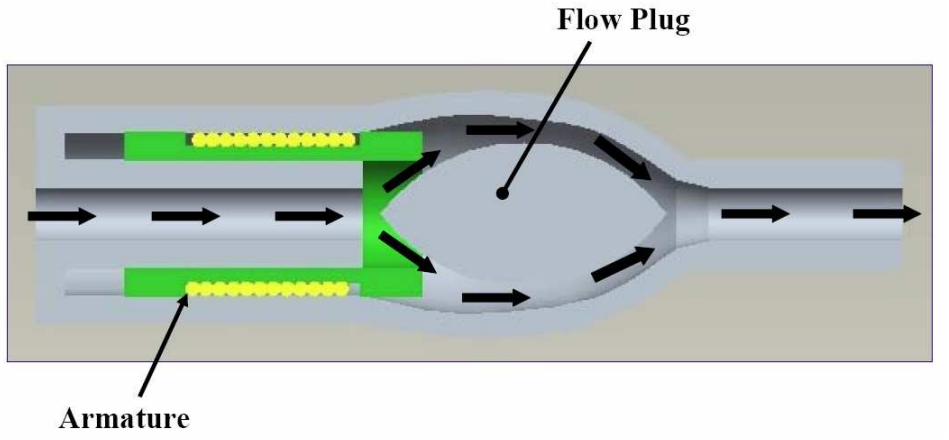

Figure 37: Original "football" valve design.

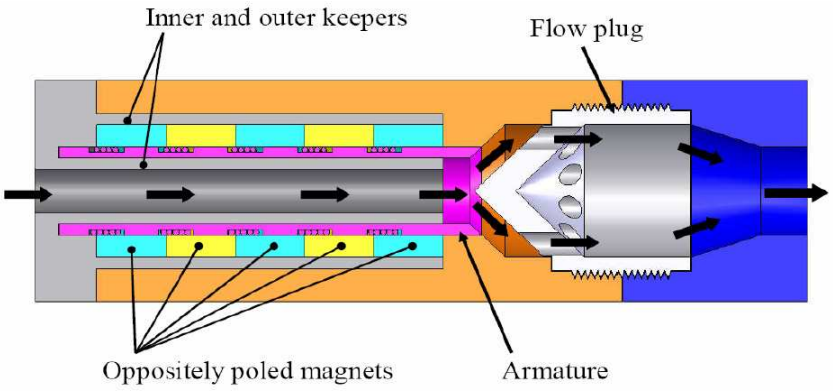

Figure 38: Split-flow plug valve (TV3) assembly.

inary valve design, as shown in Figure 39. The primary difference in these two valve assembly designs lies within the means of actuation: Figure 23 relies on a piezoelectric Thunder^{TM} brand actuator while Figure 39 incorporates the electromagnetic design discussed in the previous chapter. This valve design operates by aligning (or conversely misaligning) the holes in the armature with the mating holes in the barrel plug. Since the mating holes are relatively small, the total travel for this design is slightly less than the diameter of the mating holes, which is desirable in terms of satisfying the bandwidth requirement (i.e. fast-actuating due to a short throw).

The two valves in Figures 39 and 38 offer many advantages over competing designs. Foremost is their compactness and lack of impinging flows that can bind the moving parts or create undue forces for the actuator to overcome. Rather, the axi-symmetry balances the flow forces equally in the radial direction to preclude binding. Further, by allowing the flow to go through the center of the actuator (another advantage of the radial magnetic field that was inspired by pancake motor designs), additional compactness can be achieved along with some inherent cooling ability for the coils. Although multiple magnets (and coils) are shown in the figure, the exact number could be much less.

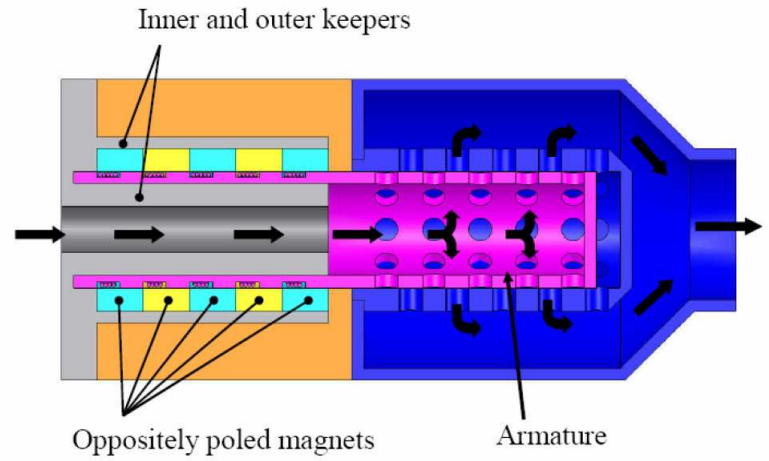

Figure 39: Barrel valve (TV1) design.

4.2.3 Preliminary Prototype Valve Designs

Since the valve designs that are being created must be tested, practical and simplified prototype valve designs were required that would accommodate relatively quick construction and low pressure, cold-flow testing at the University of Pittsburgh and NETL Morgantown. Therefore, the preliminary valve designs seen in Figures 38 and 39 were stripped of the electromagnetic actuator components and modified to create the prototype designs seen in Figures 40 and 41, respectively.

The method of actuation in the two preliminary prototype valve designs is via the threaded mating sections of the mock armature and the manual actuator (the purple and red components, respectively). When an adjustment needs to be made during an experiment, the system is depressurized and the entire mock armature and manual actuator subassembly is removed. The coarse adjustment (by threading the mock armature and manual actuator together) is made and the sub-assembly is replaced in the valve. A set screw is used on the inlet end of the manual actuator to provide fine adjustment of the mock armature position as needed.

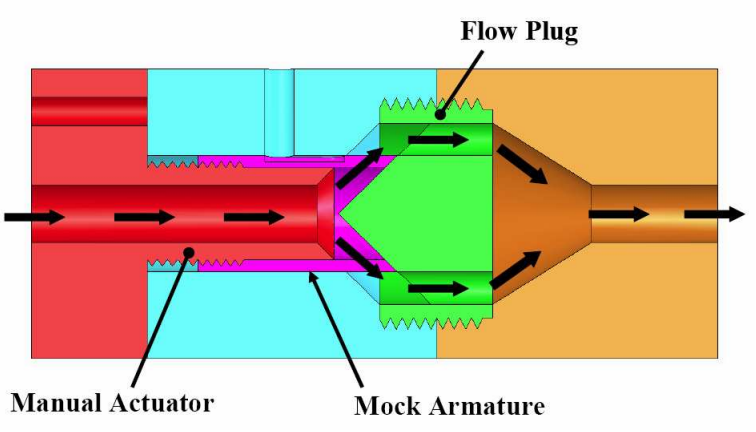

Figure 40: Prototype design for split-flow plug valve.

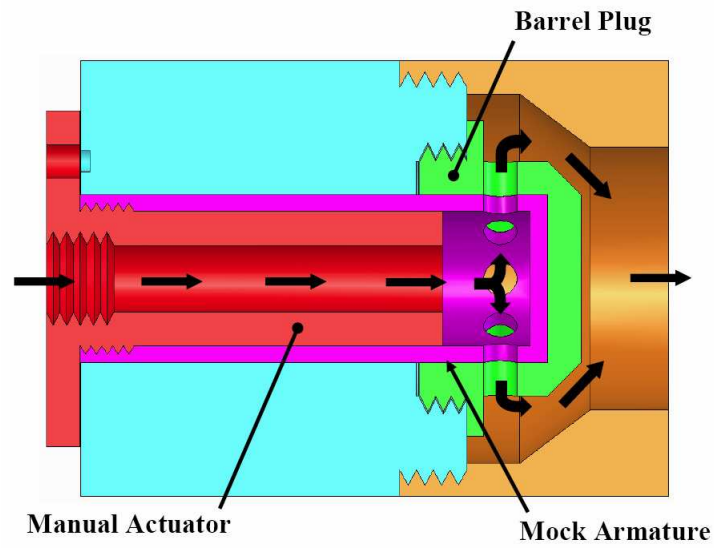

Figure 41: Prototype design for barrel valve.

4.2.4 Computational Fluid Dynamics

Fluid dynamics play a very important role in the performance of a valve, therefore in-depth CFD analyses were conducted on both of the the preliminary prototype designs devised for the ACT valve. All CFD analyses were performed by Dr. Mary Anne Clark and Jordan Musser at West Virginia University. To evaluate the feasibility of the designs, the analyses focused on the determination of the force acting on the internal components of the valve (especially the armature component), fluid velocity, pressure drop and stress throughout the valve (i.e. the static pressure on all internal components). All tests took place in 2006 and 2007 at Dr. Clark's lab.

The CFD analyses aided in the task of further refining and modifying the preliminary prototype valve designs (seen in Figures 40 and 41) into the final prototype designs, which will be introduced in the following chapter. Areas within the valve that were especially susceptible to stagnant flows, impinging flow areas and especially turbulent sections were identified and modifications were made to the designs based on the results of the CFD analyses.

4.2.5 Stress Analysis

Prior to finalization of the prototype valve designs for preliminary cold flow testing and flow characterization, a thorough stress analysis was conducted to assure the chosen material (cast acrylic) could withstand the compressed air pressures the valves would be subjected to. Of special concern were the threaded sections that were present in the prototype designs. As the final ACT valves will include an integrated actuator, these threaded sections will not be included and are therefore of no concern for those designs. However, safety was of paramount concern with the prototype valves since testing would require close human interaction at sometimes relatively high compressed air pressures.

The stress analysis conducted on the prototype valve designs included both manual calculations and FEA. To analyze the stress distributions in the prototype valve designs, an initial stress analysis of simplified components (i.e. no intricate features, such as set screw grooves, etc.) was manually conducted, then an FEA program was used to model

the simplified components. The manual analysis was compared to the simplified FEA in order to validate the FEA software. The FEA software was then used to further explore the stresses with more accurate component and assembly models. For both the manual analysis and the FEA, each assembly was assumed to be statically charged at 240 psi, since this is the pressure that the prototype valves should be hydrostatically charged and tested for structural integrity prior to being cold flow tested. This pressure was chosen since the valves would at most be subjected to 120 psi air, and as such need to be hydrostatically tested at twice the maximum operating pressure.

The manual stress analysis and stress FEA conducted for the prototype valve designs also created a framework for future valve designs (i.e. the metal-bodied, integrated designs) to be analyzed with minimal effort. A few parameters may need to be changed to accommodate new design changes, but these alterations should be minimal.

4.2.5.1 Manual Analysis The valve designs seen in Figures 40 and 41 are axisymmetric, therefore a simplified manual stress analysis was easy to execute using traditional solid mechanics theory for the individual components using the thick-walled equations introduced in Equations 3.3–3.6 to determine von Mises stress. Simplified component geometry was also utilized in order to create loading and restraint conditions that could easily be mimicked using the FEA software.

4.2.5.2 Thread Analysis For the case of analyzing the thread stresses, only manual analyses were utilized since any further analyses are prohibitively time intensive. Equations 3.7 - 3.9 were used for the determination of the shear stress for thread stripping in all threaded components in both valve designs. These values were then compared the the ultimate shear strength of the material used to assure a factor of safety (FOS) above unity was attained for every threaded component. The FOSs were calculated assuming a conservative ultimate shear stress value for cast acrylic of 10,000 psi.

4.2.5.3 Finite Element Analysis After completing manual stress analyses of all valve components, FEA was performed using SolidWorks® COSMOSWorks [38], which is part of

the SolidWorks® software package. The FEA was first validated using the results from the manual stress analyses. For very simple loading scenarios, simplified valve components were created void of any intricate features. The FEA was then validated by applying similar end restraints and loading conditions for the maximum testing pressures anticipated and comparing the manual calculations to such simplified FEA cases (240 psi). Once validated, the fully-featured components could then be analyzed under similar loading scenarios and the stress distributions within the intricate features previously removed could be trusted as adequate approximations of the actual stress distributions since hand calculations cannot be employed for such detailed features. In this manner, both valve designs' components were analyzed to insure adequate FOSs were present for the given dimensions.

After FEA was performed on individual components, analyses were performed on both prototype valve assemblies to determine maximum stresses present. These stresses were compared to the material properties to determine the FOSs for each valve assembly.

4.2.6 Prototype Valve Fabrication

After the prototype valve designs were finalized, three valves of each design were machined at the University of Pittsburgh's machine shop. All components were machined mostly on computerized numerical controls (CNC) machines out of cast acrylic purchased from a commercial supplier. Acrylic was chosen as to allow some transparency during testing to aid in adjustment of the armature and possibly for viewing fluid flow using smoke or other visual aids during testing. Two of the three valves of each designed were submitted to NETL Morgantown for testing while one valve of each design was retained for preliminary testing at the University of Pittsburgh.

4.2.7 Preliminary Prototype Valve Flow Testing

The preliminary cold-flow tests were conducted at the University of Pittsburgh with house-supplied compressed air at inlet pressures up to 45 psi and flow rates up to 1,000 standard liters per minutes (SLPM) of house supplied compressed air. Several types of tests were conducted, including constant pressure drop flow tests as well as arbitrary back pressure tests.

Table 7: Preliminary flow testing conducted at UOP on prototype valves.

Experiment	Pressure Range (psi)	Backpressure?
Constant Inlet Pressure	5 – 45	Y
Constant Pressure Drop	5 – 65, with pressure drop of 5 psi	Y

Each test conducted was repeated a total of three times in order to provide some statistical relevance. For all tests, five groups of tests were created for each valve by increasing the inlet pressure from 5 psi to 45 psi in increments of 10 psi. Table 7 lists the range of the preliminary experiment.

Figure 42 shows a picture of the experimental setup for preliminary flow testing. A down stream gate valve was included to provide throttling capabilities in order to vary the pressure drop across the test specimen as desired. Both the inlet pressure and flow rate was measured using an Omega FMA-1613A electronic mass flow meter. Potential errors are avoided with the sensor, which does not require corrections for gas density and pressure, as with the rotameters used in previous experiments. A downstream electronic pressure sensor measures the pressure after the test specimen, but before the throttling valve. The particular setup shown is one where there is an arbitrary back pressure applied to the system. For the constant pressure drop experiments, the downstream gate valve is adjusted so that the specified pressure drop can be attained.

The preliminary valve testing will allow more improvements to be made upon both designs prior to making prototype valves out of metal and equipped with the electromagnetic actuator. Essentially in parallel, the other prototype valves were tested at NETL Morgantown to compare to the flow data taken at the University of Pittsburgh. The corroboration of data will further improve the ability of the ACT valve to sufficiently modify the prototype valve designs prior to live testing with metal-bodied valves.

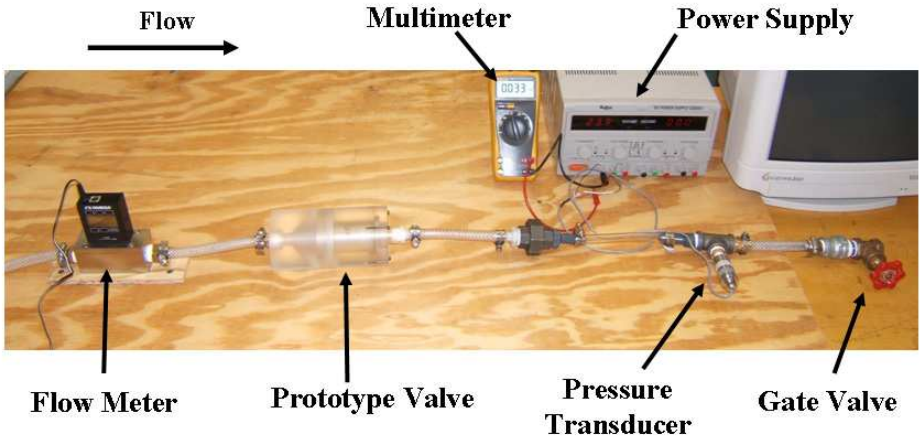

Figure 42: Preliminary valve testing setup.

4.3 THERMAL ANALYSIS

Since such a high operating temperature requirement was indicated in Table 1 (650°F), analyses of the thermal expansions of valve components and potentially the analysis of thermally induced stresses for any bonded or connected parts must be conducted. In order to analyze the thermal expansion, the heat transfer within the valve assembly must be determined beforehand. Once determined, it can be applied to all components within the valve assembly since the it is assumed to be in a steady-state (i.e. constant temperature).

4.3.1 Heat Transfer Analysis

Using Equations 3.10 - 3.24 and the process listed in section 3.3 for determining heat transfer, the heat transfers for the preliminary valve designs seen in Figures 39 and 38 were manually calculated. As stated in the previous chapter, conduction and convection (both forced and free) were considered for the valve designs while radiation was negligible. A "thermal circuit" was created such that the approximate equivalent thermal resistivity of each valve design could be calculated. The general thermal circuit for both valves is depicted in Figure 43 for the cross section shown in Figure 44. Table 8 lists the mode of heat transfer that

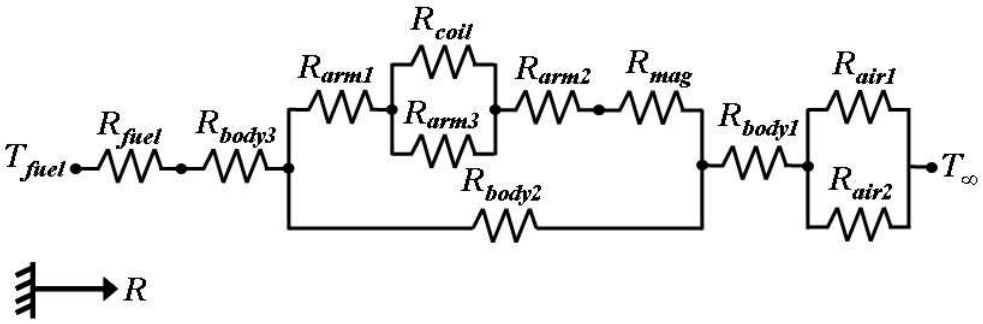

Figure 43: Thermal circuit for heat transfer analysis.

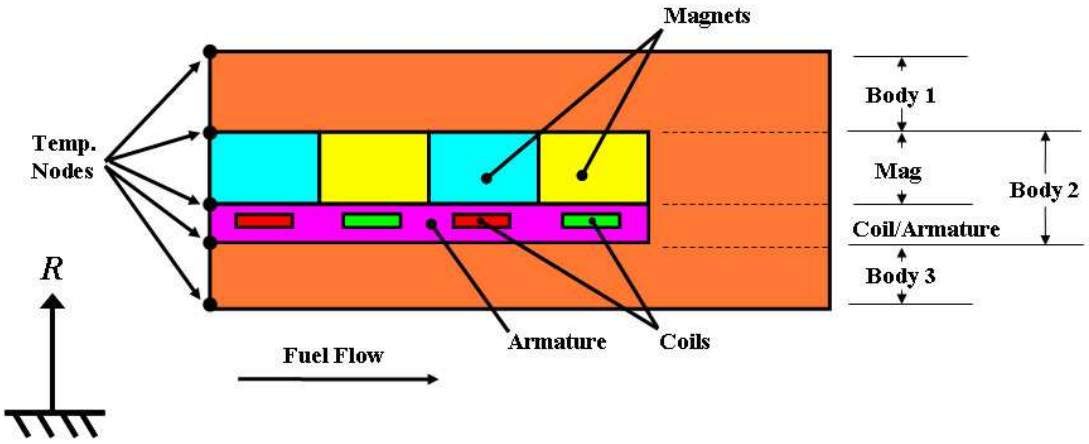

Figure 44: Cross section of valve used for thermal circuit.

corresponds to each of the individual thermal resistances shown in both the thermal circuit and valve cross section. The equivalent thermal resistance for the circuit seen in Figure 43 was calculated to be:

$$R_{equivalent} = R_{fuel} + R_{body1} + \frac{R_{air1}R_{air2}}{R_{air1} + R_{air2}} + \frac{R_{body2}(R_{arm3} + R_{coil})}{R_{arm3} + R_{coil} + R_{body2}[(R_{arm3} + R_{coil})(R_{arm1} + R_{arm2} + R_{mag}) + R_{arm3}R_{coil}]} \quad (4.2)$$

After calculation the heat transfer manually, Ansoft ePhysics^{TM} [39] FEA software was used to numerically determine the heat transfer of the valve designs. The manual calculations were essentially used to verify the FEA thermal analysis. Once the heat transfer values obtained were declared valid, the temperatures at all component interfaces (called "nodes" in Figures 43 and 44) could be determined using Equation 3.10, the corresponding thermal resistance(s) and the heat transfer value. The temperature difference was then used for calculating the thermal expansions per the following section.

4.3.2 Thermal Expansion Analysis

Thermal expansions can occur in all directions. The changes in length dimensions (e.g. a relative lengthening of the armature) may slightly affect the flow characteristic of the valve. The radial expansion is considered more critical, however, since materials with dissimilar linear coefficients of thermal expansion (CTE) could cause binding or undue thermal stresses. To calculate the linear thermal expansion in the radial directions, Equation 3.25 was used.

Upon further investigation, however, it becomes apparent that the potential to generate thermally induced stresses could be mitigated to some extent by careful selection of materials by matching the CTEs as closely as possible. Therefore, research was conducted into the material selection of the valve components, keeping in mind that the magnetic material was already selected (Sm_2Co_{17}). By finding materials with CTEs that differ at most by only a few percentage points, the clearance between components to account for thermal expansion becomes minimal (assuming the components in question have the same temperature), often eliminating altogether the need for a separate analysis of the thermally induced stresses.

Table 8: List of thermal resistances for ACT valve cross section and the corresponding mode of heat transfer.

Name	**Heat Transfer Mode**
R_{air1}	free convection
R_{air2}	radiation
R_{arm1}	conduction
R_{arm2}	conduction
R_{arm3}	conduction
R_{body1}	conduction
R_{body2}	conduction
R_{body3}	conduction
R_{coil}	conduction
R_{fuel}	force convection
R_{mag}	conduction

5.0 RESULTS AND DISCUSSION

5.1 ACTUATOR DESIGN

5.1.1 Summary of Actuator Decision Matrix for Actuator Down-Selection

A summary of the actuator decision matrix results can be seen in Table 24 in Appendix D. As indicated by the table, the five top ranking technologies were the SmCo solenoid, servo motors, solenoids, piezoelectric devices and stepper motors, respectively. These top candidates were more closely examined by the ACT project team to determine which one was best suited to fulfill the goals of the project. Note that all but piezoelectric devices of the top technologies are capable of utilizing high-strength permanent magnet materials such as samarium cobalt. Ultimately, however, the SmCo solenoid technology was chosen as has already been disclosed in a previous chapter. After additional research, it was determined that this technology has the best prospect of being able to simultaneously fulfill all of the actuator related requirements in Table 1.

5.1.2 Electromagnetic Benchmark Modeling Comparison Results

As seen in the comparison plot of the simulation data (magenta curve) and the experimental data (dark blue curve) in Figure 45, the electromagnetic benchmark modeling results are quite favorable. While the simulation data is linear, the experimental data is somewhat nonlinear. The linear trend line seen in Figure 45 yields an R^2 value of 0.9549, indicating that the experimental data is not quite linear. Non-linearities may arise from the fact that

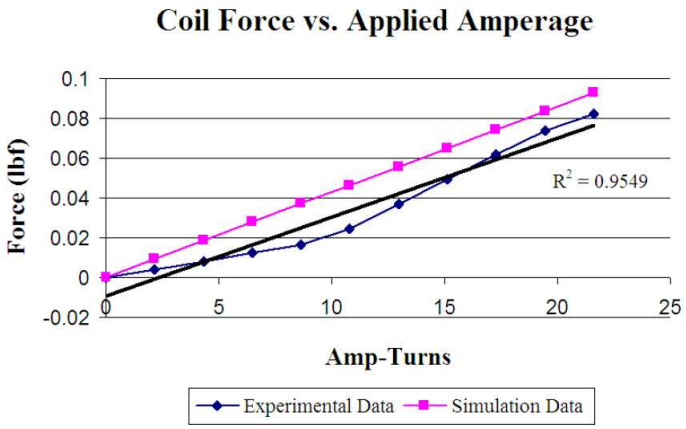

Figure 45: Experimental and simulation results for hard drive benchmark model with linear fit line (solid black) and R^2 value.

even though the springs are assumed to be linear throughout the range used, they are in fact not quite linear. The rotation of the actuator also changes the angle of application of the spring force.

The resulting data set of the hard drive experiment as well as the simulation can be seen in Table 9. Also given in Table 9 is the ratio of simulated to experimentally measured forces. The highest errors occur at low currents (e.g. 2.24 lbf at $I_{coil} = 0.4$ A), owing to the nonlinearities. At higher currents, the ratio is slightly better than 1 (1.13 at $I_{coil} =$ 0.1 amps). Results are considered good when agreement within a factor of two is achieved between the experimental and numerical results, indicating that the modeling effort is a success [40].

5.1.3 Electromagnetic Analyses of Valve Actuator Design

5.1.3.1 Saturation Analysis Results Using Ansoft Maxwell® 2D [37], minimum inner and outer keeper thicknesses were heuristically determined for three magnet thicknesses: 1/8", 1/4" and 1/2." For these magnet thicknesses, configurations of a single magnet ring to four magnet rings were considered. The keeper material for these analyses is a non-linear

Table 9: Experimentally measured and simulated force data for the computer hard drive actuator.

I_{coil} (A)	Coil Amp-turns	F_{exp} (lbf)	F_{sim} (lbf)	F_{sim}/F_{exp}
0	0	0	-0.0004	—
0.01	2.16	0.0041	0.0089	2.17
0.02	4.32	0.0082	0.0182	2.21
0.03	6.48	0.0123	0.0275	2.23
0.04	8.74	0.0164	0.0368	2.24
0.05	10.30	0.0246	0.0460	1.87
0.06	12.96	0.0369	0.0553	1.50
0.07	15.12	0.0493	0.0646	1.31
0.08	17.28	0.0616	0.0739	1.20
0.09	19.44	0.0739	0.0832	1.13
0.10	21.60	0.0821	0.0925	1.13

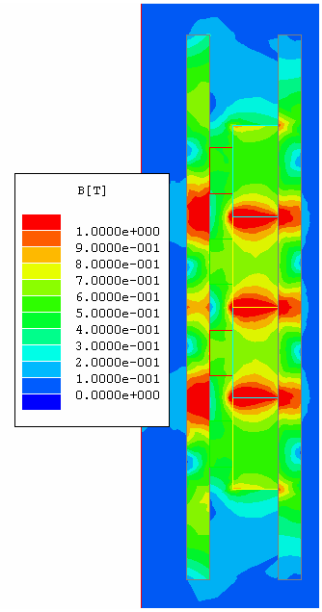

Figure 46: $\vec{B}$-field plot for 2D actuator model with 1/4" thick magnets, 1/2" in length with 1/8" thick keepers and 4 magnet rings.

iron material with a conservative saturation magnetization (M_s) of 1.0 T and a relative permeability (μ_r) of 101. Using these values and the corresponding B-H curve for the iron material, seen in Figure 34, saturation was detected by examining B-field plots created by Ansoft Maxwell® 2D. Flux plots were also created and examined to help determine saturation.

For instance, recalling Figure 33, a similar model was created with magnets 1/4" thick and 1/2" long, 1/8" thick keepers and four magnet rings was used in Ansoft Maxwell® 2D to produce the B-field plot shown in Figure 46 as well as the magnetic flux plot seen in Figure 47. In Figure 46, the red shading in both the inner and outer keepers indicate saturation since the non-linear iron material used for the keepers has a saturation magnetization (M_s) of 1.0 T (10,000 Gauss). The flux plot in Figure 47 supports this conclusion, since the flux in the outer keeper is escaping from the keeper into the surrounding area outside of the actuator model. Likewise, multiple scenarios were examined using Ansoft Maxwell® 2D to determine reasonable minimum keeper thicknesses

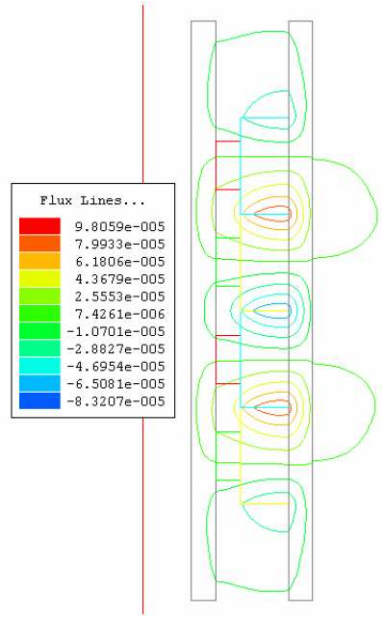

Figure 47: Flux plot for 2D actuator model with 1/4" thick magnets, 1/2" in length with 1/8" thick keepers and 4 magnet rings.

Starting from a 1/8" initial keeper thickness, both keeper thicknesses were increased until saturation was no longer detected in the keepers. These thicknesses were identified as the threshold thicknesses of the keepers in order to avoid saturation. These results along with the force produced by the actuator for each configuration can be seen in Table 10.

The results of the saturation analysis do not necessarily provide any unanticipated insight to the actuator design, but rather confirm that the theory considered during the design of the electromagnetic actuator holds true: as the magnet thickness increases, the required keeper thickness to avoid saturation increases, as does the force produced. This result was predicted and provides no design alterations.

5.1.3.2 Force Analysis Results Using the saturation analysis results, varying amounts of current were applied in Ansoft Maxwell® 2D to determine how the force varied with the coil current for the actuator configurations depicted in Table 10. According to theory, there should be a linear relationship between force and applied coil current when there is

Table 10: Results of saturation analysis showing the minimum keeper thicknesses for various magnet thicknesses with a magnet axial length of 0.5" and coils of 100 turns at 1 ampere.

Magnet Thickness (in.)	Number of Rings	Inner Keeper Thickness (in.)	Outer Keeper Thickness (in.)	Force (N)
1/8	1	0.1250	0.1250	2.322
	2	0.1875	0.2500	6.815
	3	0.1875	0.2500	10.667
	4	0.1875	0.2500	14.422
1/4	1	0.1250	0.1250	2.873
	2	0.5000	0.4375	15.439
	3	0.5000	0.4375	22.664
	4	0.5000	0.4375	30.713
1/2	1	0.1875	0.1875	4.561
	2	0.6250	0.5625	20.146
	3	0.6250	0.5625	28.992
	4	0.6250	0.5625	39.030

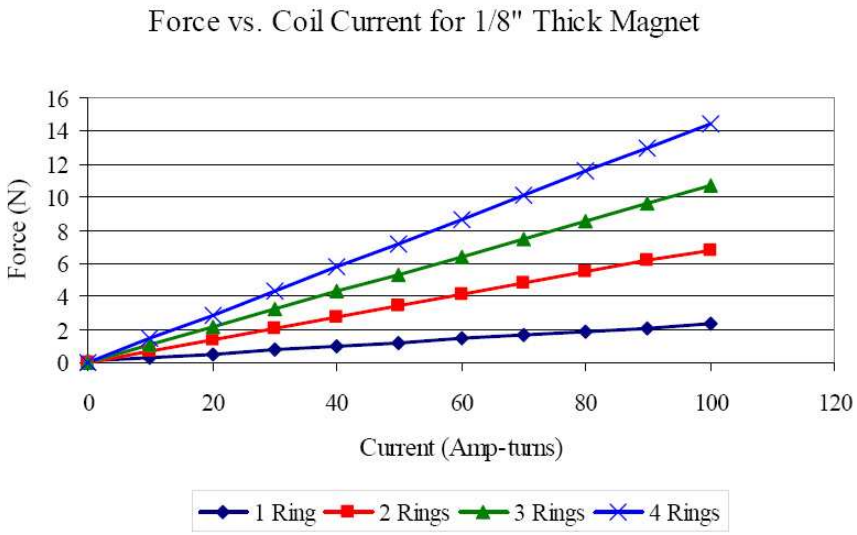

Figure 48: Plot of force vs. applied coil current for Ansoft Maxwell® 2D model of actuator with 1/8" thick magnets.

no saturation present. As previously stated, the keeper thicknesses listed in Table 10 are threshold thicknesses where saturation is no longer present in the keepers. Therefore, the force analysis data should support a linear relationship between the force and the applied coil current.

For the analysis, the coil current was varied from 0 to 1 A in 0.1 A increments. The force data were tabulated and plotted for each of the three magnet thicknesses and for one, two, three and four magnet ring configurations. The resulting plots were all linear, confirming that the keepers were not saturated at the threshold thicknesses. Figures 48, 49 and 50 depicts all four magnet configurations for magnet thicknesses of 1/8," 1/4" and 1/2," respectively. As seen in these plots, the force produced by the actuator increases with magnet thickness and with the number of magnet rings in the actuator configuration. Refer to Appendix E for individual force plots for each of the magnet configurations mentioned for all three magnet sizes.

Closely examining Figures 48, 49 and 50, one notices that the force does not double when the thickness increases nor when the number of magnets doubles for a given magnet

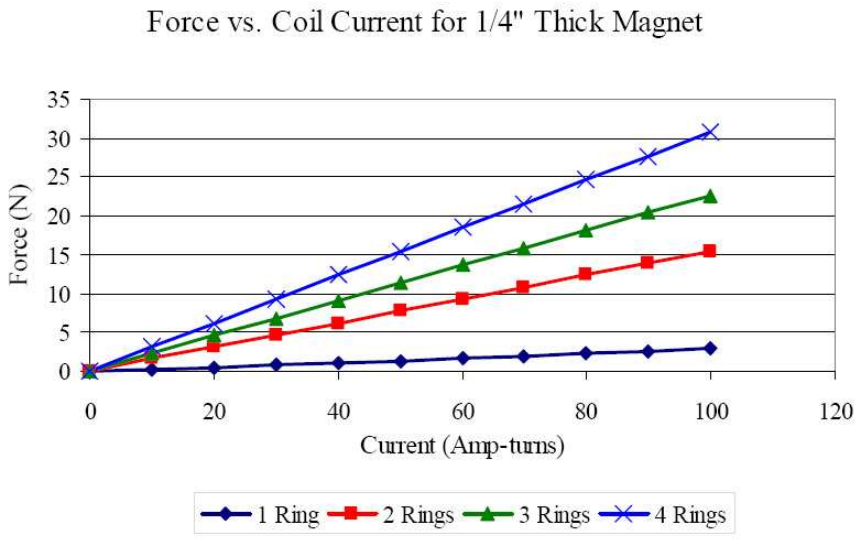

Figure 49: Plot of force vs. applied coil current for Ansoft Maxwell® 2D model of actuator with 1/4" thick magnets.

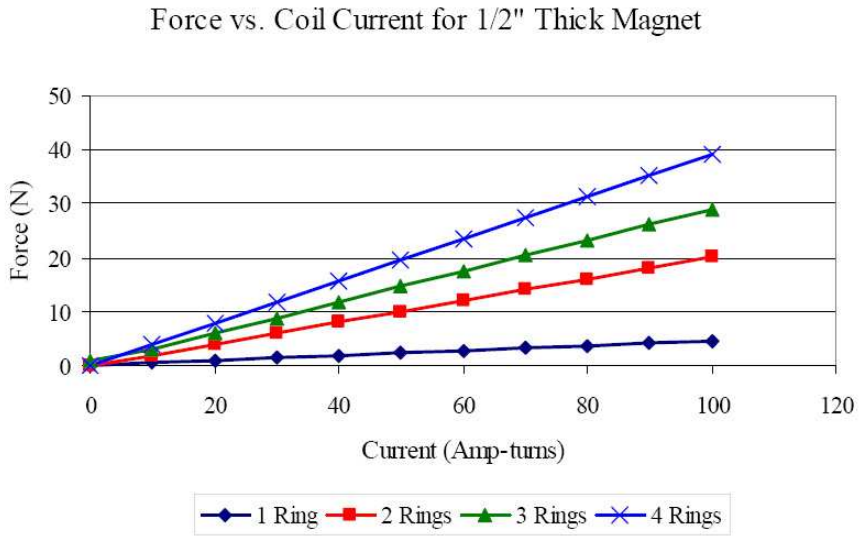

Figure 50: Plot of force vs. applied coil current for Ansoft Maxwell® 2D model of actuator with 1/2" thick magnets.

thickness. It is initially non-intuitive that the force does not double when the number of magnet rings for a given configuration doubles, or even when the magnet thickness doubles. Recall Equation 3.1: the electromagnetic force depends on I (coil current) and $\vec{B}$ ($\vec{B}$-field, or magnetic flux density). When increasing the number of magnet rings for a given configuration, $\vec{B}$ does not double. The $\vec{B}$-field in the air gap (i.e. where the coil is located) is not directly proportional to the number of magnets present in the actuator. Also, when three or more magnet rings are present, the $\vec{B}$-field from coil to coil may be different as well, further preventing direct proportionality between magnets and force. Similarly, doubling the thickness of a magnet does not double the $\vec{B}$-field in the air gap. The amount of $\vec{B}$-field in the air gap is related to the magnet volume, which more than doubles each time the thickness doubles from 1/8" to 1/4" (volume increases by approximately 220%) and from 1/4" to 1/2" (volume increases by approximately 150%).

5.2 VALVE DESIGN

5.2.1 Summary of Valve Decision Matrix for Valve Down-Selection

The valve decision matrix results are summarized in Table 26 in Appendix F. According to the totals presented in the summary, the top two valve designs are the linear barrel valve and the globe valve, in that order. These valve designs were further considered and researched. The globe valve was ultimately eliminated, but the linear barrel valve became the inspiration for the TV1 valve assembly seen in Figure 39.

5.2.2 Braided Sleeving Valve Concept Testing Results

While the braided sleeving valve was initially believed to offer some promise of finding an innovative design, the results of the testing seen in Figure 51 indicates otherwise. As seen in the flow versus inlet pressure plot, regardless of the amount of compression applied to the

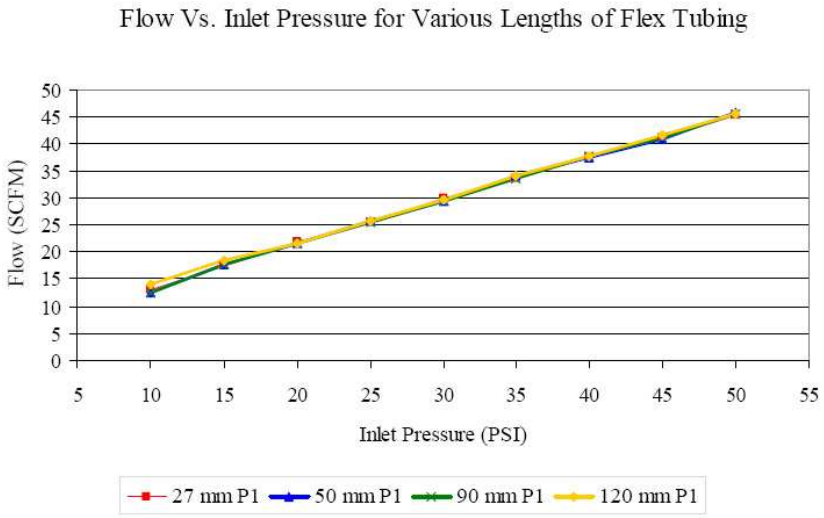

Figure 51: Results from braided sleeving experiment.

braided sleeving (i.e. valve position), the flow through the valve does not change enough to satisfy a ±10% variance in flow. Therefore, the braided sleeving valve design was abandoned early in the design process.

5.2.3 Computational Fluid Dynamics

The primary results of the CFD analyses were some refinements that were made to the preliminary prototype valve designs as well as reversing the flow direction originally intended through the valves. The flow direction indicated in Figures 40 and 41 was reversed after the CFD analyses revealed lower pressure drops in that direction. Design refinement of the prototype designs included the creation of flow splitters on both designs as well as removal of some sharp corners originally found on the internals of the valves.

Static pressure versus position plots were produced by the CFD analyses, including the plot seen in Figure 52. This plot was produced for the preliminary prototype valve design of Figure 41, but with the flow reversed relative to the indicated path of that figure. In Figure 52, notice that there is a pressure drop of nearly 40 psi through the length of the valve, mainly due to excessive turbulence. This exceeds the maximum pressure drop listed

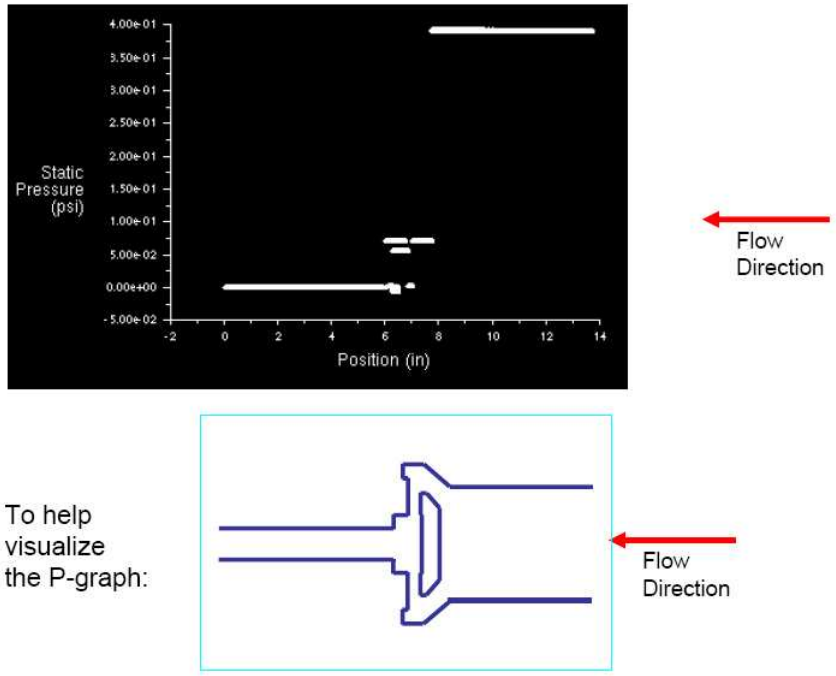

Figure 52: CFD analysis of the barrel valve variant preliminary prototype design.

in Table 1 by a factor of four. Taking this into account, it was decided that flow splitters needed to be added to the internal components of the valves to reduce the large pressure drop. Figure 53 depicts the static pressure versus position plot for the barrel valve variant with flow splitters. Due to the reduced turbulence, the pressure drop now is approximately 6 psi, which is within the 10 psi maximum allowed for the ACT valve.

It was initially believed that the force acting on the armature of the valves would be determined by the CFD analyses in order to properly size the electromagnetic actuator components. Unfortunately, only very preliminary force results came to fruition for the valve seen in Figure 40 with flow in the direction indicated in the figure. As previously stated, it has since been determined that the fluid will flow in the opposite direction, therefore voiding the force results obtained.

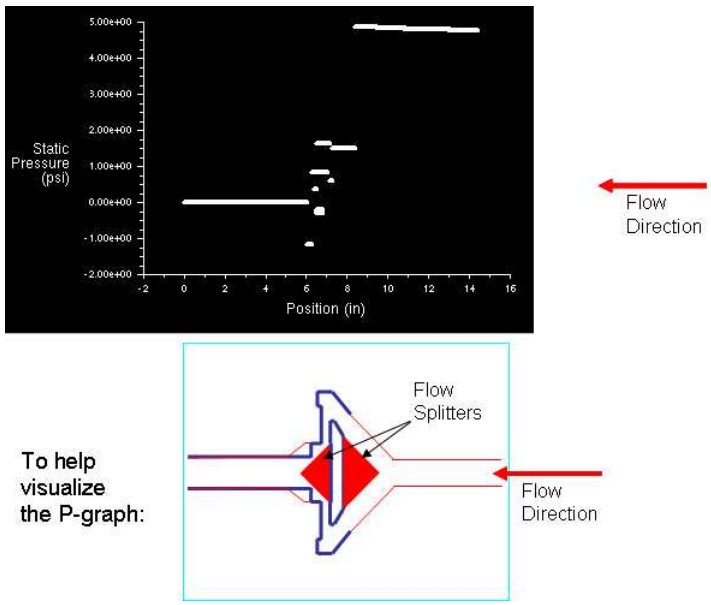

Figure 53: CFD analysis of a modified barrel valve variant prototype design with flow splitters.

5.2.4 Final Prototype Valve Designs

The final prototype valve designs take into account the CFD results mentioned in the previous section as well as design improvements conceived to make adjustment of the valves easier and quicker. Figures 54 and 55 depict the final prototype designs. In addition to the flow splitters and new adjustment mechanism, a few other changes are reflected in these designs. Minor changes in the flow path include chamfering the mock armature (purple component) ends as well making both inlet and outlet dimensions 1/2."

5.2.5 Stress Analysis

5.2.5.1 Manual Analysis Using the theory and equations and methods introduced in previous chapters, the various components of each of the prototype designs were approximated as thick-walled cylinders and analyzed according to the von Mises criterion in order to provide a baseline to validate the FEA software used for the brunt of the stress analysis.

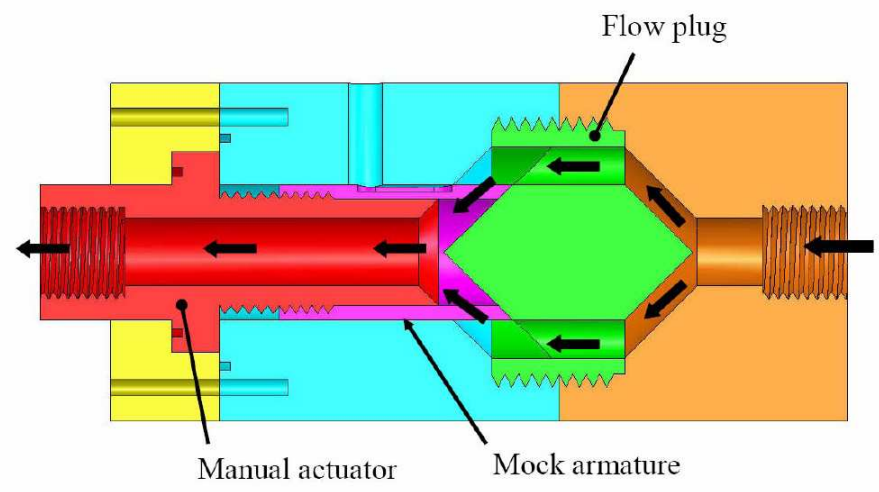

Figure 54: Prototype design of split-flow plug valve (TV3).

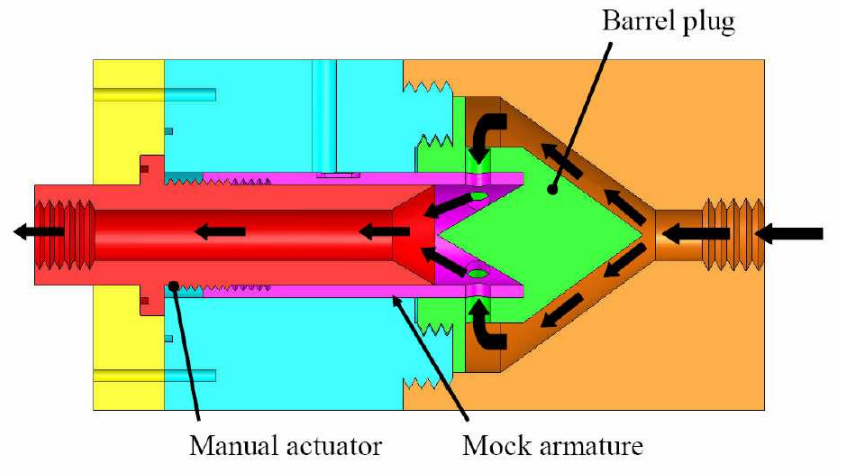

Figure 55: Prototype design of barrel valve (TV1).

Table 11: Summary of manual stress analysis and FEA results for TV1 prototype design.

	TV1															
	Manual Actuator		Mock Armature		Inlet Casing				Outlet Casing				Middle Casing			
	Single X-Sec.		Single X-Sec.		Thin X-Sec.		Thick X-Sec.		Thin X-Sec.		Thick X-Sec.		Thin X-Sec.		Thick X-Sec.	
	Inner	Outer	Inner	Outer	Inner	Outer	Inner	Outer	Inner	Outer	Inner	Outer	Inner	Outer	Inner	Outer
σ_{rr} (psi)	-240	0	-240	0	-240	0	-240	0	-240	0	-240	0	-240	0	-240	0
$\sigma_{\theta\theta}(psi)$	400.00	160.00	1093.33	853.33	1204.58	964.58	250.00	10.00	366.81	126.81	282.67	42.67	717.80	477.30	311.47	71.47
σ_{zz} (psi)	0	0	0	0	0	0	0	0	0	0	0	0	0	0	0	0
σ_{Mises} (psi)	560.00	160.00	1231.01	853.33	1340.78	964.58	424.38	10.00	366.81	126.81	282.67	42.67	863.20	477.80	478.92	71.47
FEA Results (psi)	540	160	1200	860	1380	970	340	9	500	120	430	40	880	500	450	80
% Difference	3.64	0.00	2.55	0.78	2.88	0.56	22.08	10.53	5.70	5.52	5.24	6.45	1.93	4.54	6.23	11.26

A summary of the manual stress analysis results can be seen in Tables 11 and 12. At the bottom of each table is also a comparison of the FEA results that will be discussed in a subsequent section. For a more detailed summary of the manual stress results, including the values used along with Equations 3.3- 3.6, refer to Tables 27 – 30 in Appendix G. Also, refer to Appendix H for the simplified valve component models used for both the manual stress analysis as well as for the simplified stress FEA used for validation.

5.2.5.2 Thread Analysis Shear stress for thread stripping was evaluated for each threaded component, yielding the results seen in Tables 14 and 13. As seen in the thread stress results, there are two sets of data: one for conservative calculations, the other for typical calculations. The difference lies in whether or not the full load of the force experienced by

Table 12: Summary of manual stress analysis and FEA results for TV3 prototype design.

	TV3																	
	Manual Actuator				Mock Armature		Inlet Casing				Outlet Casing				Middle Casing			
	Thin X-Sec.		Thick X-Sec.		Single X-Sec.		Thin X-Sec.		Thick X-Sec.		Thin X-Sec.		Thick X-Sec.		Thin X-Sec.		Thick X-Sec.	
	Inner	Outer	Inner	Outer	Inner	Outer	Inner	Outer	Inner	Outer	Inner	Outer	Inner	Outer	Inner	Outer	Inner	Outer
σ_{rr} (psi)	-240	0	-240	0	-240	0	-240	0	-240	0	-240	0	-240	0	-240	0	-240	0
$\sigma_{\theta\theta}(psi)$	574.82	334.82	400.00	160.00	985.75	745.75	751.94	511.94	260.00	20.00	498.99	258.99	331.43	91.43	756.68	516.68	331.43	91.43
σ_{zz} (psi)	0	0	0	0	0	0	0	0	0	0	0	0	0	0	0	0	0	0
σ_{Mises} (psi)	725.24	334.82	560.00	160.00	1125.11	745.74	896.37	511.94	433.13	20.00	652.95	258.99	496.98	91.43	900.98	516.68	496.98	91.43
FEA Results (psi)	710	320	530	160	1140	790	890	530	340	23	640	260	470	80	930	520	480	90
% Difference	2.12	4.53	5.50	0.00	1.32	5.76	0.71	3.47	24.09	13.95	2.00	0.39	5.58	13.33	3.17	0.64	3.48	1.57

Table 13: Summary of thread stress analysis for TV1 prototype design.

	TV1						
	Mock Armature	Manual Actuator	Inlet Casing	Middle Casing	Middle Casing	Middle Casing	Plug
	Internal Th.	External Th.	Internal Th.	Internal Th.	External Th.	Tapped Holes	External Th.
$\tau_{s,conservative}$ (psi)	719.01	1961.27	2774.43	3206.62	3133.06	7153.29	3711.37
FOS (conservative)	13.91	5.10	3.60	3.12	3.19	1.40	2.69
τ_s (psi)	52.10	148.58	346.80	533.02	391.63	357.66	662.74
FOS	191.93	67.30	28.83	18.76	25.53	27.96	15.09

Table 14: Summary of thread stress analysis for TV3 prototype design.

	TV3					
	Mock Armature	Manual Actuator	Inlet Casing	Middle Casing	Middle Casing	Plug
	Internal Th.	External Th.	Internal Th.	Internal Th.	Tapped Holes	External Th.
$\tau_{s,conservative}$ (psi)	599.41	1414.93	819.39	819.39	4195.90	936.20
FOS (conservative)	16.68	7.07	12.20	12.20	2.38	10.68
τ_s (psi)	74.93	84.22	128.03	102.42	209.80	65.01
FOS	133.46	118.73	78.11	97.63	47.67	153.81

the threads are evenly distributed to all of the threads in the threaded region (the typical approach), or conversely all of the force is handled by the first thread (the conservative approach). The theory behind the conservative approach is that due to manufacturing inconsistencies, only the first thread in a threaded region actually supports the entire load. Should the load be too much for the single thread, it may deform or break, then the load is transferred to the next thread in tact in the threaded region. As seen in Tables 13 and 14, both the conservative and typical approaches result in FOS's greater than unity. Therefore, at 240 psi, there is very little chance that the mode of failure would occur by shear thread stripping due to the shear stress applied to the threads.

5.2.5.3 Finite Element Analysis Using similar simplified geometrical models of the valve components as used for the manual stress analysis, SolidWorks® COSMOSWorks [38] was used to perform static FEA for comparison with the manual results. Tables 12 and 11 summarize and compare the manual stress analysis and FEA in order to validate the COSMOSWorks software as a valid FEA program.

As seen in both Table 11 and 12, all but the inlet casing components give percent differences less than 12% between the manual analysis and the static FEA. Therefore, SolidWorks® COSMOSWorks was accepted as a valid FEA software package for conducting stress analysis for the fully-feature prototype valve components and assemblies. For more complete details of the analysis, including the applied forces and dimensions, see Tables 27 - 30 in Appendix G.

The FEA performed on the fully-featured individual components (i.e. including such intricate features as the set screw groove in both mock armature components) as well as the complete assemblies resulted in the summary seen in Table 15. Refer to Appendix I for a complete collection of stress distribution figures of all components and both assemblies.

It is important to note that the FEA performed on the components is a very conservative one. For instance, all components were only restrained on one face or end, while in reality perhaps other restraints were present. For example, the mock armature component for both prototype designs were restrained only by the threads that attach them to the manual actu-

Table 15: Summary of FEA results for both TV1 and TV3 prototype designs.

	TV1			TV3		
Component	Minimum Stress (psi)	Maximum Stress (psi)	Factor of Safety	Minimum Stress (psi)	Maximum Stress (psi)	Factor of Safety
Actuator	6	3250	3.08	28	1560	6.41
Armature	2	3630	2.75	5	2770	3.61
Plug	1	710	14.08	1	1690	5.92
Inlet Casing	1	1100	9.09	3	680	14.71
Middle Casing	2	710	14.08	1	1470	6.80
Outlet Casing	4	1880	5.32	4	1030	9.71
Assembly–Open	1	1200	8.33	7	900	11.11
Assembly–Closed	1	1310	7.63	5	1020	9.80

ator component, when in the assembly the mock armature is actually additionally restrained by the middle casing component as well. The result is a very conservative one.

For a yield strength of 10,000 psi, it is clear that at a static pressure of 240 psi, no valve components or assemblies will fail due to the stress distribution present, even with a fairly conservative analysis. The 240 psi static pressure value came from the fact that 120 psi was believed to be the maximum pressure that the prototype valves would be tested at during the cold flow testing phase. For safety purposes, it was proposed that the prototype valves be hydrostatically tested at double the maximum operating pressure to ensure the safety of those working with the valves. As the actual operating pressure of the prototype valves in fact less than half of the 240 psi used throughout the calculations, there is virtually no chance of either prototype design failing due to the cold flow testing.

5.2.6 Prototype Valve Fabrication

The prototype valve designs shown in Figures 55 and 54 were machined at the University of Pittsburgh's School of Engineering Machine Shop out of cast acrylic purchased from a

commercial supplier. Cast acrylic was chosen for several reasons: price, ease of machinability and transparent/translucent nature. Using mainly computerized numerical controls (CNC) machines, three prototypes of each design were created. Figures 56 and 57 depict the final models that were used for cold flow, low pressure testing at both University of Pittsburgh and NETL Morgantown. The machine shop drawings used to create the designs seen in Figures 56 and 57 can be found in Appendix J.

Figure 56: Finished TV1 valve assembly prototype of cast acrylic.

Figure 57: Finished TV3 valve assembly prototype of cast acrylic.

5.2.7 Preliminary Prototype Valve Flow Testing

While the preliminary cold flow testing has many differences from the actual application (lower pressure, higher pressure drops, lower temperature), many things can be gleaned from the tests. For example, the controllability, the flow characteristic, the linearity, and

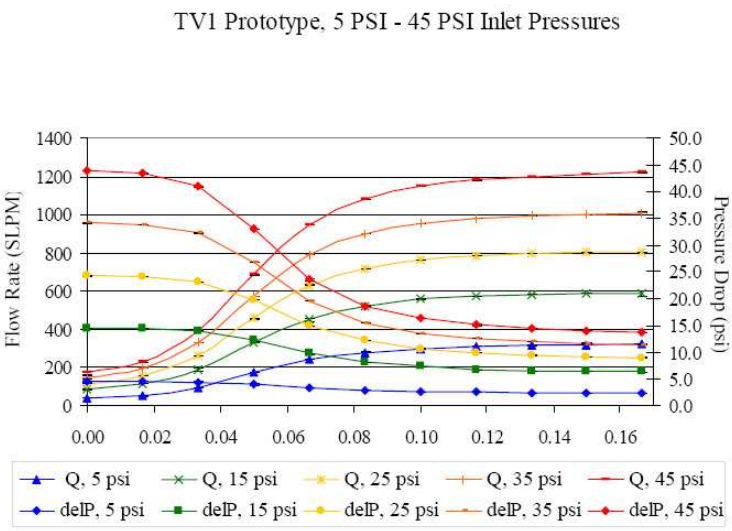

Figure 58: Plot of installed flow characteristic for TV1.

pressure drop characteristics of the valve can all be better understood by the tests conducted. In turn, improvements can potentially be made prior to fabricating the final prototype valves which include the electromagnetic actuation.

The results of the preliminary prototype provided useful information about the current valve designs. Figures 58 and 59 depict results from the arbitrary back pressure testing, which produces a plot referred to as an "installed flow characteristic" due to the varying pressure drops across the valve at each valve position [41]. Such a flow characteristic can allude to each valve's performance, but for direct comparisons of flow characteristics, a constant pressure drop is needed. Figures 60 and 61 are results from the constant pressure drop tests and are referred to as an "inherent flow characteristic" [41].

For each inlet pressure in the Figures 58 and 59, the flow rate (left y-axis) and pressure drop (right y-axis) are given as a function of valve position. For Figures 60 and 61, only the flow rate is given as a function of valve position since a constant pressure drop was

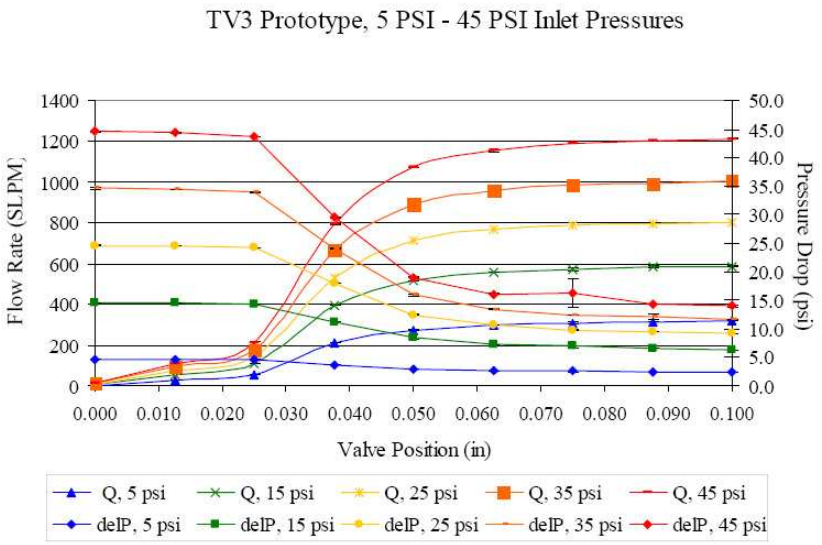

Figure 59: Plot of installed flow characteristic for TV3.

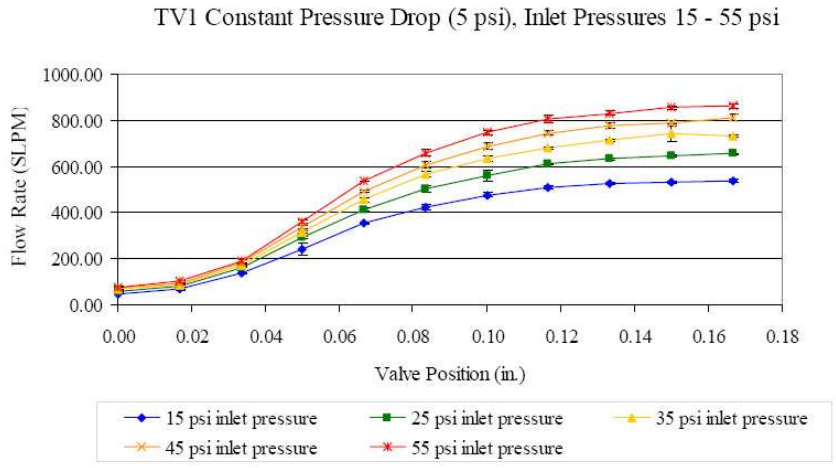

Figure 60: Plot of inherent flow characteristic with 5 psi pressure drop for TV1.

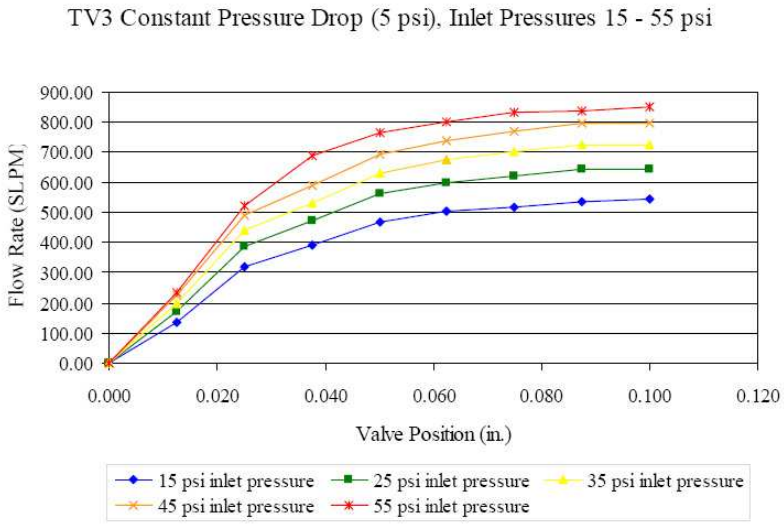

Figure 61: Plot of inherent flow characteristic with 5 psi pressure drop for TV3.

maintained during testing. Plots of each individual case (inlet pressure) for both tests can be found in Appendix K. In all cases, the average values (across three tests) are presented, along with standard deviation bars. Given that the tests were fairly repeatable, the standard deviation bars are not very visible in most of the plots.

The installed characteristic plot of TV3 seen in Figure 59, is somewhat different in many respects. The valve is observed to open very slowly from 0.00–0.025 inches, after which it rapidly opens until about 0.04 inches. From 0.05–0.1 inches, the valve again responds slowly. Each of these three regions represents an approximately linear region. Focusing just on the 45 psi inlet pressure case (also see Figure 131 in Appendix K), a similar $\pm 10\%$ range

corresponds to the valve position between 0.05–0.08 (throw = 0.03 inches). The linearity in this region is not bad. In addition, the corresponding pressure drop of between 15–18 psi is half of that of TV1, making TV3 more appealing in this respect.

Recalling Figures 61 and 60, a direct comparison reveals that TV3 is in fact closer to a quick acting valve versus TV1. The TV1 prototype again has a longer, more linear region than that of TV3. While the constant pressure drop do not necessarily add any additional insight as to the performance of the valves, it does verify that TV3 is the faster acting valve of the pair, which may make it more desirable in the sense of requiring a shorter throw and therefore smaller magnet segments for the final integrated valve and actuator assembly.

Both types of characteristics curves obtained (installed and inherent) indicate that both valves are somewhere between linear in nature and quick-opening. Noticing the installed characteristic plot of TV1 in Figure 58, the flow characteristic is relatively linear in the region of 0.03–0.07 inches. Focusing on the 45 psi case (also see Figure 126 in Appendix K), if the valve is operated between 1,000 to 1,200 SLPM, that would represent the $\pm 10\%$ change in flow that is required for the ACT application. This region corresponds to valve positions between 0.07–0.13 inches, which corresponds to a very modest required actuator throw of 0.06 inches. Although the accompanying pressure drop is quite high (33 psi), it should be much lower in the actual application, given that the gas is highly compressed (inlet pressure of 450 psi). In addition, the valve is relatively quick opening. By 0.12 inches, the flow rate has almost achieved its full range.

All data sets collected indicated a maximum flow coefficient (C_v) in the neighborhood of 1.7. The flow coefficient is a dimensionless, relative measure of a valve's efficiency of flowing fluid through it. The maximum values of C_v obtained were with the valves at their maximum opening (a travel of 0.17" for TV1 and 0.1" for TV3). Table 16 provides of summary of the range of maximum C_v. Note that the red cell shading for the three values of C_v that are around 1.5 indicates that choked flow. The lower C_v value is most likely related to the occurrence of choked flow, which typically reduces the effectiveness of valves.

In general, there is little difference in the flow characteristics in the upper range of operation of both valves (where the pressure drop is lowest, and hence a more desirable operating range). While the lower pressure drop of TV3 is likely appealing, the larger

Table 16: Flow coefficients (C_v for preliminary flow testing.

	TV1		**TV3**	
Inlet P [psi]	Installed	Inherent	Installed	Inherent
5	1.787	N/A	1.749	N/A
15	1.693	1.744	1.713	1.782
25	1.506	1.781	1.704	1.754
35	1.501	1.765	1.696	1.744
45	1.507	1.766	1.766	1.733
55	N/A	1.721	N/A	1.689

required throw for TV1 is also likely appealing. A larger required throw would help mitigate thermal expansion issues in the armature, which is an integral part of the valve action. Although electromagnetic actuators are analog devices capable of fine motions, the additional operating range will help with precision and also minimize sensitivity in the valve.

5.3 THERMAL ANALYSIS

5.3.1 Heat Transfer Analysis

Manual analysis of the heat transfer rate yielded the thermal resistances seen in Table 17. The names of resistances correspond to the thermal circuit and valve actuator cross section in Figures 43 and 44, respectively.

Manual analysis of the heat transfer rate yields a value of 57.02 W for the actuator model. This indicates that the valve design is capable of dissipating 57.02 W of energy in the form of heat for the scenario presented (343°C fuel flowing through the valve in an environment that is room temperature: 21°C). Since metal is a very good conductor of heat

Table 17: Thermal resistances manually calculated for thermal analysis.

Name	Resistance [K/W]
R_{air1}	16.761
R_{air2}	7.993
R_{arm1}	0.327
R_{arm2}	0.132
R_{arm3}	1.738
R_{body1}	0.016
R_{body2}	0.070
R_{body3}	0.042
R_{fuel}	0.115
R_{coil}	0.004
R_{mag}	0.156

(indicated by relatively high thermal conductivity values, k), a large value of heat transfer is to be expected. Also recall that the thermal analysis was assumed to be in steady-state conditions, therefore the heat transfer will be a constant value throughout the valve.

A smaller design was used for the thermal analysis than the prototype designs, pictured in Figures 54 and 55 as the metal-bodied integrated valve design underway will be considerably smaller than the prototype designs. With an overall outer diameter of 2" and AISI 1020 steel acting as both the valve body and keeper materials, the total length of the actuator section was approximated to be 1.7" (6 magnets at 0.2" length, plus an extra 0.5" at the end of the actuator to simulate where the integrated valve would be connected. From the heat transfer rate calculation, it was also determined that the inner wall temperature (flow passage) is 336.4°C and the outer wall temperature (outside of valve body) is 329.6°C for a fuel temperature of 343°C. This is a reasonable result, as the actuator design is quite small (i.e. unable to dissipate as much heat as the TV1 prototype valve design made of similar material, for instance). As this was a worse case scenario, the temperature far away

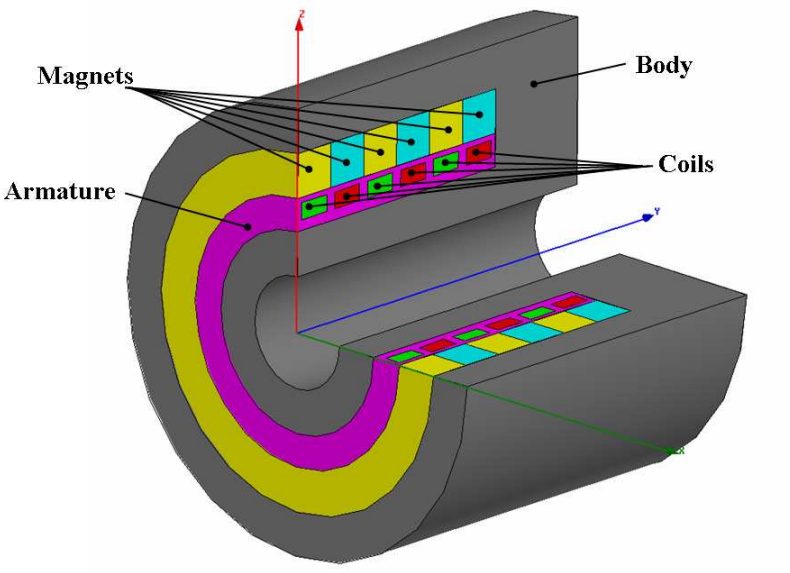

Figure 62: Cutaway of actuator model created in Ansoft ePhysics™ for thermal FEA.

from the valve (i.e. T_∞) was taken to be at room temperature (21°C) to give the largest possible temperature difference. This temperature difference will be used in the next section to determine the thermal expansion of the actuator.

The manual heat transfer and temperature gradient calculations were next used to verify the validity of Ansoft ePhysics™ software [39], as it would then be used for examining more closely the temperature distribution through the actuator design as well as possible future use for determining thermally induced stresses within valve and/or actuator components. Creating a three dimensional version similar to the one seen in Figure 44 in Ansoft ePhysics™ results in the model seen in Figure 62.

The FEA results of the thermal analysis can be seen in Figures 63, 64, and 65. Figure 63 shows the temperature distribution through the valve, indicating an inner wall temperature of approximately 320°C and an outer wall temperature of approximately 290°C. Figures 64 and 65 depict the inner and outer surface temperatures, respectively. After close inspection of the plots, it appears the outer valve surface is 316°C while the inner surface is 293°C. This differs from the manual analysis by 20°C on the inner surface and more than 30°C on

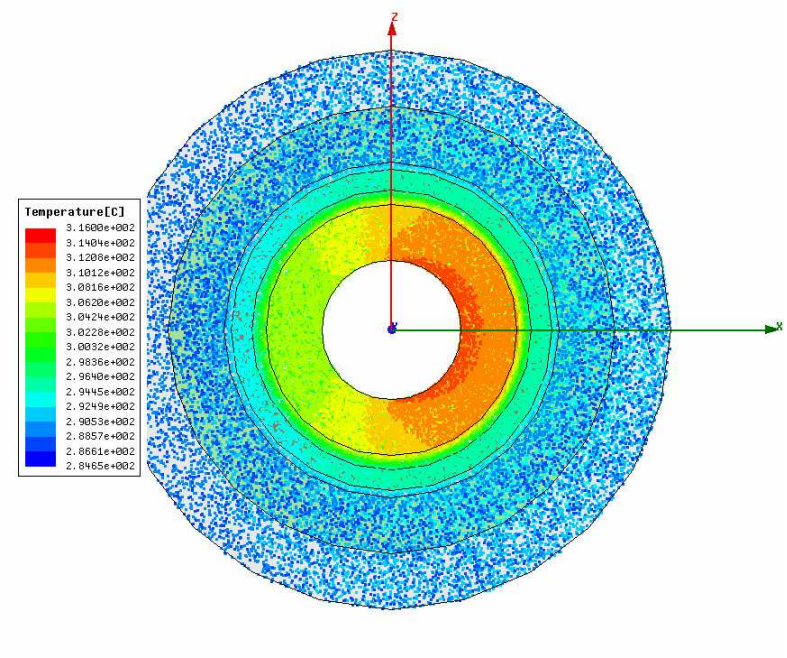

Figure 63: Top down (longitudinal) temperature cloud plot of actuator model.

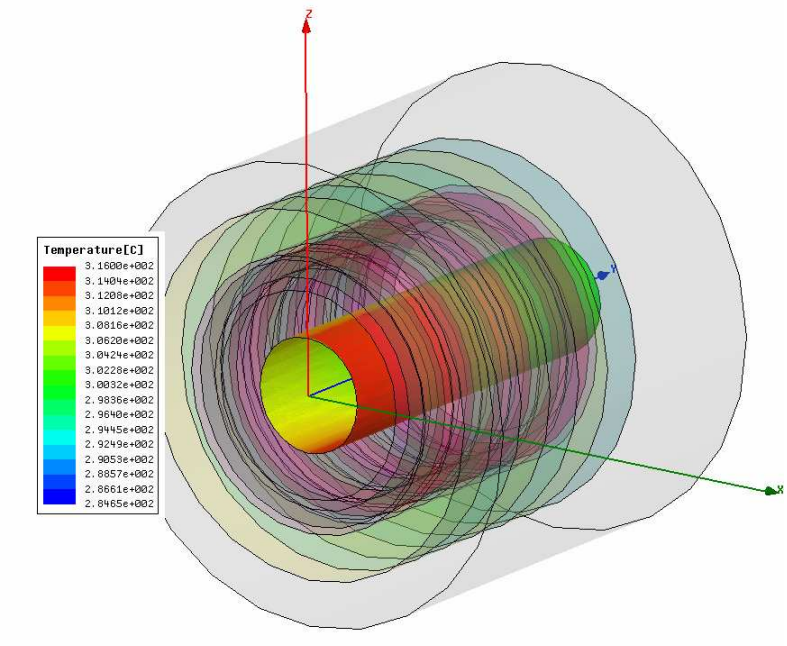

Figure 64: Inner surface temperature plot of actuator model.

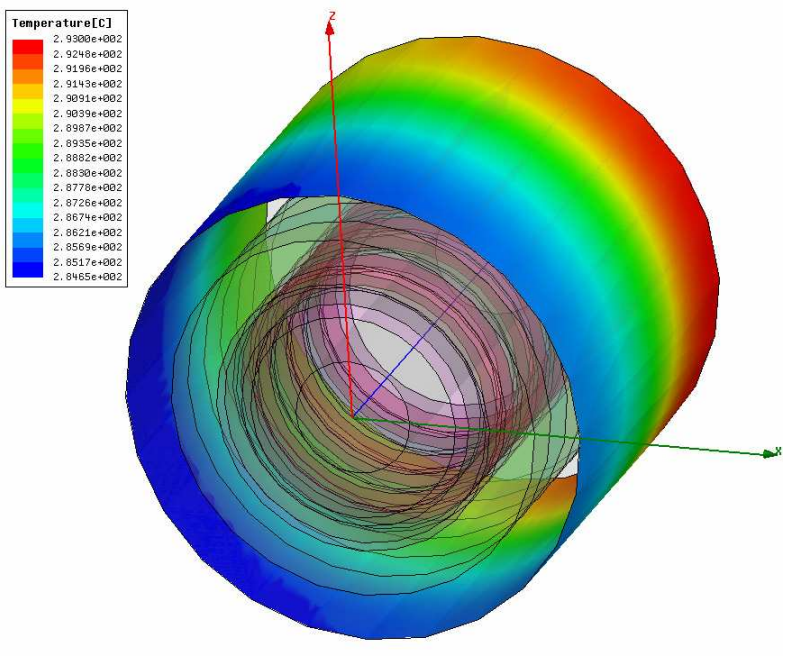

Figure 65: Outer surface temperature plot of actuator model.

the outer surface. Table 18 summarizes the results and differences between the manual and FEA results. Since both the inner and outer temperatures obtained using Ansoft ePhysics™ were at least 3% lower than the manual calculations, it is apparent that the actuator design seen in Figure 62 is better at dissipating heat than indicated by the manual analysis. Note that the manual analysis will give a more conservative thermal expansion analysis and will therefore be used in the following section rather than the temperatures obtained using Ansoft ePhysics™.

5.3.2 Thermal Expansion Analysis

The primary concerns addressed by the thermal analysis are reduction of the armature's clearance and thermally induced stresses. In particular, the brittle magnet material may become stressed should the adjacent components expand at a different rate than the magnets. Computing the thermal expansion manually using the results from the heat transfer analysis

Table 18: Comparison of manually calculated temperatures and temperatures obtained using Ansoft ePhysics™.

	Manual	FEA	% Absolute Difference
$T_{inner,wall}$ [°C]	336.4	316	3.4
$T_{outer,wall}$ [°C]	329.6	293	6.3

resulted in an expansion that does not impinge on the magnets. Only two diametral interfaces had resulting impingements due to thermal expansion: the interface between the outer radius of R_{body3} and the inner radius of R_{arm1} (approximately 4e-4 inches) and the interface between the outer radius of R_{coil} and the inner radius of R_{arm2} (approximately 1e-2 inches). These expansions are minimal and most likely not within most machinists' machining tolerances. A summary of the thermal expansion analysis can be found in Table 19. Refer to Figure 44 in a previous chapter to identify what the individual components are referred to in the table.

Largely, these favorable results are due to careful material selection for the valve body and keepers. AISI 1020 steel was chosen for the material as both the keeper material and valve body material due to its favorable magnetic properties, mechanical properties, availability and especially due to the fact that it has a coefficient of thermal expansion (CTE) very close to that of Sm_2Co_{17}. Tables 22 and 23 in Appendix C list several such materials that were identified for potential use for the fabrication of the final metal-bodied valve prototypes. As seen in Table 23, AISI 1020 steel alloy was chosen in particular due to there being no difference in the CTEs of the steel and Sm_2Co_{17}. The other materials considered for use in the metal-bodied prototype all have very low percentage differences relative to the chosen magnetic material. Even though the CTEs nearly match for 1020 steel and the magnetic material, it was still believed that such a thermal analysis would be beneficial as to confirm that thermal expansion would not hinder operation or structural integrity of the actuator/valve assembly.

Table 19: Summary of radial dimensions of thermal expansion analysis.

	Material	Original [in]	New [in]	% Change
$r_{body1,outer}$	AISI 1020 steel	1.000	1.00420	0.41950
$r_{body1,inner}$	AISI 1020 steel	0.800	0.80336	0.41950
$r_{mag,outer}$	Sm_2Co_{17}	0.800	0.80328	0.41004
$r_{mag,inner}$	Sm_2Co_{17}	0.600	0.60246	0.41004
$r_{arm2,outer}$	Glass Mica	0.600	0.60208	0.34696
$r_{arm2,inner}$	Glass Mica	0.575	0.57700	0.34696
$r_{coil,outer}$	Copper	0.575	0.57808	0.53621
$r_{coil,inner}$	Copper	0.500	0.50268	0.53621
$r_{arm1,outer}$	Glass Mica	0.500	0.50174	0.34696
$r_{arm1,inner}$	Glass Mica	0.450	0.45156	0.34696
$r_{body3,outer}$	AISI 1020 steel	0.450	0.45189	0.41950
$r_{body3,inner}$	AISI 1020 steel	0.250	0.25105	0.41950

6.0 CONCLUSIONS AND FUTURE WORK

6.1 CONCLUSIONS

Half way through the second phase of the Active Combustion Throttle (ACT) project, much progress has been made toward the goal of creating a throttle valve for gas turbine engines. An extensive examination of literature and an exhaustive, periodic patent search confirmed that no commercially available off-the-shelf valve assemblies exist that can simultaneously meet all requirements for the ACT project listed in Table 1. The results of a survey of various existing and newly conceived valve technologies (or variants of existing designs) were compiled into a white paper. Likewise, various actuation technologies were also cataloged and contrasted. The actuator was seen as the most potentially limiting of the two and hence was designed first. Of the actuators, the most viable technology was electromagnetic using high temperature (Sm_2Co_{17}) permanent magnets. A unique style linear actuator was conceived in conjunction with Lambeth Systems, which has a magnetic design inspired by pancake motors used in computer hard drives and operates somewhat similarly to a speaker voice coil. This unique design will reduce the potential for saturation of the keepers and also permit the gas to flow through the center of the actuator to enhance the compactness and potentially provide some cooling for the actuator coils. Modeling for the actuators was performed using Ansoft Maxwell® 2D and Maxwell® 3D [37]. Given the similarities, initial benchmark modeling was performed on a computer hard drive and was validated with a companion experimental testing program. In general, the models agreed by a factor of two

or better, which is considered good agreement. Modeling was later extended to the actual valve actuator. A parametric study demonstrated how the hardware can be optimized based upon size and force requirements as well as to prevent saturation of the magnetic circuit (i.e. the keepers).

Two valve designs were down-selected for modeling and testing. Each has an axial flow characteristic that well complements the linear voice coil actuator design. One valve was inspired by an original design termed the "football" valve. A moving cylindrical armature mates with a cone shaped piece to increase or decrease the gap between them and increase or decrease the flow, respectively. The second valve was created by drilling holes through two closed concentric right circular cylindrical shells. As the cylinders move relative to one another, the respective holes will align or misalign. Since the gas flow is forced to go through these holes, the flow can be modulated. Computational fluid dynamic (CFD) modeling of both valves was performed by West Virginia University (WVU). From the lessons learned, improvements to the internal geometry were made to the geometries of the initial designs to reduce excessive recirculation and thus pressure drop through the valves. Results also predicted the valve positions for the controllable region for the valve designs. The performance was modeled for the low-pressure, low-temperature preliminary flow tests that were conducted with air. Given the complexity of the modeling, the models for the design case (methane at 650°F and 450 psi) were not completed before CFD funding discontinued.

Final prototypes of just the valves were designed for cold-flow testing at the University of Pittsburgh and NETL Morgantown. Cast acrylic material was used to create the valves, given the good machinability and the translucent nature, which permits the internal structure of the valves to be observed. The valves were designed such that the mock armature can be repositioned without fully disassembling the valve. A manual, simplified stress analysis determined that the factor of safety was at least eight. Finite element analysis (FEA) predicted the factor of safely to be closer to three, which is believable since it will take into account stress concentration factors that were ignored in the manual analysis. Two specimens of each design were delivered to NETL Morgantown for preliminary flow testing. A third specimen was kept at the University of Pittsburgh for testing and refinement purposes.

Initial cold-flow tests at the University of Pittsburgh determined that both prototypes are viable designs and the internal flow paths are in need of no further refinement. Inherent flow characteristics (constant pressure drop) as well as installed flow characteristics (varying pressure drop) were determined and compared. Flow modulation of ±10% was observed for both TV1 and TV3 within the throw range tested (0.17" for TV1 and 0.1" for TV3). Both designs were found to have linear regions with relatively short throws, while TV3 was found to be slightly more of a quick-opening design (i.e. shorter throw). Testing at NETL Morgantown confirmed testing at the University of Pittsburgh, providing similar characteristic curves and flow coefficient values (C_v) of up to 1.7.

Given the high temperature operation of the valve, considerations for thermal design were taken into account. It is best to minimize the mismatch in coefficient of thermal expansion (CTE) for the various materials used in the device. Several materials with similar CTEs were identified that should work well in the final prototype valves that will be created in phase II. Specifically, 1020 mild steel to be used for the keepers (and possibly valve body) has a CTE that is nearly equivalent to the Sm_2Co_{17} magnetic material. Alternate body materials include certain stainless steels or Haynes 230 alloy, which is already used in high-temperature gas turbine components. Machinable glass-mica ceramic could make a suitable armature, given its similar CTE and resistance to abrasion and chemical attack.

Even though careful material selection has greatly reduced the possibility of thermally induced stresses, conservative manual heat transfer and thermal expansion analyses were coupled with thermal FEA by Ansoft ePhysics™ [39] to ensure no unexpected thermal growth would damage the valve designs when in operation. A thermal resistance analysis was used in order to determine the heat transfer of the valve due to all three modes of heat transfer (conduction, convection and radiation). The results were used to determine radial growth of all components and confirmed that no major thermally induced stresses would significantly effect the valve actuator design chosen. The thermal FEA further confirmed the heat transfer and thermal expansion calculations.

6.2 FUTURE WORK

The primary concentration for the next design iteration of the ACT valve will focus on an integrated valve assembly design (i.e. including the electromagnetic actuator) in a smaller, metal-bodied package. Preliminary, work designs can be seen in Figures 66 and 67. These

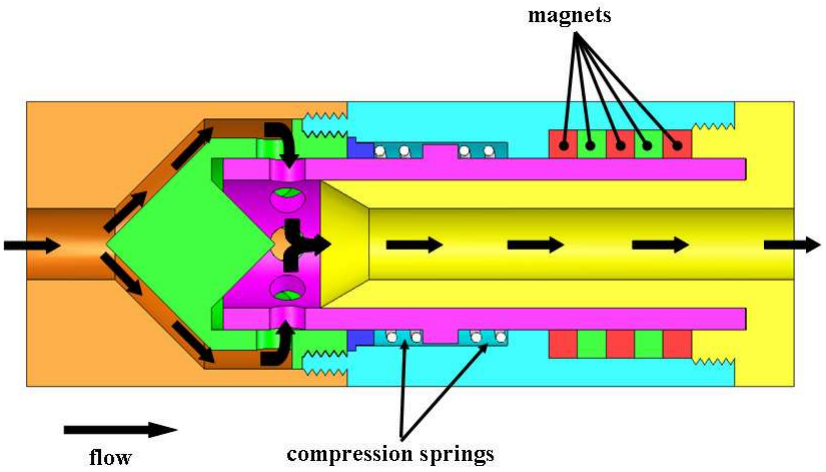

Figure 66: Preliminary integrated valve and actuator design for metal-bodied prototype TV1.

valve assemblies include a fail nominal feature per item 11 of Table 1. This feature will function by including counteracting springs that provide pretension from both directions during operation of the valve. If power is lost or the actuator fails electrically, the springs will return it to the predesigned position that provides the desired nominal flow rate. The overall design will incorporate an integrated valve body/magnetic keeper design of mild 1020 steel. Preliminary saturation analysis of the actuator in the slimmer design has been conducted and will continue throughout the design process to assure the actuator is properly sized for the valve designs. In order to solidify the design of the flow path for both valves, however, a non-dimensional analysis needs to be conducted. Such analysis will give a clearer

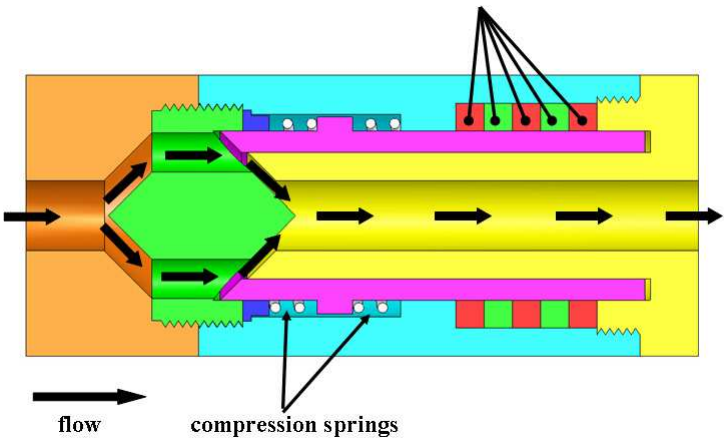

Figure 67: Preliminary integrated valve and actuator design for metal-bodied prototype TV3.

picture of the behavior of the fluid through the valve designs at the full operating pressure of 450 psi and flow rate of 3,000 SCFH. While the cold-flow, low-pressure tests are encouraging, further non-dimensional analysis will help determine the final flow passage size through the metal-bodied valve designs.

Since the final dimensions for the electromagnetic actuator design were not determined due the lack of CFD force analysis, the cold-flow testing data will be manipulated in order to extrapolate the forces required by the actuator. Dimensionless analysis may be required for this operation, in which the Buckingham Pi Theorem will be employed.

Parallel flow testing of the current acrylic prototype valves will also be conducted using dual electronic mass flow meters in order to gain more insight into how these valves will operate in such a configuration. Ultimately, the ACT valve will be used in such a system and thus far, no data or testing has been conducted in a parallel flow loop with such designs. The parallel flow loop at the University of Pittsburgh is currently being assembled. Parallel flow testing will be commencing by the end of April 2008.

An actuator proof-of-concept model is also being designed and is currently undergoing saturation analysis. The saturation analysis will aid in finalizing the dimensions of the design for the neodymium iron boron (NdFeB) magnets purchased for the model. A cross section of

the preliminary prototype design can be seen in Figure 68. The flanged design provides easy manufacturing as well as assembly of the model. Once completed, the model will (along with the hard drive benchmark electromagnetic modeling) further validate the actuator design.

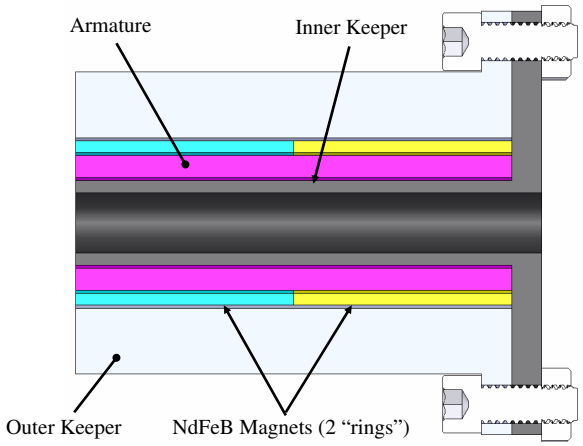

Figure 68: Cross section of preliminary proof-of-concept prototype of electromagnetic actuator.

APPENDIX A

ACTUATOR ADVANTAGES/DISADVANTAGES

In an effort to determine the most likely valve design candidates to incorporate into the ACT project, Table 20 was created. The advantages and disadvantages of the various designs were taken into consideration and aided members of the ACT design team in ranking each design in several metrics in Table 24 on page 119.

Table 20: Comprehensive list of actuation technologies' advantages and disadvantages.

Advantages	**Disadvantages**
Stepper Motors	
Angle of rotation is proportional to the input voltage	Resonances can occur if not properly controlled
Excellent response to starting, stopping and reversing	Not easy to operate at extremely high speeds (≈1,000 – 2,000 rpm max.)
The life of the motor is simply dependent on the life of the bearing since there are no contact brushes	Current maximum operating temperature for magnetic versions stands at ≈ 300 °C
Able to be controlled effectively in an open loop system	Performance is compromised with the smaller diameter models
Can operate under a wide range of rotational speeds since speed is proportional to the frequency of the input pulse	Rotational speed does not increase when subject to heavier loads
Can have extremely small diameters	Cogging
Responds very quickly to input pulse	Controller required
Simple design allows motor to be fabricated by user	Relatively complex
Relatively inexpensive (≈ $100 – $200)	
Servo Motors	
As with a stepper motor, the angle of rotation is proportional to the input pulse	Due to the motor's circuitry, the motor lags behind its input pulse
Precise positioning and repeatability greater than that of a stepper motor	Since the motor lags, it must be used in a closed loop system
Able to adjust rotational speed when heavier loads are applied	Unresponsive to starting, stopping and reversing (can lead to undesired vibrations)
Easy to control even at very high speeds (≈ 3000 – 5000 rpm max.)	Has complex circuitry which generally must be purchased

Continued on next page

Table 20 (continued)

Advantages	**Disadvantages**
The life of the motor is simply dependent on the life of the bearing since there are no contact brushes	Relatively expensive: ≈ 400 – 500
Can operate under a wide range of rotational speeds since speed is proportional to the frequency of the input pulse	Current Maximum operating temperature stands at ≈300 °C
Can have extremely small diameters	
Hydraulic Valves	
Provides a great deal of power compared to the actuator inertia	Systems tend to leak, creating messy and potentially dangerous conditions
Rapid response to starting, stopping and reversing	High temperatures can cause hydraulic fluid to vaporize or ignite
Can be operated under continuous, intermittent, reversing, and stalled conditions without damage to the system	Potential hydraulic fluid contamination can cause a loss in actuator efficiency
Can have diameters as small as 1/4 in.	Relatively expensive: ≈ $200 – $600
Requires less space than most electrical actuators	Hydraulic systems' natural frequency is proportional to the diameter of its cylinders
The pressure inside of a hydraulic actuator can be held constant without the need for more energy while creating a constant torque in an electric or electromagnetic motor could lead to overheating	If the maximum load for a certain diameter hydraulic system is exceeded, the system can come susceptible to a resonant frequency
Operates at approximately 1,000 – 5,000 psi	
Can be driven linearly or rotationally	
Pneumatic Valves	
Compressed air can be easily transported over large distances more easily than hydraulic fluid	While pneumatic actuators provide good power compared to their inertia, the power produced by pneumatics is significantly less than that of hydraulics
Able to operate at high speeds	Like hydraulic actuators, pneumatic actuators are susceptible to leakage
The actuator can stall at high speeds without damage	In order for pneumatic actuators to work effectively, the system must be free of dirt and condensate
Pneumatic devices are relatively insensitive to	Can only operate at pressures between 80 – 100 psi
temperature fluctuations and can therefore operate	Need an air supply
under very extreme conditions	Pneumatic actuators have poor controllability
Pneumatic actuators, unlike hydraulic actuators, offer	Lags can occur when conveying air over long distances
no risk of explosion or fire	
Can operate linearly or rotationally	
Can have a diameter as small as 1/10 in.	
Relatively inexpensive: ≈ $50 – $200	
Solenoids	
Can install where hydraulic or pneumatic actuators cannot be used	Generally, solenoids are reserved for linear motion
Excellent response time to input pulses	Unlike stepper and sero motors, solenoids have a very limited range of motion; they can only be either fully open or fully closed
Much less complicated than hydraulic or pneumatic actuators and are therefore easier to install	Lacks the precise positioning and controllability that stepper motors and servo motors offer
Highly reliable and have long operation life	Current maximum operating temperature stands at approximately 210 °F (≈ 100 °C)
Can have diameters as small as 1/2 in.	Does not produce as much force as any of the previously described actuators and are therefore reduced to operating relatively smaller valves
Simple design allows motor to be fabricated by user	
Relatively inexpensive: ≈ $50 – $200	
Piezoelectrics	
The input voltage supplied is linear to displacement of the actuator	Piezoelectric materials and therefore piezoelectric actuators are extremely dependent on temperature
Piezoelectric actuators can exert forces of several 10,000 N with only micron changes to the actuator's displacement	High operating temperatures negatively affect performance (loses all piezo effect above the Curie temperature)

Continued on next page

Table 20 (continued)

Advantages	Disadvantages
Piezoelectric actuators have a very low power consumption in relation to the power they produce	Long term creep of piezoelectric materials can be as high as 15%
Virtually resistant to wear and tear	Brittle and susceptible to fracture
Excellent response to starting, stopping and reversing	Severely strain limited
Can be cheap or expensive depending on the application	
Electrochemical	
Consume low energy and yield significant forces up to 30 kN	Can only operate up to a temperature of approximately 250 °F (≈ 120 °C)
The chemical reaction which drives the actuator can be halted during the reaction without compromising the buildup of pressure produced to that point	Leakage of gas can be problematic if the actuator is operated over a long period of time
Both natural gas and hydrogen can be the products of oxidation reduction reactions	Unknown long-term stability
Electrochemical actuators can easily replace either hydraulic or pneumatic actuation systems	Electrochemical actuators are only as fast as the chemical reaction which drives the actuator
Reaches target diameter of 1/2 in.	Can only operate at a bandwidth of about 60 Hz
	Both natural gas and hydrogen can be the products of oxidation reduction reactions, creating an explosion hazard
	Inconvenient to supply reactants and get rid of by-products
Electrostrictive	
Electrostrictive materials are less susceptible to creep over time	The PMN material which is used to create electrostrictive actuators has a higher coefficient of thermal expansion than PZT thus making PMN more sensitive to temperature changes
Unlike piezoelectric materials, electrostrictive materials are non-polarized	
Being non-polarized, electrostrictive actuators can respond to a charge of either polarity and are able to operate in either direction if designed as a stack	Electrostrictive actuators can only operate up to a temperature of 300 °F (≈ 150 °C)
Electrostrictive actuators can operate at frequencies exceeding 1000 Hz	Strain limited
Electrostrictive actuators are more responsive to sudden changes in input voltage and therefore have a lower hysteresis, 2%, than PZT	Requires very high voltage
	Nonlinear operation
	Requires bias voltage to create AC actuation
Along with these characteristics, PMN also retains all other important characteristics of PZT while creating strains 10 times that of PZT	
Magnetostrictive	
Magnetostrictive actuators have the ability to produce large forces	Strength of the magnetic force produced depends on temperature
Excellent response time to input signals	Magnetostrictive actuators are generally brittle and difficult to machine
Magnetostrictive actuators can operate at temperatures of 720 °F (≈ 380°C)	In order to maintain the magnetic field about the actuator, electrical power is always required even if the actuator is static
Magnetostrictive actuators can also operate at frequencies above 1200 Hz	Magnetostrictive material is not very common thus making it expensive compared to piezoelectric materials
Unlike piezoelectric and electrostrictive actuators, magnetostrictive actuators are not required to have a stack design	
Excellent response to starting, stopping, and reversing	
Generally have diameters less than 1/2 in.	
Able to emit large forces relative to its small displacement	
Electrorheological Dampers	
Electrorheological dampers produce comparable force to that of hydraulic actuators	Not an actuator per se, but rather an actively tailored passive device

Continued on next page

Table 20 (continued)	
Advantages	**Disadvantages**
Since the electrorheological effect is directly controlled by the electric field being supplied to the actuator, these dampers have excellent response to starting, stopping, and reversing	The electrorheological effect is highly dependent upon temperature and this effect can be lost at temperatures above 250°F (≈ 120°C)
	Unpredictable long-term behavior
	There are numerous effects which can disturb the electrorheological effect
The response time of electrorheological dampers is on the order of milliseconds	The power that is needed to drive an electrorheological damper is on the order of several hundred watts
	These dampers can only operate in a frequency range of about 40 - 50 Hz
Magnetorheological Dampers	
Magnetorheological dampers do not require much power to operate	Not an actuator per se, but rather an activley tailored passive device
MR fluids are much less susceptible to contamination than ER fluids	The magnetic properties of a magnetorheological damper deteriorate over time
The forces that can be generated in a magnetorheological damper are greater than those in an electrorheological damper by one order of magnitude	Careful considerations must be taken to ensure material compatibilities
Unlike ER fluids, the rheological effect in a MR damper does not dissipate with increased temperature (it should be noted though that MR dampers have been tested at a temperature of 300°F (≈ 150°C))	MR dampers require the use of magnetic circuitry in addition to the actuator itself
Short response time on the order of milliseconds (i.e. can operate on the order of 1,000's of Hz)	

APPENDIX B

VALVE ADAVANTAGES/DISADVANTAGES

In an effort to determine the most likely valve design candidates to incorporate into the ACT project, Table 21 was created. The advantages and disadvantages of the various designs were taken into consideration and aided members of the ACT design team in ranking each design in several metrics in Table 26 on page 129.

Table 21: Comprehensive list of valve technologies' advantages and disadvantages.

Advantages	**Disadvantages**
Globe Valve	
High flow controllability (i.e. efficient throttling)	Moderate flow resistance (i.e. high pressure drop)
Wide availability of pressure ranges	Can become fouled from debris buildup on seat
High accuracy of flow control	Relatively expensive
Very linear flow expected	May be quite noisy and cause undesirable vibration
Low pressure drop expected	
Needle Valve	
Very high flow controllability	Moderate to high flow resistance
Precise operation can be achieved	Can become fouled from debris buildup on seat
Low pressure drop expected	Requires precise machining (increased cost)
Possible to create a very small footprint	Typically small and therefore prone to corrosion
Very linear flow expected	May be quite noisy and cause undesirable vibration
Gate Valve w/1 Gate	
Low flow resistance (low pressure drop)	Difficult to control flow in throttling applications
Less costly compared to other valves	Often have long stroke
Available in high capacity models	Can become fouled from debris buildup on seats
Tight shutoff (not needed for the ACT valve, however)	Cavitation may occur at low pressure drops
Easy to model (low complexity)	Poor, inaccurate control
"Fail nominal" requirement more easily implemented than other valve types	
Gate Valve w/2 Gates	
Low flow resistance (low pressure drop)	Complex flow control
Multitude of gate shapes and therefore possible valve characteristics	Still may result in poor, inaccurate control

Continued on next page

Table 21 (continued)	
Advantages	**Disadvantages**
Does not completely impede flow	Can become fouled from debris buildup on seats
Does not require seating on pipe surface	Cavitation may occur at low pressure drops
Tight shutoff (again, not needed for the ACT valve)	
"Fail nominal" requirement more easily implemented than other valve types	
Butterfly Valve	
Thin elements have low flow resistance	Cavitation and choked flow at high pressures and lower flows
90 degree turn operation	Throttling requires special designs
High pressure-recovery factor (partially due to low pressure drop)	Typically low pressure applications
Relatively inexpensive	High torque required for control in many cases (not easy to actuate)
High capacity models available	"Fail nominal" requirement may not be met - difficult to implement
Low maintenance	Can become fouled from debris buildup on seats
Ball Valve	
High rangeability	Dramatic geometry change when throttling
High controllability	Larger balls reduce actuation for control
Suitable for high pressure application	Often prone to cavitation
Low flow resistance when fully open	"Fail nominal" requirement may be difficult to implement
Relatively tight sealing without requiring much torque	Not very linear flow expected
Little leakage	Special ball needed for throttling applications, otherwise quite poor throttling characteristics
Low maintenance	
Single Orifice Valve	
High precision is easily achievable	May be prone to clogging based on how small the orifice is
Low pressure drop expected	High machining costs for a miniaturized orifice
Fast actuating design	Difficult to actuate
High controllability	Overall footprint may be relatively large
Linear flow	May be quite noisy and cause undesirable vibration
	High frictional flow losses if orifice is too small
Multi-Orifice Plate Valve (MOV)	
Ideal for stroke-limited actuators since multiple passages are employed	May be prone to clogging based on how small the multiple orifices get
Horizontal or vertical actuation possible (or both for two degrees of freedom, if needed)	High firictional flow losses with small orifices
Allows small device footprint	High machining costs for miniaturized orifices
Low pressure drop	Difficult to model (high complexity)
MOV Gate Valve (Linear Flow)	
Reduced control gap length is ideal for stroke-limited actuators, such as electromechanical or electromagnetic devices	Design optimization a must for this valve type
Allows small device footprint	May be prone to clogging based on how small the multiple orifices get
Linear flow	High frictional flow losses with small orifices
Low pressure drop	High machining costs for miniaturized orifices
Fast actuating design	Difficult to model (high complexity)
MOV Gate Valve (Non-Linear Flow)	
Reduced control gap length is ideal for stroke-limited actuators, such as electromechanical or electromagnetic devices	Design optimization a must for this valve type (could be time intensive)
Allows small device footprint	May be prone to clogging based on how small the multiple orifices get
Low pressure drop	High frictional flow losses with small orifices
Fast actuating design	High machining costs for miniaturized orifices
	Non-linear flow
	Difficult to model (high complexity)

Continued on next page

Table 21 (continued)

Advantages	Disadvantages
Constricting Pinch Valve	
Valve body acts as a built-in actuator, eliminating costly hydraulic, pneumatic, or electric operators	Typically not high temperature valves due to elastomeric body
Good for control of abrasives and/or corrosives since no contact between metal parts and transport media	Not suggested for high-pressure flow and for use with gases
Design good for cleanliness, drainage and ease of cleaning	High modeling complexity for braided sleeving design (change in porosity)
Low maintenance, low weight (due to the largely plastic body), and suitable for use in systems requiring explosion-proof line closure	May be slow actuating
Good for use in sterile lines and for product purity	Expensive design for such a harsh environment
No obstruction to flow passage	
Low pressure drop	
Thunder-Like Valve	
Low cost, high efficiency piezoelectric devices having improved piezoelectric characteristics including improved mechanical output	Insufficient actuator throttling
The actuator is pre-stressed which gives it a characteristic curve or bend, ideal for creating a nominal flow	Poor erosion resistance
Very simple design (easy to model and build)	Could become a large device footprint
Low pressure drop	
Fast actuating design	
Linear Barrel Valve	
Ideal for stroke-limited actuators since multiple holes will allow a relatively substantial amount of flow to be modulated using very minimal stroke	Conceived design requires flow to drastically change direction
Low pressure resistance	High complexity (difficult to model and build)
Low pressure drop	May be prone to clogging based on how small the multiple orifices get
High controllability	Relatively larger device footprint
Fast actuating design	
Barrel Valve w/2 DOF Motion	
Embodies two colinear degrees of freedom for actuation	Complex to machine and assemble as high precision would be required
Ideal for stroke-limited actuators since multiple holes will allow a relatively substantial amount of flow to be modulated using very minimal stroke	High complexity (difficult to model and build) - even more so than the linear barrel valve
Low pressure drop	May be prone to clogging based on how small the multiple orifices get
Fast actuating design	Relatively large device footprint
High controllability - more so than the linear barrel valve since has 2 DOF vs. 1	
DAHENV	
Embodies two degrees of freedom for actuation	Complex to machine and assemble as high precision would be required
Ideal for stroke-limited actuators	Expensive
Compact construction	May be prone to clogging based on how small the multiple orifices get
Expected linear flow	Difficult to actuate
Fast actuating design	
High controllability	
Low pressure drop	
Turbine Throttles	
Low pressure resistance	Expensive to machine or buy acceptable turbines for such an application
Actuator could conceivably be unattached to turbines and therefore out of the flow path	Easy to clog since turbines would be relative small
	Difficult to imlement “fail nominal” requirement
	Difficult to model such a design
	Low controllability

Continued on next page

Table 21 (continued)	
Advantages	**Disadvantages**
Football Valve	
Low resistance and therefore low pressure drop	Expensive to manufacture a football-shaped component
Could be quite compact - small device footprint	Difficult to suspend a football-shaped component within a valve body without making sacrifices to the pressure drop
Fast actuating design	
Easy to model since low complexity	

APPENDIX C

THERMAL ANALYSIS

A primary focus of the thermal analysis performed on the actuator model and summarized in Section 5.3.2 was ultimately to reduce the amount of thermal expansion that occurred by matching as closely as possible the coefficient of thermal expansion (CTE) of all of the materials used in the valve assembly. Therefore, data were gathered on multiple prospects to determine their feasibility in the ACT project. Tables 22 and 23 summarize the data gathered for these materials.

The highlighted rows in both tables represent the materials that looked to be promising, including the Sm_2Co_{17} magnetic material (item 7), copper coil material (item 3), and mild steel keeper material (e.g. AISI 1020 steel - item 6). In addition, a light-weight, high-temperature material is needed to construct the armature to support the coils and provide valve actuation. Properties for many high temperature polymers (items 13-15) along with a machinable ceramic material (item 16) are given in the table. These all have excellent chemical and abrasion resistance. Note that the polymers, although light weight and self-lubricating, have service temperatures (final column) somewhat less than the desired operating temperature of 650°F. Further, the CTE (column 3 of Table 22) is an order of magnitude higher than the keeper material (1020 steel, item 6). Thus the potential for binding exists, once the valve is heated to operating temperature. Using the machinable ceramic (item 16) is a better choice, given that the CTE is better matched (only 15% lower) and the operating temperature is within range (up to 750°F). Further, the thermal conductivity (column 4 in Table 22) is somewhat higher than the polymers, improving heat

Table 22: Properties for various materials being considered for the final valve design.

Item	Material	Coeff. of Thermal Expansion α (1/°C)	Thermal Conductivity Btu-in/ft^2 °F	Electrical Resistivity ohm - cm	Magnetic Permeability	Max. Service Temperature
1	Al	2.300 E-05	1460	2700 E-06		N/A
2	Fe	1.550 E-05	529	8.900 E-06		N/A
3	Cu	1.600 E-05	2670	1.700 E-06		N/A
4	1010 steel	1.370 E-05	360	1.430 E-05		N/A
5	1015 steel	1.320 E-05	360	1.590 E-05		N/A
6	1020 steel	1.300 E-05	360	1.590 E-05		N/A
7	Sm_2Co_{17}	1.300 E-05	70	5.00 E07 – 6.00 E07		N/A
8	430 stainless steel	1.080 E-05	181	6.00 E-05	600 – 1100	N/A
9	403 stainless steel	1.130 E-05	173	5.70 E-05		N/A
10	409 stainless steel	1.190 E-05	173	6.000 E-05		N/A
11	Haynes 230 Alloy	1.300 E-05	62	1.250 E-04		Combustor Matl.
12	304 stainless steel	1.728 E-05	112	7.200 E-05	1 – 8	N/A
13	PTFE (Teflon)	1.350 E-04	1 – 30	1 E10 – 1 E18		550 def F
14	Rulon	1.200 E-04	1.7 – 2.3	1.000 E15		500 def F (if reinforced)
15	PEEK (glass filled)	1.080 E-04	1.75 – 6.7	1 E15 – 2 E16		600 def F (if reinforced)
16	Glass-Mica Ceramic	1.100 E-05	8	1 E10 – 1 E14		750 def F

Table 23: Thermal expansion for each material for 580°F temperature change.

Item	Material	Coeff. of Thermal Expansion α (1/°C)	Thermal Expansion ($\alpha \cdot \Delta$T)	Expansion Difference from Sm_2Co_{17}
1	Al	2.300 E-05	1.33%	0.58%
2	Fe	1.550 E-05	0.90%	0.15%
3	Cu	1.600 E-05	0.93%	0.17%
4	1010 steel	1.370 E-05	0.79%	0.04%
5	1015 steel	1.320 E-05	0.77%	0.01%
6	1020 steel	1.300 E-05	0.75%	0.00%
7	Sm_2Co_{17}	1.300 E-05	0.75%	0.00%
8	430 stainless steel	1.080 E-05	0.63%	-0.13%
9	403 stainless steel	1.130 E-05	0.66%	-0.10%
10	409 stainless steel	1.190 E-05	0.69%	-0.06%
11	Haynes 230 Alloy	1.300 E-05	0.75%	0.00%
12	304 stainless steel	1.728 E-05	1.00%	0.25%
13	PTFE (Teflon)	1.350 E-04	7.83%	7.08%
14	Rulon	1.200 E-04	6.96%	6.21%
15	PEEK (glass filled)	1.080 E-04	6.26%	5.51%
16	Glass-Mica Ceramic	1.100 E-05	0.64%	-0.12%

dissipation from the coils. A particularly fortuitous result is that 1020 steel keeper material (item 6) and Sm_2Co_{17} magnetic material (item 7) each have equivalent CTEs. As a result, these materials will not experience high thermally induced stresses despite being in physical contact with one another. The valve body could be made of stainless steel. The choices in items 8-11 in Table 22 have CTEs similar to that of the Sm_2Co_{17} and 1020 steel. A perfect CTE match can be achieved by making the valve body out of the keeper material. Alternately, if better corrosion resistance is needed, Haynes 230 alloy (item 12) can be used. This material is already used for many high temperature environments, including combustors and other gas turbine components.

The thermal expansion for each material in Table 22 was computed and given in Table 23. The third column again reports the CTE, while the fourth column reports the maximum thermal expansion for the T = 580°F. It is not the total expansion that is important, but rather the relative expansions for each material. As such, the final column in Table 23 compares the thermal expansion of a particular material with the Sm_2Co_{17}. The preferred (highlighted) materials are within 0.17% of the magnetic material. Only the copper is 0.17%, which is somewhat inconsequential given that the copper will be wound around the mandrel such that thermal stresses will likely not result. The next highest relative expansion for the preferred materials is for the glass-mica ceramic at -0.12%. If this material is selected for the armature, then the clearance for the inner diameter should be high enough to account for this relative contraction. For example, if the inner diameter of the armature is 0.75 inches, the relative contraction would be: -0.0012 0.75 = -0.0009 inches. Thus, less than one mil of additional clearance is required for thermal expansion considerations. In contrast, using PTFE (Teflon) would require additional clearance in the outer dimension of the armature, given the positive relative expansion of 7.08% (although the material can't operate at 650°F). For illustrative purposes, if the armature has an outer diameter of 1 inch, the relative expansion is: 0.0708 0.75 = 53.1 mils.

The flowchart seen in Figure 69 is meant to be used in conjunction with Section 3.3.3.1 and 3.3.3.1 in order to find the convective heat transfer coefficients, h. As previously mentioned, this flowchart is specifically tailored for the the analysis conducted in the ACT project thermal analysis. Additional checks and formulations of the dimensionless parameters mentioned throughout exist for different situations and conditions.

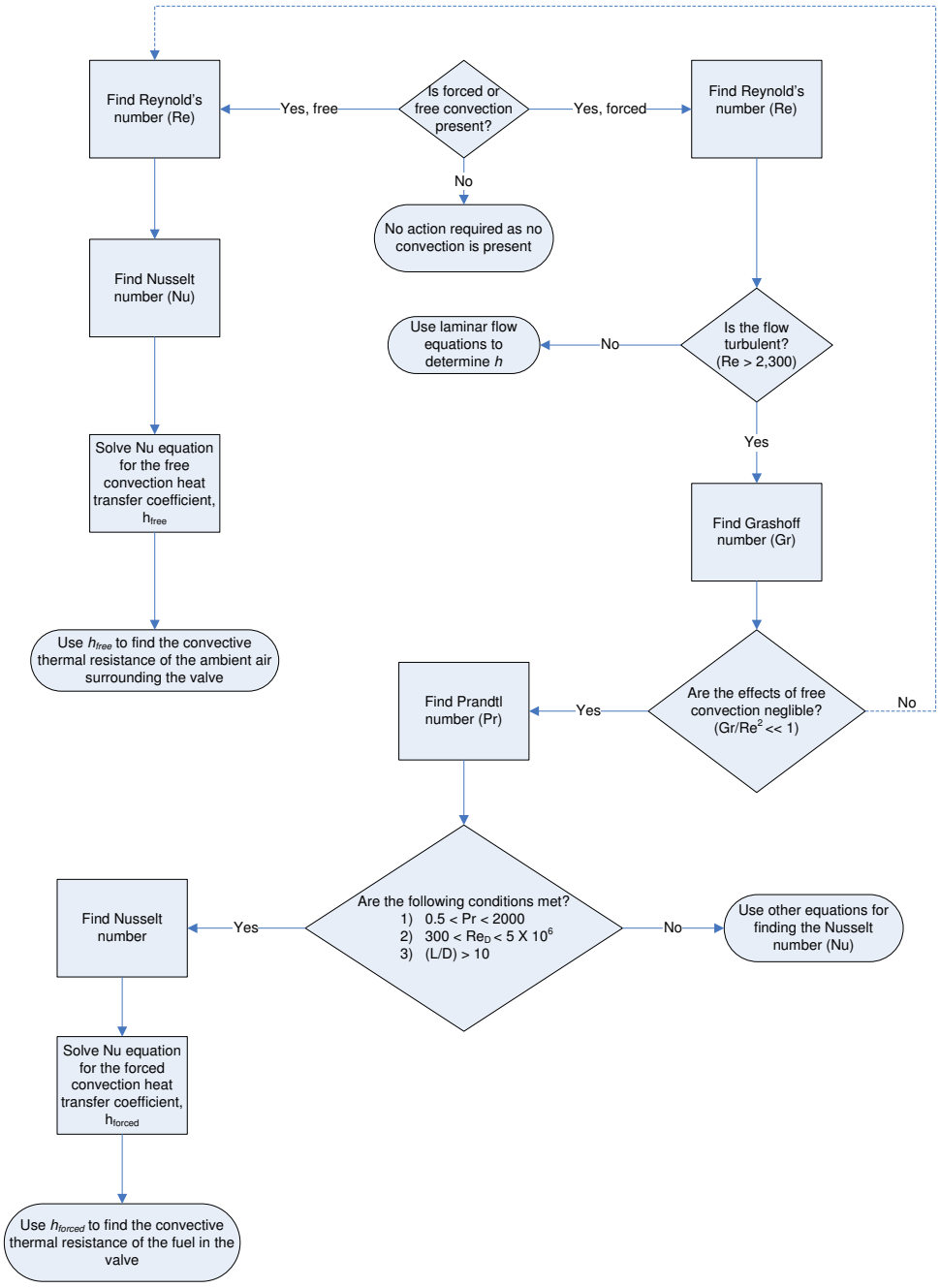

Figure 69: Flowchart summarizing the process of finding convective heat transfer coefficients for the ACT valve.

APPENDIX D

ACTUATOR DECISION MATRIX SUMMARY

One tool used to determine feasibility of actuator designs early in the design process is an evaluation matrix. This matrix includes a myriad of features vital to the actuator design and ranks each feature for each design. This tool was used largely in a subjective context, where each member of the design team ranked the features based on knowledge and intuition. Table 24 summarizes the results from all group members that completed the evaluation matrix, while Table 25 gives a description for the comment codes in Table 24. The desired actuation features can be seen as the row headings in Table 24, while the actuation technologies can be seen as the column headings. Each feature was ranked on a scale of 1 to 3, where 1 is very unfavorable performance and 3 is very favorable performance. The final row in Table 24 gives the total score for each actuation technology (higher is better). The dark green shading in the "total" row indicates technologies that were to be further investigated, while the lighter green shading represents the technologies that could possibly still be viable options should the dark green shaded designs fail. Although many technologies had high scores (¿20), only the leftmost three columns are high-temperature technologies. No shading represents the technologies that were believed to not be viable options in any case. The various actuation technologies are discussed at greater lengths in the white paper on valve and actuation technologies produced for NETL [42].

Table 24: Results of evaluation matrix for actuator design.

	SmCo Motor	Pneumatic Actuators	Chemical	Piezoelectric	Servo Motors	Solenoids no PM	Stepper Motors w/PM	Piezo Ultrasonic, etc.	Electrostrictive	Hydraulic Actuators	Piezo Flexure	Magnetostrictive	Magnetorheological	Electrorheological
	High Temp			Low Temp									Act/Pass	
Force/Torque	2.3	2.0	3.0	3.0	2.3	2.0	2.0	2.5	2.8	2.8	2.0	3.0	1.5	1.5
Energy Density	2.7	1.3	3.0	2.7	2.0	1.7	2.3	2.5	2.5	2.7	2.0	3.0	1.0	1.0
Stroke/Throw	3.0	3.0	3.0	1.0	3.0	3.0	3.0	2.0	1.5	3.0	1.7	1.3	1.5	1.5
Bandwidth	2.0	1.7	1.7	3.0	1.7	2.0	2.3	2.5	3.0	1.7	2.7	2.3	2.5	2.5
Cost	1.7	2.3	1.3	2.3	2.7	2.7	2.0	1.5	1.5	1.3	1.7	1.7	2.0	2.0
Simplicity	2.7	1.3	1.0	2.7	2.7	2.7	2.3	1.5	2.0	1.0	2.0	1.3	1.0	1.0
Linearity	3.0	2.3	1.3	3.0	3.0	2.7	2.3	2.5	1.5	1.3	3.0	2.0	1.0	1.0
Convenience	3.0	1.0	1.0	2.3	3.0	3.0	2.3	2.2	2.5	1.0	2.0	2.0	1.5	1.0
Temp	3.0	3.0	1.7	1.0	1.7	2.0	1.7	1.0	1.5	1.3	1.0	1.0	0.3	0.7
Comment		A		T			N			F,H			D,P	D,P
Total	23	18	17	21	22	22	20	19	19	16	18	18	12	12

Table 25: Descriptions of comments used in actuator design evaluation matrix.

Comment	Description
A	Would require air supply and controls.
D	Actively tuned variable dissipation mechanisms.
F	Flammable.
H	Would require hydraulic fluid supply and controls. Hydraulic systems are nonlinear.
N	Could be made high temperature.
P	These are passive devices in terms of force/stroke. Cannot do positive work on the system.
T	There is a new "Thermiezo" material reported, but it's not available; still stroke limited.

APPENDIX E

ELECTROMAGNETIC FORCE ANALYSIS RESULTS

The individual electromagnetic force versus applied coil current plots produced from the electromagnetic force analysis can be seen in Figures 70 - 81. All of these plots were created from data obtained using the threshold dimensions shown in Table 10. Ansoft Maxwell® 2D [37] FEA software was used exclusively for all of the electromagnetic analysis that yielded these figures.

As previously mentioned, all actuator configurations and magnet size combinations demonstrated a linear relationship between actuator force produced (the dependent, y-axis) and the applied coil current (the independent, x-axis). This was an expected result and further confirms that the threshold dimensions determined for the keeper do in fact reduce saturation to a minimal value. For direct comparison of all magnet configurations for a given magnet size, refer to Figures 48, 49 and 50 for thicknesses of 1/8," 1/4" and 1/2," respectively.

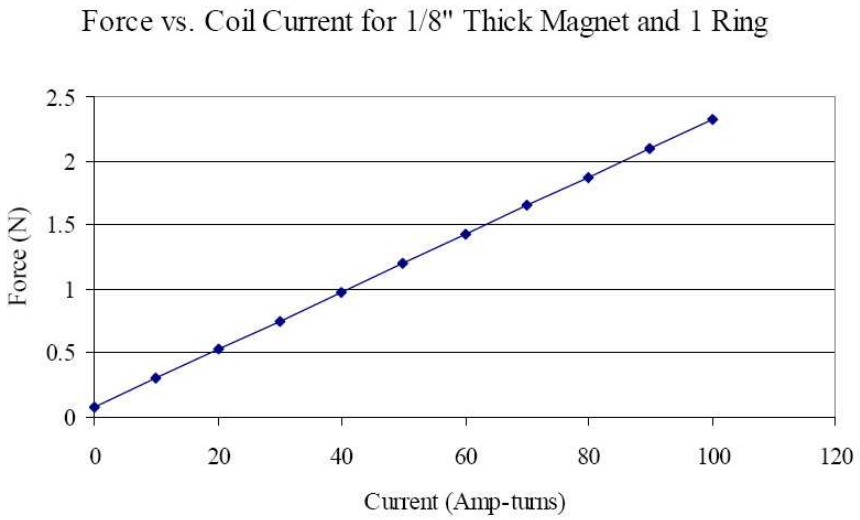

Figure 70: Plot of force vs. applied coil current for 1/8" thick magnets with one ring.

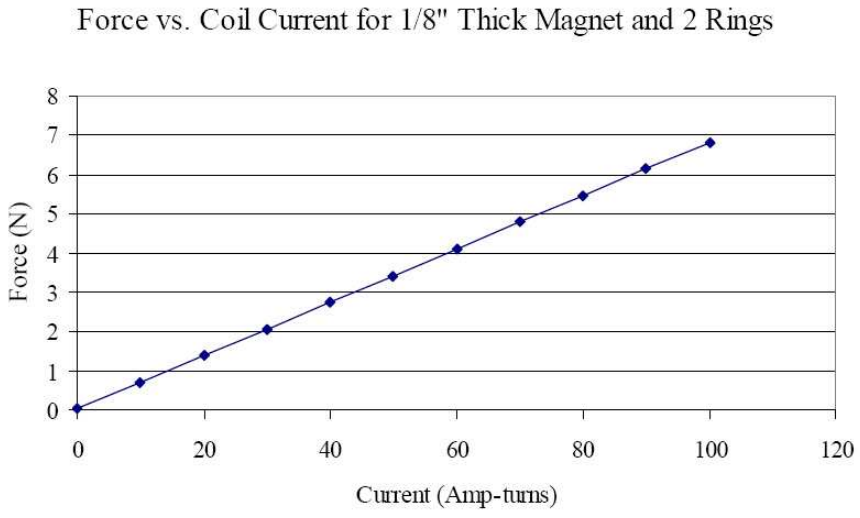

Figure 71: Plot of force vs. applied coil current for 1/8" thick magnets with two rings.

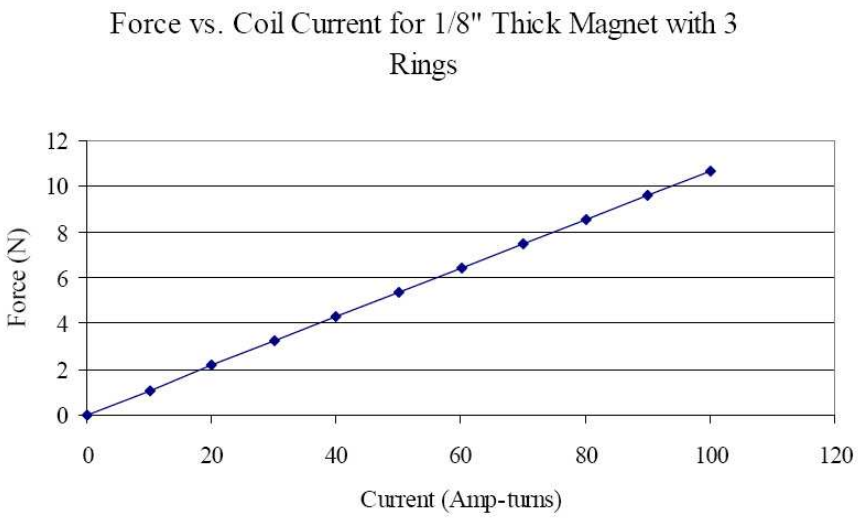

Figure 72: Plot of force vs. applied coil current for 1/8" thick magnets with three rings.

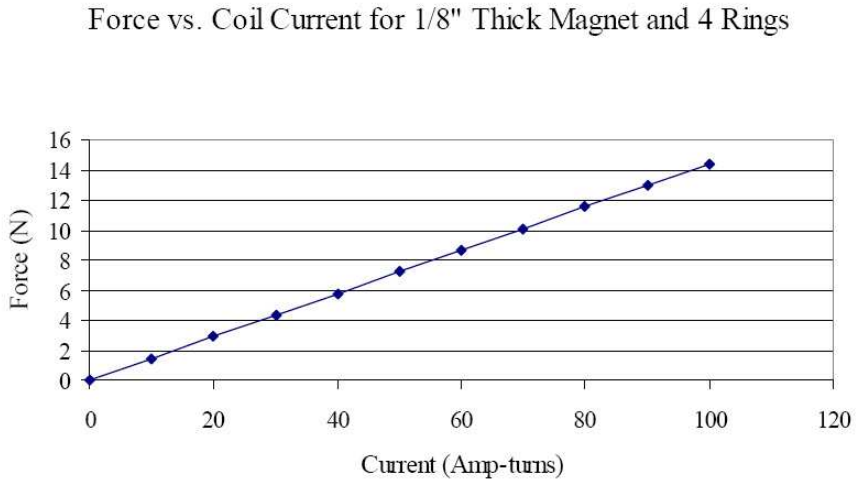

Figure 73: Plot of force vs. applied coil current for 1/8" thick magnets with four rings.

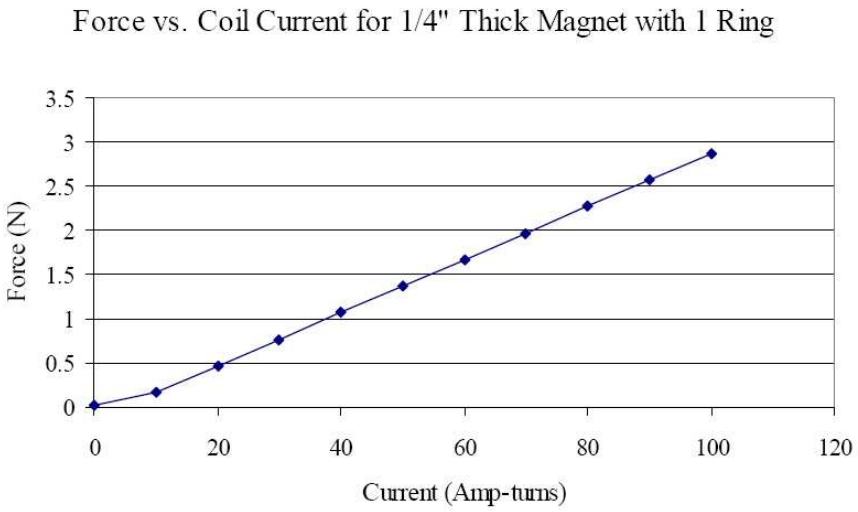

Figure 74: Plot of force vs. applied coil current for 1/4" thick magnets with one ring.

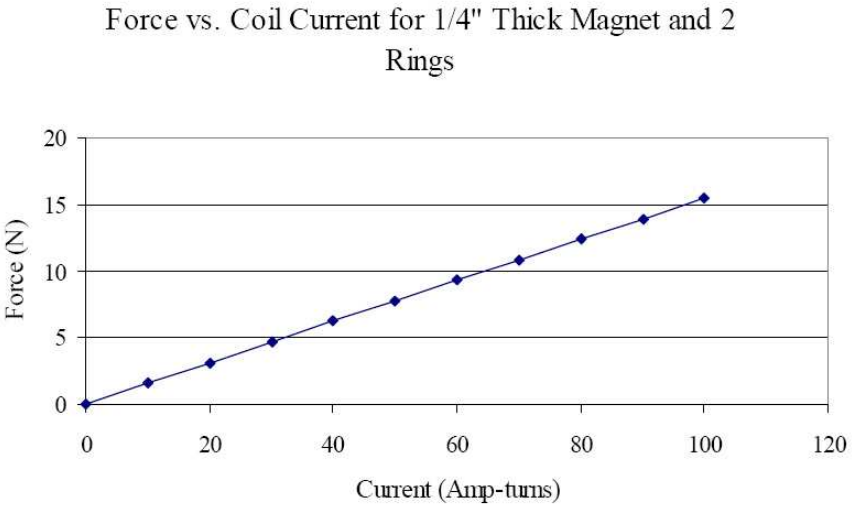

Figure 75: Plot of force vs. applied coil current for 1/4" thick magnets with two rings.

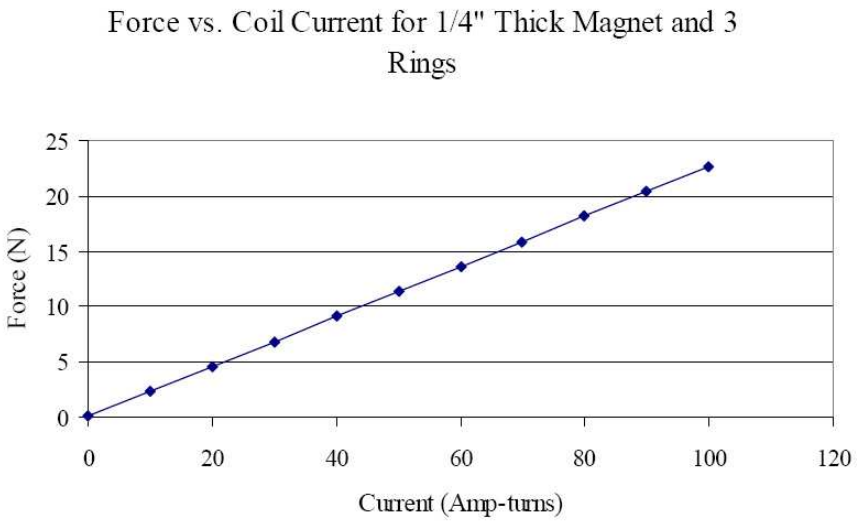

Figure 76: Plot of force vs. applied coil current for 1/4" thick magnets with three rings.

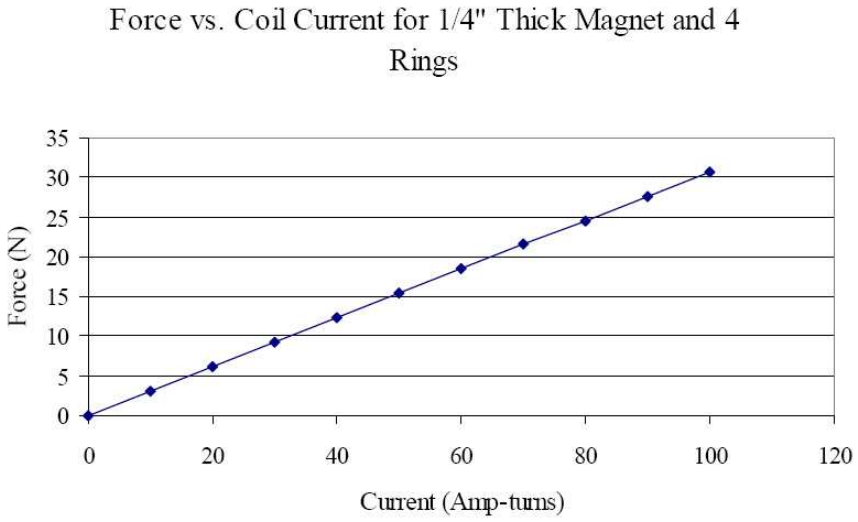

Figure 77: Plot of force vs. applied coil current for 1/4" thick magnets with four rings.

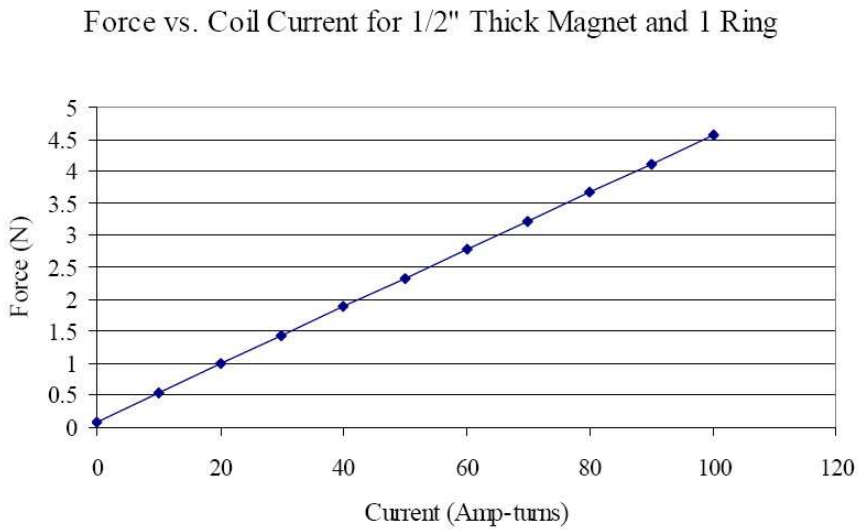

Figure 78: Plot of force vs. applied coil current for 1/2" thick magnets with one ring.

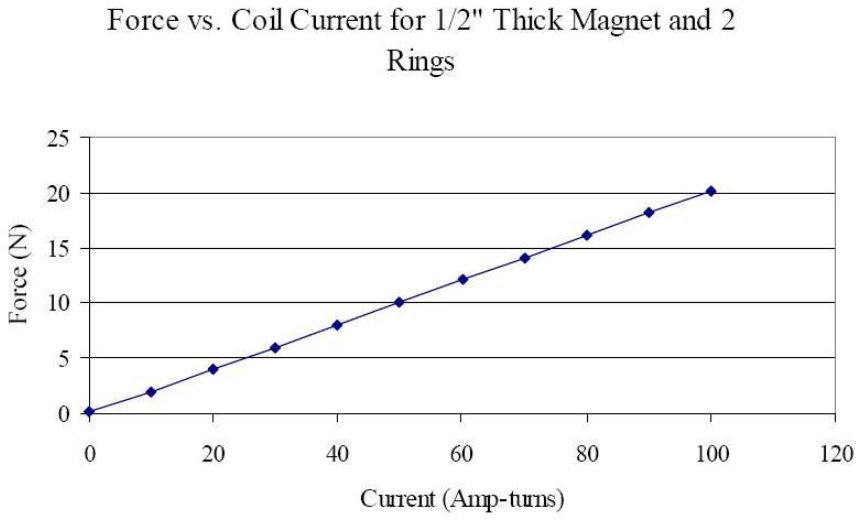

Figure 79: Plot of force vs. applied coil current for 1/2" thick magnets with two rings.

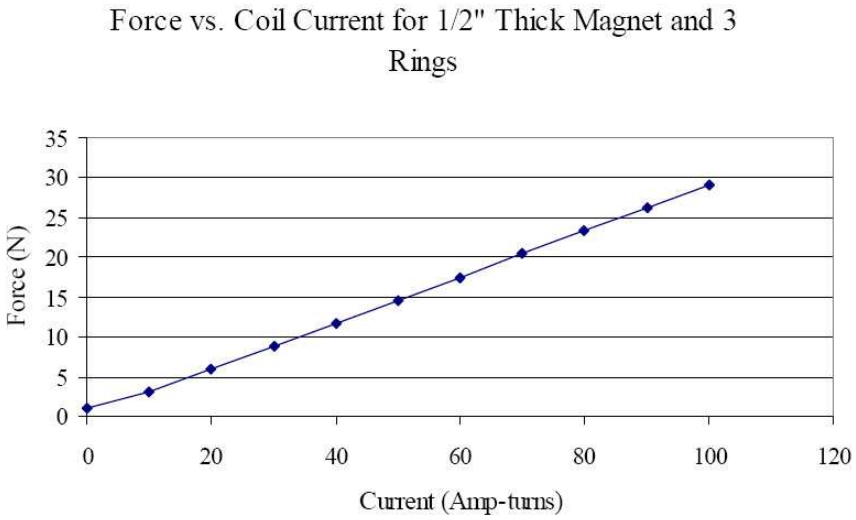

Figure 80: Plot of force vs. applied coil current for 1/2" thick magnets with three rings.

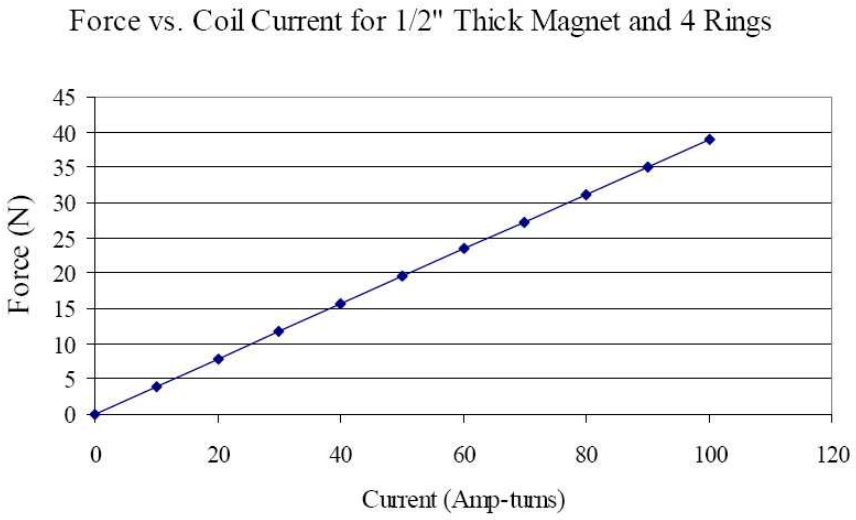

Figure 81: Plot of force vs. applied coil current for 1/2" thick magnets with four rings.

APPENDIX F

VALVE DECISION MATRIX SUMMARY

Similar to the actuator evaluation matrix explained in Appendix D, an evaluation matrix for the valve design was implemented. Features of the valves were subjectively (albeit, based on knowledge) ranked by the ACT project team and tabulated in order to determine which technologies merited further investigation. Table 26 summarizes the valve evaluation matrix.

The features of the valves are given in the row headings in Table 26 and the valve types are given in the column headings. The yellow fill in three of the row headings indicate the perceived most crucial features of the valves considered. The features were each ranked on a scale of 1 to 3, 1 being very unfavorable performance and 3 being very favorable performance in the corresponding metric. The final two rows indicate the totals of the rankings for each valve. The upper row includes objective/subjective information from a valve design handbook and the latter row does not. The dark green shading indicates the technologies that fared most favorably and merit further research, while the light green shading indicates "back-up" valve technologies that were still considered possibilities for further research. The light yellow shading indicates technologies that scored lower than the dark and light green valve types, but that still may be viable. The two highest rated valve designs are the barrel valve and the globe valve. These valves, along with the other valves listed in Table E.1, are presented in greater detail in the white paper on actuation and valve technologies [42].

Table 26: Results of evaluation matrix for valve design.

	Needle Valve	Linear Barrel Valve	Gate Valve w/2 Gates	Butterfly Valve	Globe Valve	Multi-Orifice Plate Valve (MOV)	DAHENV	MOV Gate Valve Linear Flow	Thunder-Like Valve	Gate Valve w/1 Gate	Constricting Pinch Valve (CFP Valve)	Single-Orifice Valve (F. Cell Valve)	MOV Gate Valve Non-Linear Flow	Turbine Throttles	Barrel Valve w/2 DOF Motion	Ball Valve
Complexity/Machniability	1.5	1.8	1.8	2.5	2.0	1.8	1.3	1.0	2.3	1.6	1.5	1.6	1.3	1.0	1.3	1.8
Cost	1.5	2.1	2.0	2.5	2.0	1.9	1.3	1.3	2.0	2.1	1.5	2.0	1.3	1.1	1.5	1.8
Erosion Resistance	2.0	2.0	2.0	1.8	2.3	2.3	1.8	1.8	2.0	1.5	2.0	1.3	1.5	1.3	1.5	2.0
Expected Noise/Vibration	2.0	2.3	2.3	2.3	2.0	2.3	1.8	2.0	2.5	1.5	2.8	1.8	1.5	1.5	2.0	2.5
Size	2.8	1.5	1.8	2.0	2.5	1.5	2.8	2.0	1.8	1.8	2.5	1.8	1.8	2.3	2.3	2.0
Ease of Actuation	2.3	2.5	1.8	1.6	2.3	2.0	1.8	2.3	1.8	2.0	2.0	1.8	2.3	2.5	2.8	2.0
Expected Linearity	2.8	2.3	2.3	2.0	2.5	2.3	2.8	2.8	2.0	1.8	2.0	2.0	1.8	2.0	2.0	1.3
Temperature Resistance	2.3	2.3	2.8	2.8	2.3	1.8	2.3	2.3	1.8	2.3	2.0	2.0	2.0	2.5	2.0	2.5
Pressure Resistance	2.0	3.0	2.8	1.8	2.8	3.0	2.3	2.5	1.5	2.1	2.3	1.8	2.3	3.0	2.5	2.3
Speed of Actuation	2.5	2.8	1. 3	2.3	2.5	2.8	2.8	2.8	2.3	1.8	1.5	2.8	2.8	1.1	2.5	2.0
Modeling Complexity	1.8	1.8	2.3	2.3	2.0	2.3	1.8	1.3	2.3	2.5	1.5	1.5	1.5	2.0	1.8	2.0
(Throttling) Controllability	3.0	3.0	1.8	2.3	3.0	2.5	3.0	2.5	1.8	2.0	2.0	2.8	2.3	1.5	2.5	1.8
Fail Nominally	2.3	2.8	2.0	1.0	1.5	2.8	2.3	2.0	2.5	2.0	2.0	2.8	2.0	1.8	2.0	1.0
Pressure Drop of 10 psi	2.5	2.8	3.0	2.5	2.8	2.5	2.5	2.5	3.0	3.0	2.5	2.0	2.5	2.5	2.5	2.8
Total	31	33	30	29	32.3	31	30	29	29	28	28	27.6	26.5	26	29	28
With/out "BOOK" (Pete's)	29	32	29	28	32.3	31	30	28	29	28	28	27.8	26.3	26	30	28

APPENDIX G

MANUAL STRESS ANALYSIS RESULTS

As discussed in Section 5.2.5.1, the stresses for all prototype valve components were manually calculated using simplified loading scenarios and geometry by the von Mises criterion equations, Equations 3.3 – 3.6. A complete listing of the values used for the manual stress calculations can be seen in Tables 27 – 30. Descriptions of all variables are listed in both Table 29 and 27. For more explanation, refer to Equations 3.3 – 3.6.
The simplified valve component models used for the manual stress analysis (as well for validation of the FEA analysis) can be seen in Appendix H, Figures 82 – 86 for the TV1 prototype design (seen in Figure 55)and Figures 87 – 91 for the TV3 prototype design (seen in Figure 54).
It is important to note that for all manual analyses, no longitudinal forces were considered due to the fact that Equations 3.3 – 3.6 do not take into account radial forces. For example, the chamfered ends of both manual actuators have provided a longitudinal component of force as well as a radial component of force when pressure is applied to the face. Therefore, as the simplest loading scenarios were considered for FEA software validation, only non-chamfered surfaces were assumed to be loaded with a static pressure of 240 psi for all calculations. No chamfered ends or angled sections (e.g. the angled sections seen in the inlet casings, Appendix H, Figures 84 and 89) were considered to have pressure applied to them.

Table 27: Summary of manual stress analysis results for internal components of TV1 prototype design.

		TV1(see Figure 55)			
		Manual Actuator		Mock Armature	
		Single X-Sec.		Single X-Sec.	
Variable	**Description**	Inner	Outer	Inner	Outer
a (in.)	inner radius	0.25	0.25	0.50	0.50
b (in.)	outer radius	0.50	0.50	0.625	0.625
r (in.)	evaluation radius	0.25	0.50	0.50	0.625
p_1 (psi)	inner pressure	240	240	240	240
p_2 (psi)	outer pressure	0	0	0	0
P (lbf)	longitudinal force	0	0	0	0
σ_{rr} (psi)	radial stress	-240	0	-240	0
$\sigma_{\theta\theta}$ (psi)	tangential stress	400.00	160.00	1093.33	853.33
σ_{zz} (psi)	longitudinal stress	0	0	0	0
σ_{Mises} (psi)	von Mises stress	560.00	160.00	1231.01	853.33

Table 28: Summary of manual stress analysis results for casing components of TV1 prototype design.

	TV1 (see Figure 55)											
	Inlet Casing				Outlet Casing				Middle Casing			
	Thin X-Sec.		Thick X-Sec.		Thin X-Sec.		Thick X-Sec.		Thin X-Sec.		Thick X-Sec.	
Variable	Inner	Outer	Inner	Outer	Inner	Outer	Inner	Outer	Inner	Outer	Inner	Outer
a (in.)	1.43	1.43	0.25	0.25	0.80	0.80	0.50	0.50	1.01	1.01	0.63	0.63
b (in.)	1.75	1.75	1.75	1.75	1.75	1.75	1.75	1.75	1.43	1.43	1.75	1.75
r (in.)	1.43	1.75	0.25	1.75	0.80	1.75	0.50	1.75	1.01	1.43	0.63	1.75
p_1 (psi)	240	240	240	240	240	240	240	240	240	240	240	240
p_2 (psi)	0	0	0	0	0	0	0	0	0	0	0	0
P (lbf)	0	0	0	0	0	0	0	0	0	0	0	0
σ_{rr} (psi)	-240	0	-240	0	-240	0	-240	0	-240	0	-240	0
$\sigma_{\theta\theta}$ (psi)	1204.58	964.58	250.00	10.00	366.81	126.81	282.67	42.67	717.80	477.80	478.92	71.47
σ_{zz} (psi)	0	0	0	0	0	0	0	0	0	0	0	0
σ_{Mises} (psi)	1340.78	964.58	424.38	10.00	529.33	126.81	453.15	42.67	863.20	477.80	478.92	71.47

Table 29: Summary of manual stress analysis results for internal components of TV3 prototype design.

		TV3 (see Figure 54)					
		Manual Actuator				Mock Armature	
		Thin X-Sec.		Thick X-Sec.		Single X-Sec.	
Variable	**Description**	Inner	Outer	Inner	Outer	Inner	Outer
a (in.)	inner radius	0.25	0.25	0.25	0.25	0.39	0.39
b (in.)	outer radius	0.39	0.39	0.50	0.50	0.50	0.50
r (in.)	evaluation radius	0.25	0.39	0.25	0.50	0.39	0.50
p_1 (psi)	inner pressure	240	240	240	240	240	240
p_2 (psi)	outer pressure	0	0	0	0	0	0
P (lbf)	longitudinal force	0	0	0	0	0	0
σ_{rr} (psi)	radial stress	-240	0	-240	0	-240	0
$\sigma_{\theta\theta}$ (psi)	tangential stress	574.82	334.82	400.00	160.00	985.75	745.75
σ_{zz} (psi)	longitudinal stress	0	0	0	0	0	0
σ_{Mises} (psi)	von Mises stress	725.24	334.82	560.00	160.00	1125.11	745.74

Table 30: Summary of manual stress analysis results for casing components of TV3 prototype design.

	TV3 (see Figure 54)											
	Inlet Casing				Outlet Casing				Middle Casing			
	Thin X-Sec.		Thick X-Sec.		Thin X-Sec.		Thick X-Sec.		Thin X-Sec.		Thick X-Sec.	
Variable	Inner	Outer	Inner	Outer	Inner	Outer	Inner	Outer	Inner	Outer	Inner	Outer
a (in.)	0.90	0.90	0.25	0.25	0.74	0.74	0.50	0.50	0.90	0.90	0.50	0.50
b (in.)	1.25	1.25	1.25	1.25	1.25	1.25	1.25	1.25	1.25	1.25	1.25	1.25
r (in.)	0.90	1.25	0.25	1.25	0.74	1.25	0.50	1.25	0.90	1.25	0.50	1.25
p_1 (psi)	240	240	240	240	240	240	240	240	240	240	240	240
p_2 (psi)	0	0	0	0	0	0	0	0	0	0	0	0
P (lbf)	0	0	0	0	0	0	0	0	0	0	0	0
σ_{rr} (psi)	-240	0	-240	0	-240	0	-240	0	-240	0	-240	0
$\sigma_{\theta\theta}$ (psi)	751.94	511.94	260.00	20.00	498.99	258.99	331.43	91.43	756.68	516.68	331.43	91.43
σ_{zz} (psi)	0	0	0	0	0	0	0	0	0	0	0	0
σ_{Mises} (psi)	896.37	511.94	433.13	20.00	652.95	258.99	496.98	91.43	900.98	516.68	496.98	91.43

APPENDIX H

SIMPLIFIED VALVE COMPONENTS FOR MANUAL STRESS ANALYSIS AND FEA VALIDATION

To allow a comparison between the manual stress analysis and the stress FEA, simplified component models were considered. Since the components were all considered to be relatively simple, thick-walled cylinders, all but the flow plugs for both prototype valve designs were included in a simplified form. The simplified component models for the TV1 valve prototype can be seen in Figures 82 – 86, while the simplified components models for the TV3 valve prototype can be seen in Figures 87 – 91. For dimensions of each radial dimension, refer to Tables 27 – 30 in Appendix G.

All simplified models were considered to be constrained at one end of the component (the mock armatures and the manual actuators) or along the threaded sections (all three

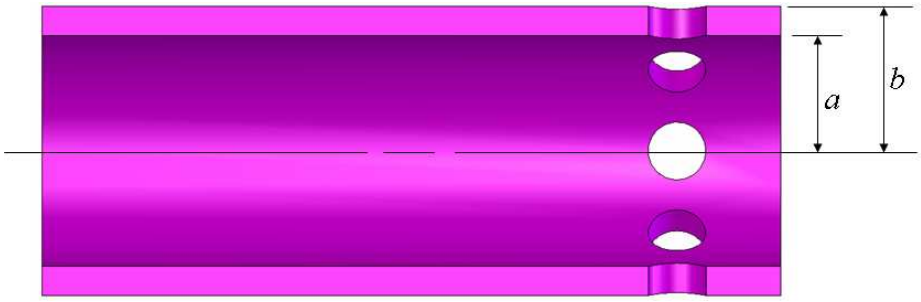

Figure 82: Cross section of simplified mock armature component for TV1.

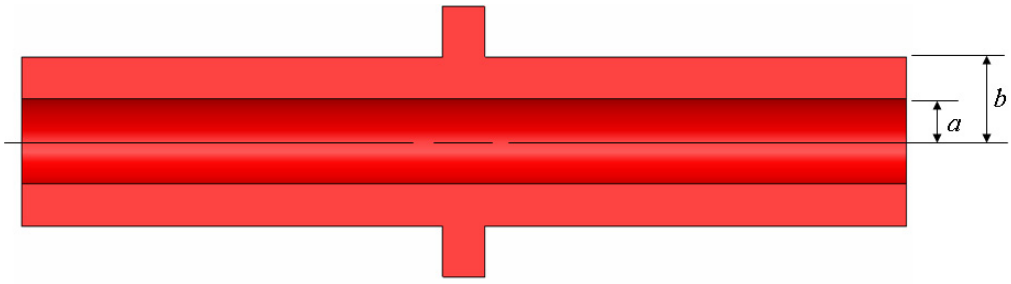

Figure 83: Cross section of simplified manual actuator component for TV1.

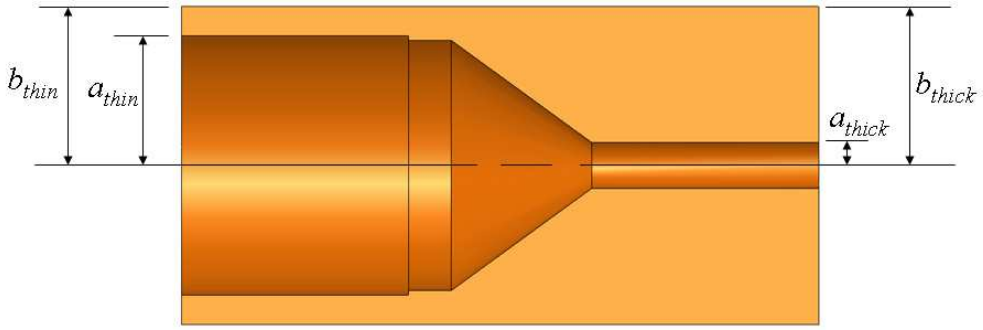

Figure 84: Cross section of simplified inlet casing component for TV1.

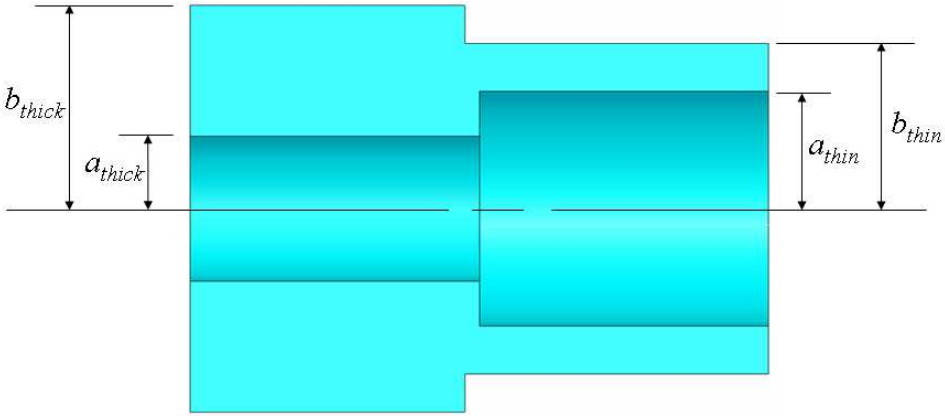

Figure 85: Cross section of simplified middle casing component for TV1.

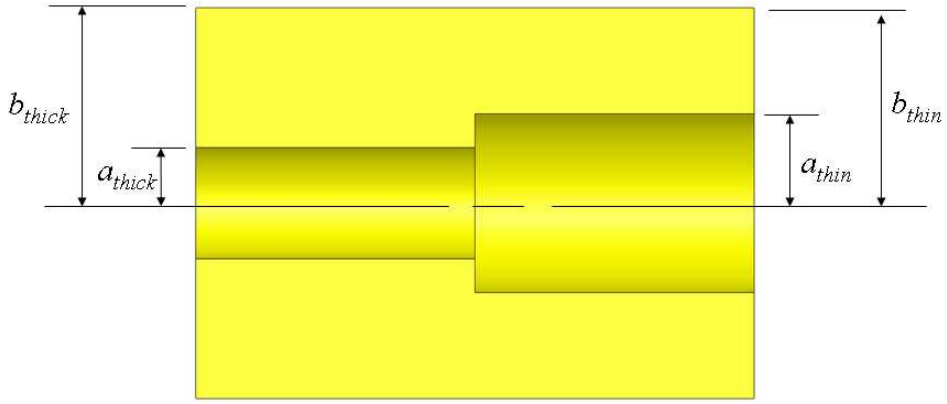

Figure 86: Cross section of simplified outlet casing component for TV1.

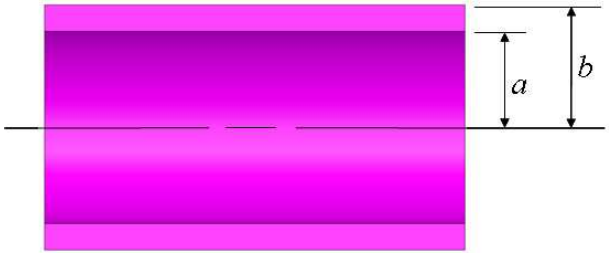

Figure 87: Cross section of simplified mock armature component for TV3.

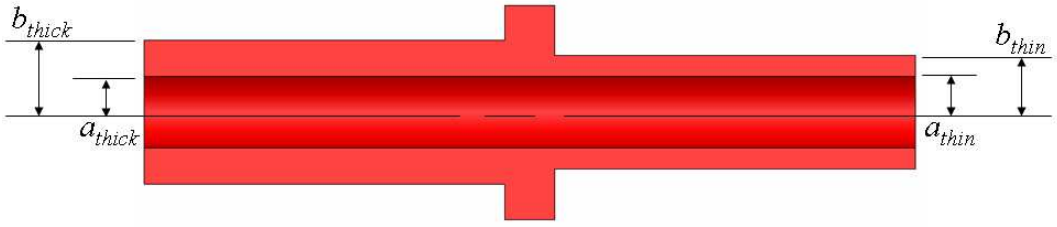

Figure 88: Cross section of simplified manual actuator component for TV3.

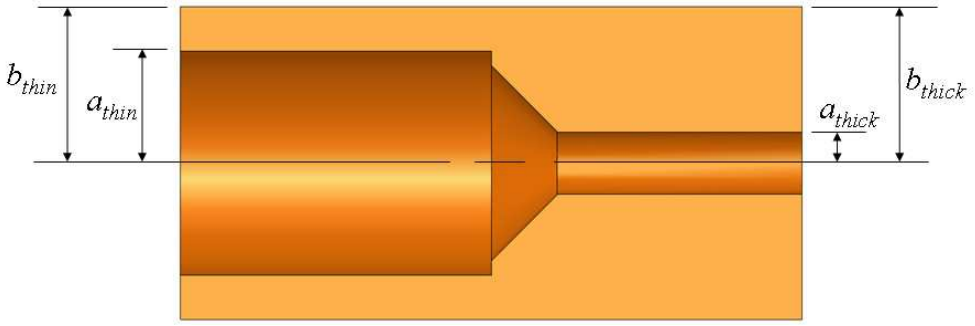

Figure 89: Cross section of simplified inlet casing component for TV3.

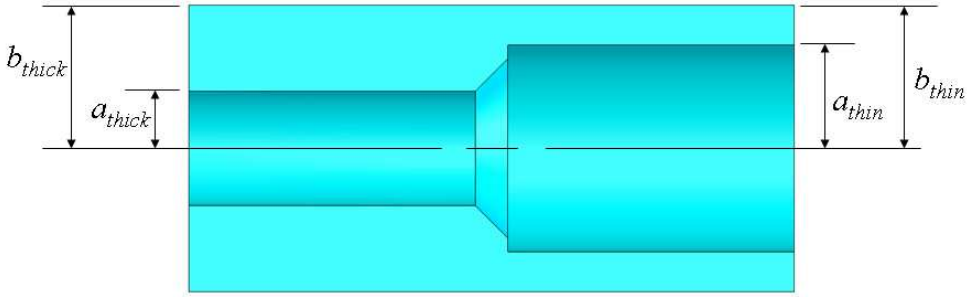

Figure 90: Cross section of simplified middle casing component for TV3.

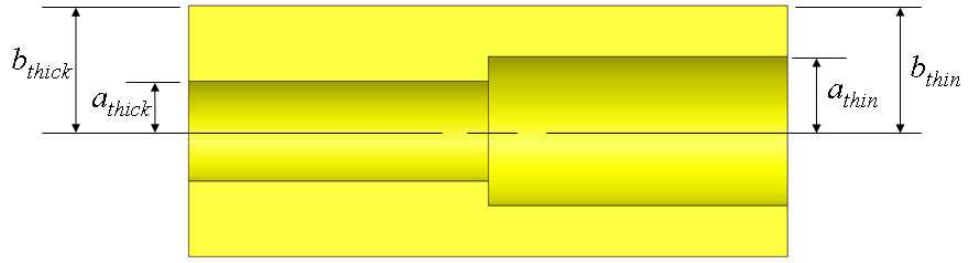

Figure 91: Cross section of simplified outlet casing component for TV3.

casings: inlet, middle and outlet) for the stress FEA. For these simplified models, the threads were approximated as smooth surfaces since other stress analyses were used to consider the thread stress.

Please note that several components (e.g. the outlet casings, Figures 86 and 91) were elongated in order to take into account Saint-Venant's Principle (refer to Section 3.2.3 for a summary). In short, the components need be long enough in order for the stress at an appreciable distance away from the constrained end to be approximately the same for an identical component with a differing end constraint. Since some of the simplified components were simply to short to apply Saint-Venant's Principle, these components were simply elongated for the sake of comparing manual stress analysis and stress FEA results.

APPENDIX I

PROTOTYPE VALVE STRESS FEA

The stress distributions for the FEA of the assemblies as well as the components of both prototype valve designs cannot easily be tabulated. Therefore, Figures 92 - 107 are very useful in determining the high-stress areas in each component. The provided cross sections of all components and assemblies lend extra insight into the reactions within each entity. Note that the FEA of individual components displays higher stress levels compared to the assembly figures (Figures 92, 93, 100 and 101). This is due to the fact that the FEA performed on the individual components was an extremely conservative one consisting of only a single restraint for each component when there were actually multiple constraints on some of the components (such as the mock armatures and manual actuators).
It is important to note some of the technical specifications of SolidWorks® COSMOSWorks FEA package [38]. COSMOSWorks uses a four-point tetrahedral solid element for meshing and two different solvers: a direct solver and an iterative solver. For all of the FEA performed on the valve assemblies and components, an automated feature was used that chooses the solver type based on several parameters of the analysis being conducted (e.g. number of elements, number of degrees of freedom, material properties, etc.). The automated feature also chose the solid element side length as well by an iterative approach.

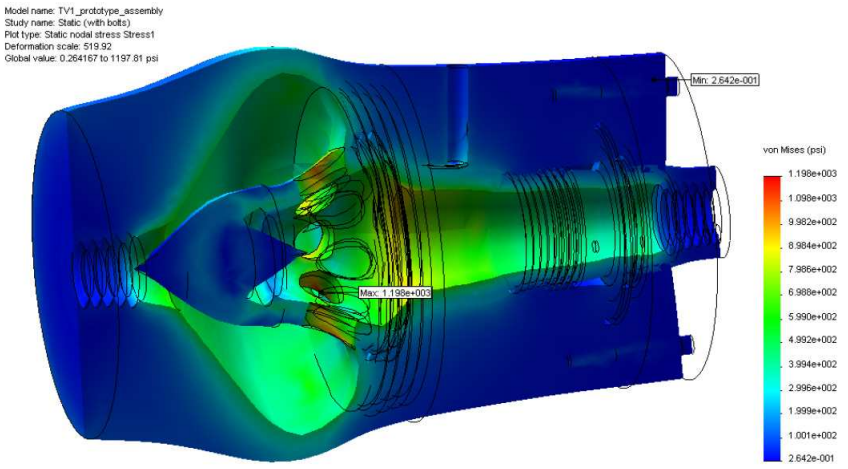

Figure 92: Stress FEA results using SolidWorks® for assembled TV1 prototype, fully open.

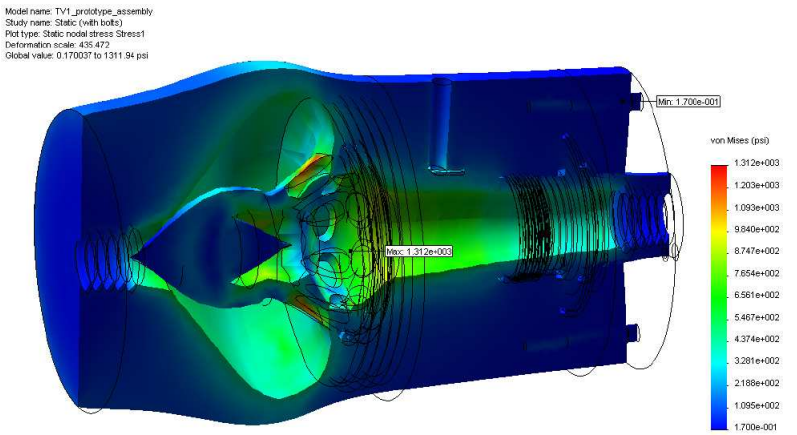

Figure 93: Stress FEA results using SolidWorks® for assembled TV1 prototype, fully closed.

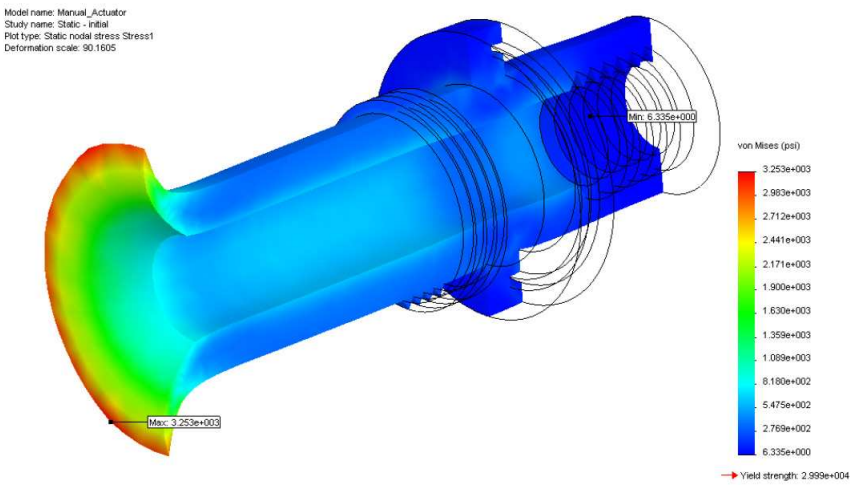

Figure 94: Stress FEA results using SolidWorks® for TV1 actuator.

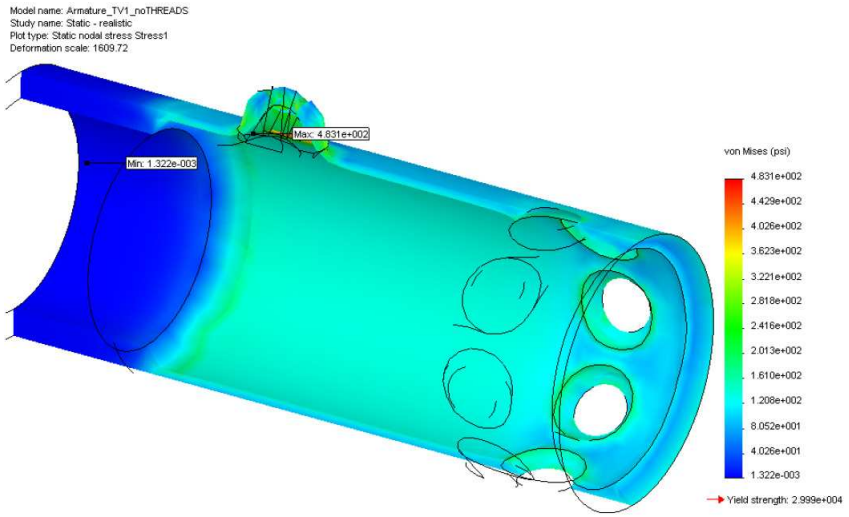

Figure 95: Stress FEA results using SolidWorks® for TV1 armature.

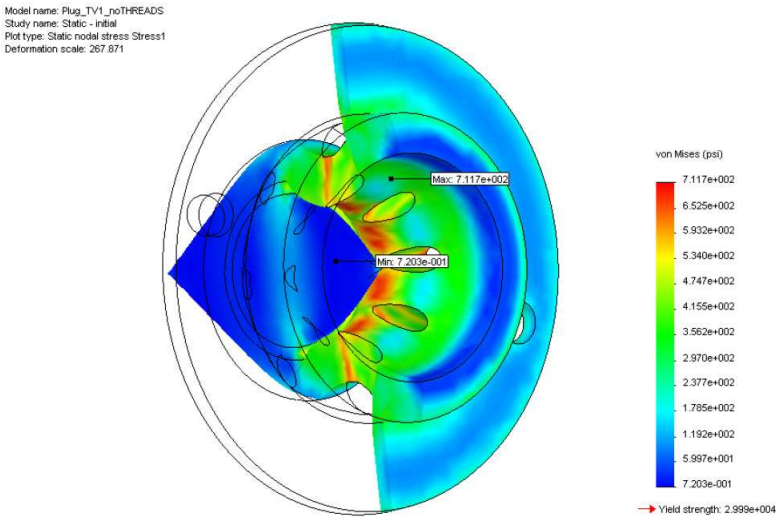

Figure 96: Stress FEA results using SolidWorks® for TV1 barrel flow plug.

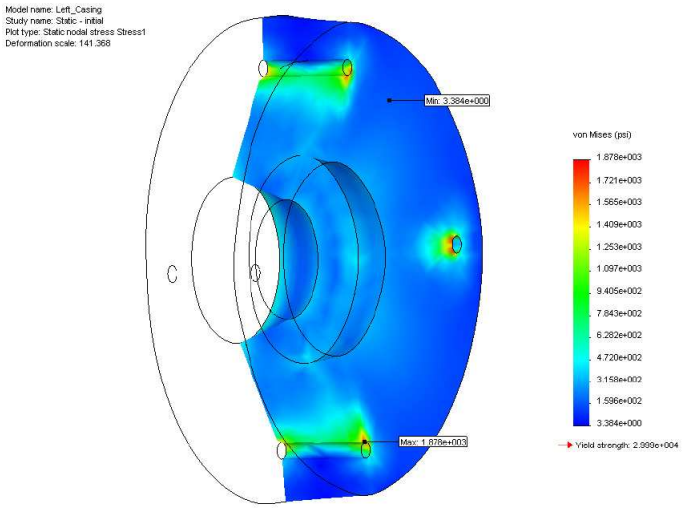

Figure 97: Stress FEA results using SolidWorks® for TV1 outlet casing.

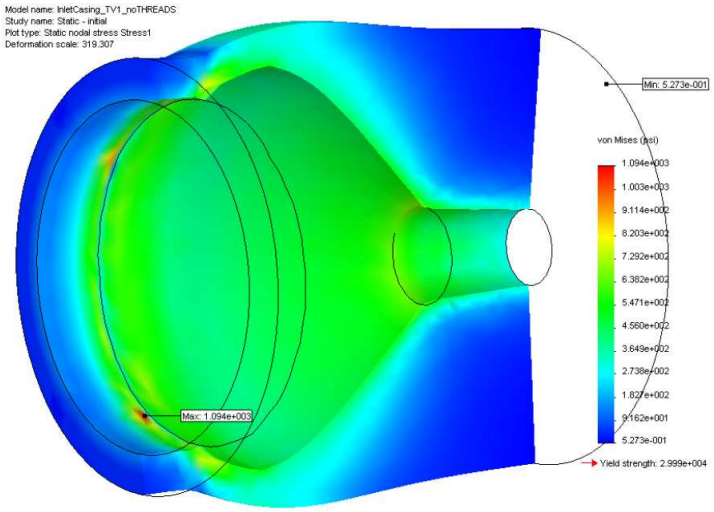

Figure 98: Stress FEA results using SolidWorks® for TV1 inlet casing.

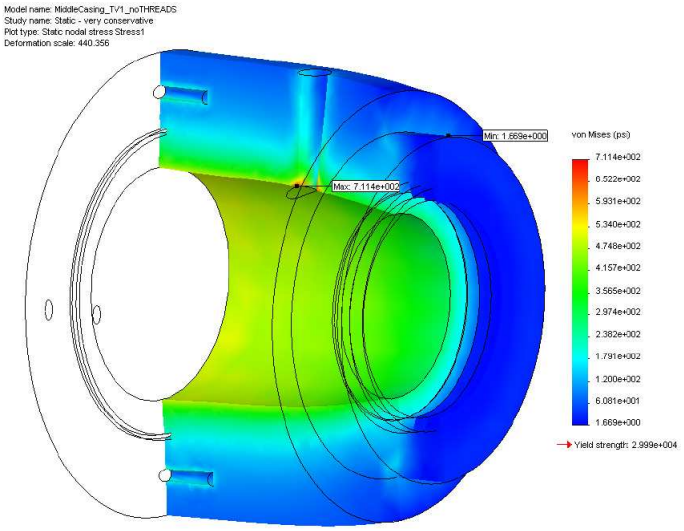

Figure 99: Stress FEA results using SolidWorks® for TV1 middle casing.

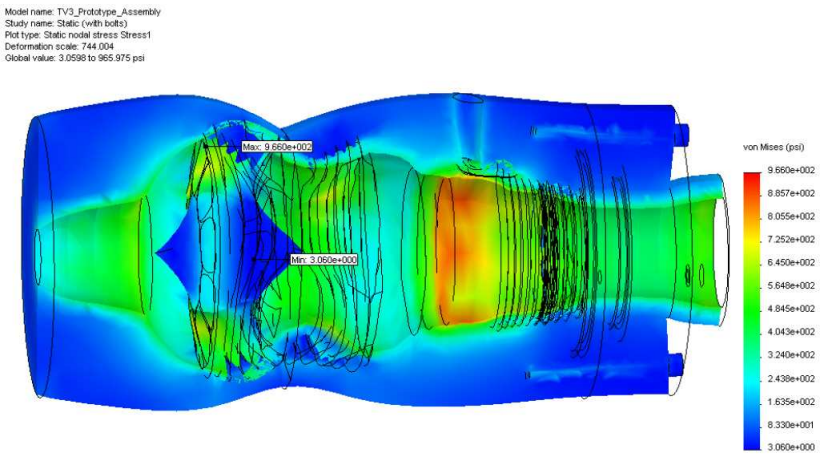

Figure 100: Stress FEA results using SolidWorks® for assembled TV3 prototype, fully open.

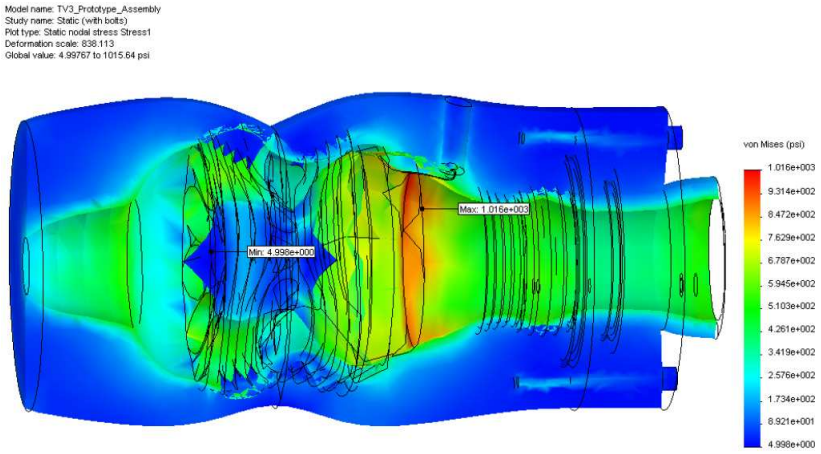

Figure 101: Stress FEA results using SolidWorks® for assembled TV3 prototype, fully closed.

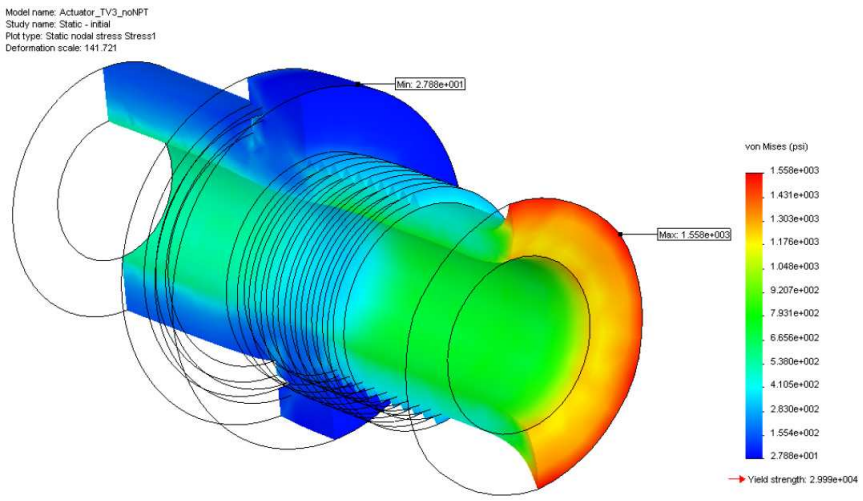

Figure 102: Stress FEA results using SolidWorks® for TV3 actuator.

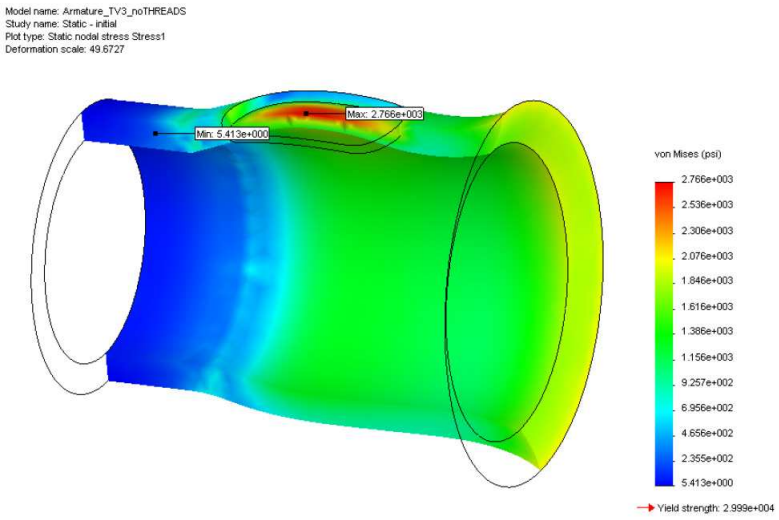

Figure 103: Stress FEA results using SolidWorks® for TV3 armature.

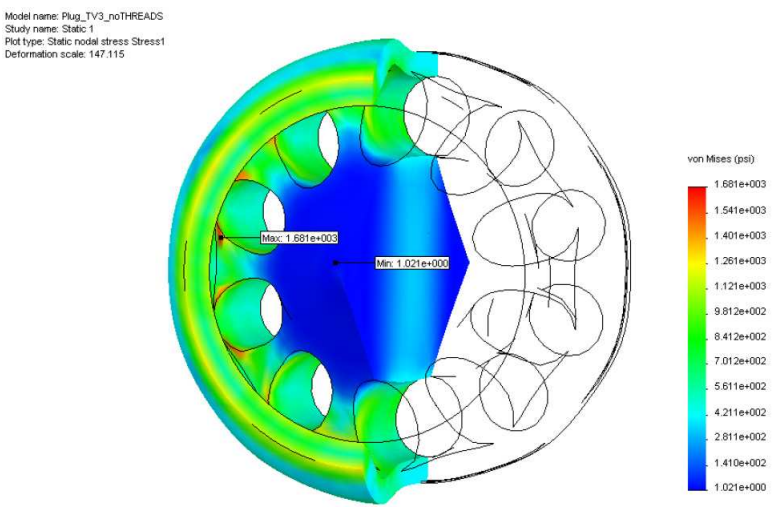

Figure 104: Stress FEA results using SolidWorks® for TV3 barrel flow plug.

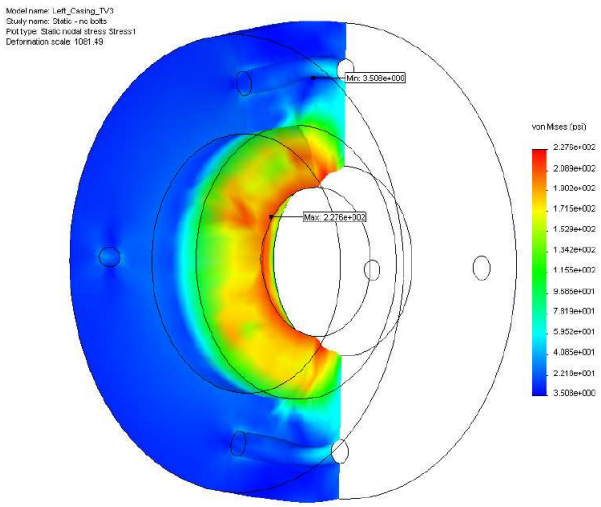

Figure 105: Stress FEA results using SolidWorks® for TV3 outlet casing.

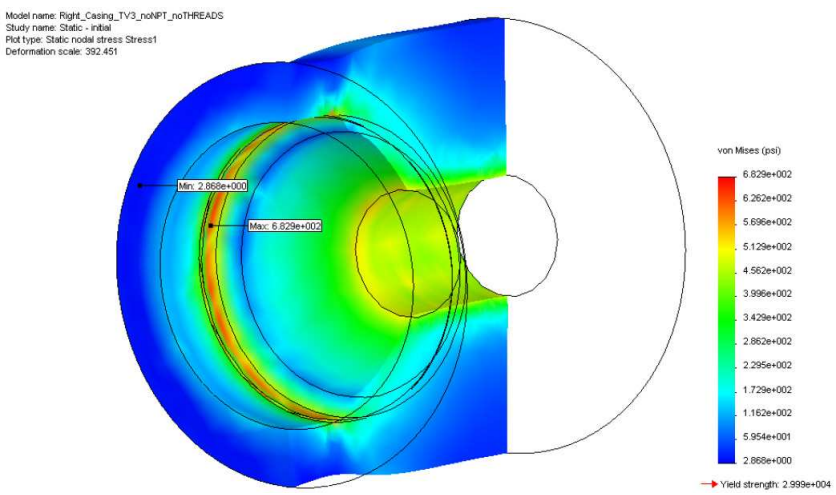

Figure 106: Stress FEA results using SolidWorks® for TV3 inlet casing.

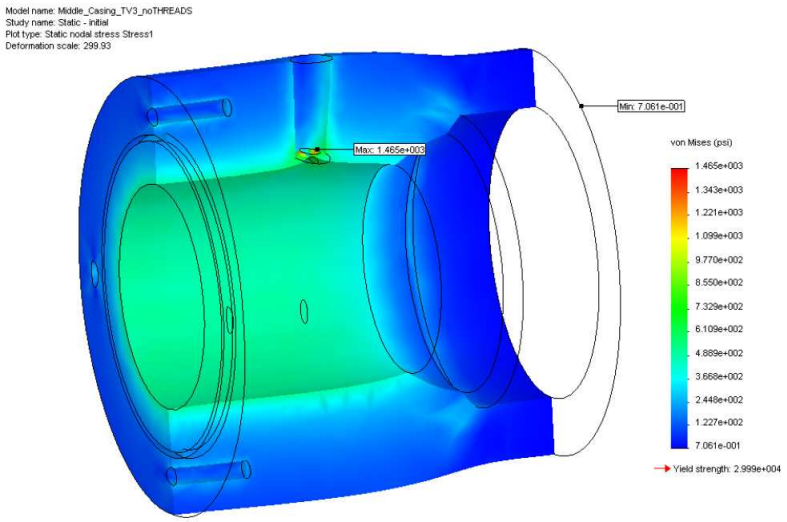

Figure 107: Stress FEA results using SolidWorks® for TV3 middle casing.

APPENDIX J

PROTOTYPE VALVE FABRICATION DRAWINGS

The following figures depict the drawings submitted for fabrication at the University of Pittsburgh machine shop. There are component drawings for each prototype valve design as well as an assembly drawing of each. Note that all components were machined of cast acrylic. All drawings were created using SolidWorks® [38].

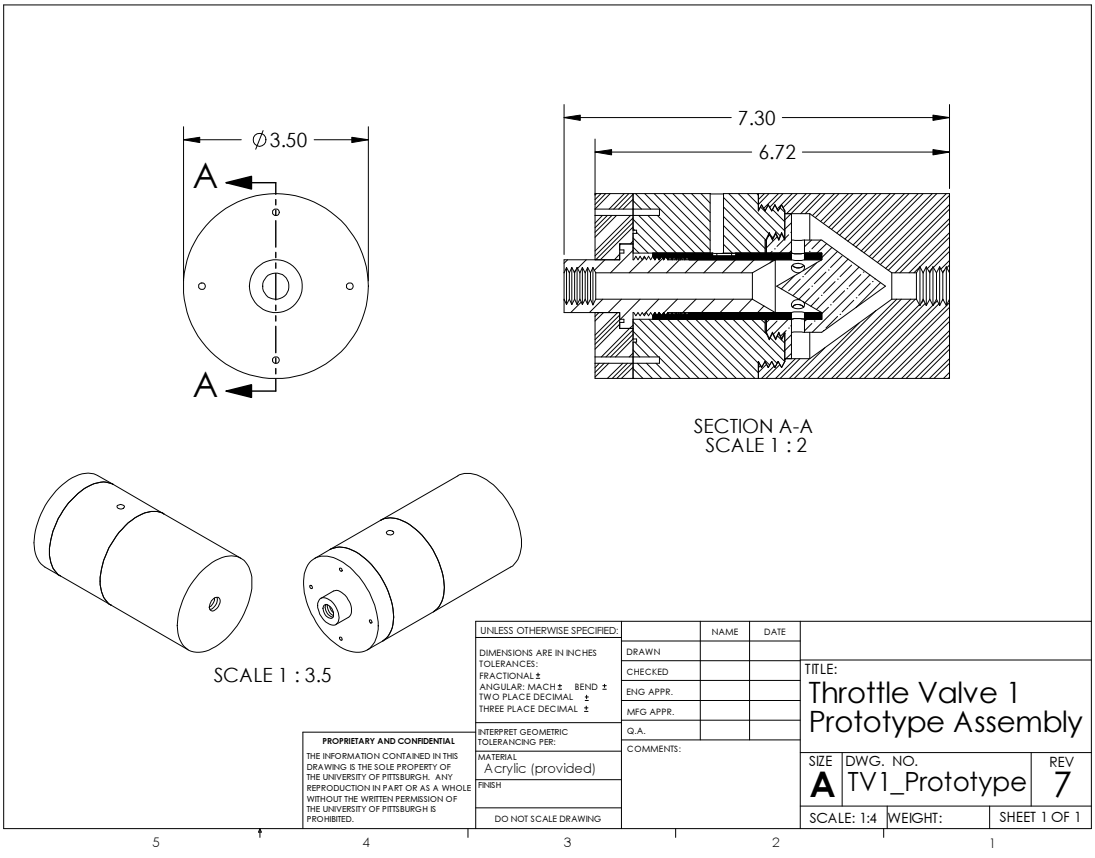

Figure 108: Assembly drawing for barrel valve prototype (TV1).

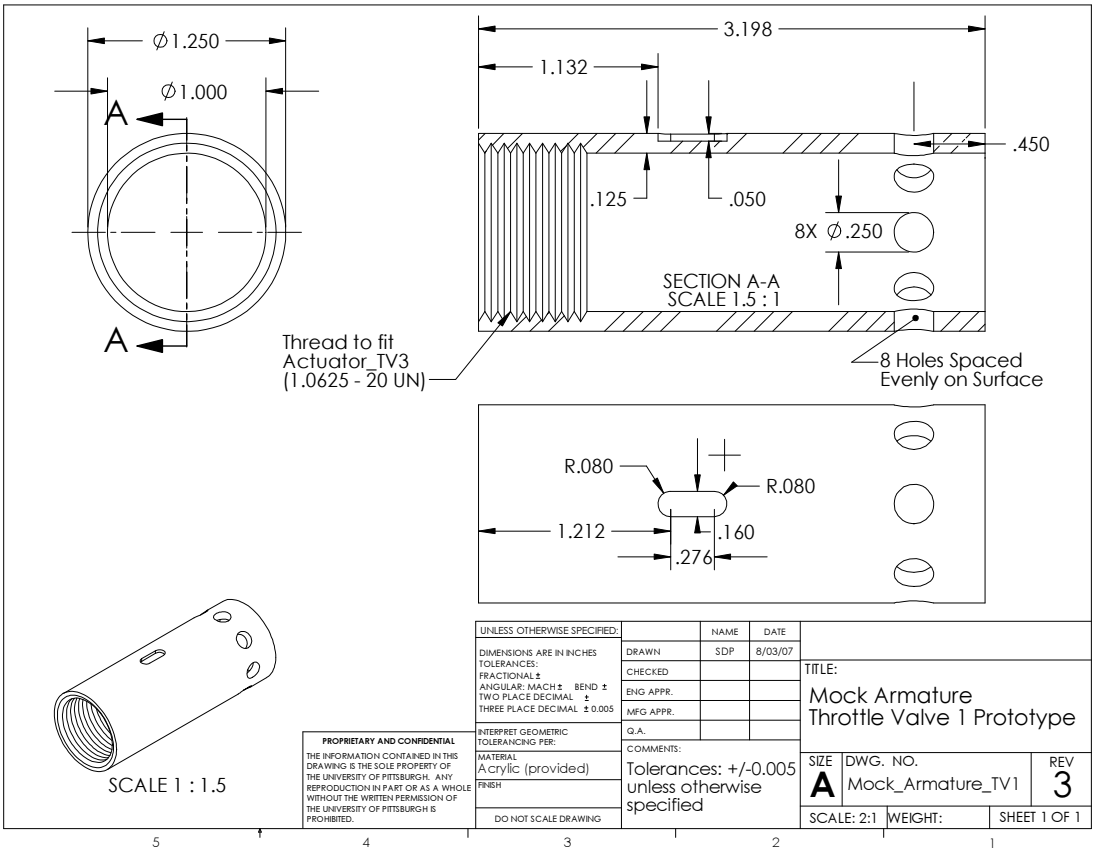

Figure 109: Mock armature component drawing for barrel valve prototype (TV1).

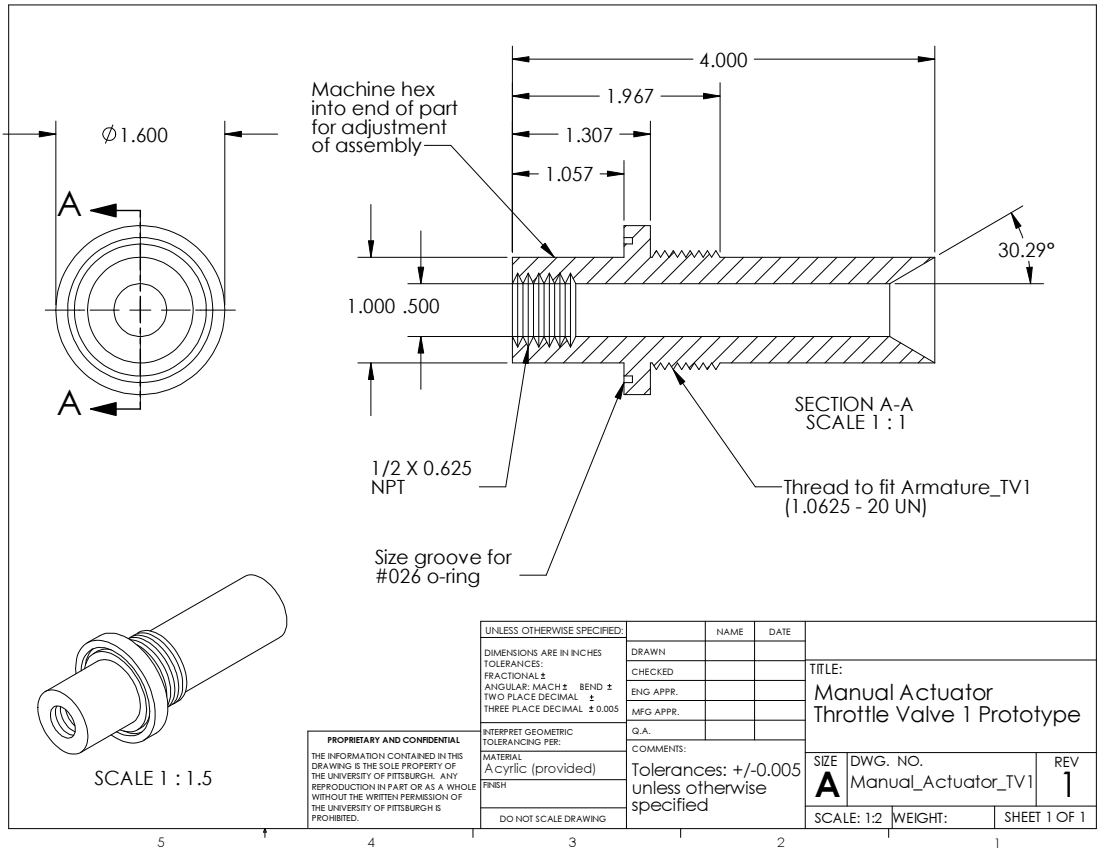

Figure 110: Manual actuator component drawing for barrel valve prototype (TV1).

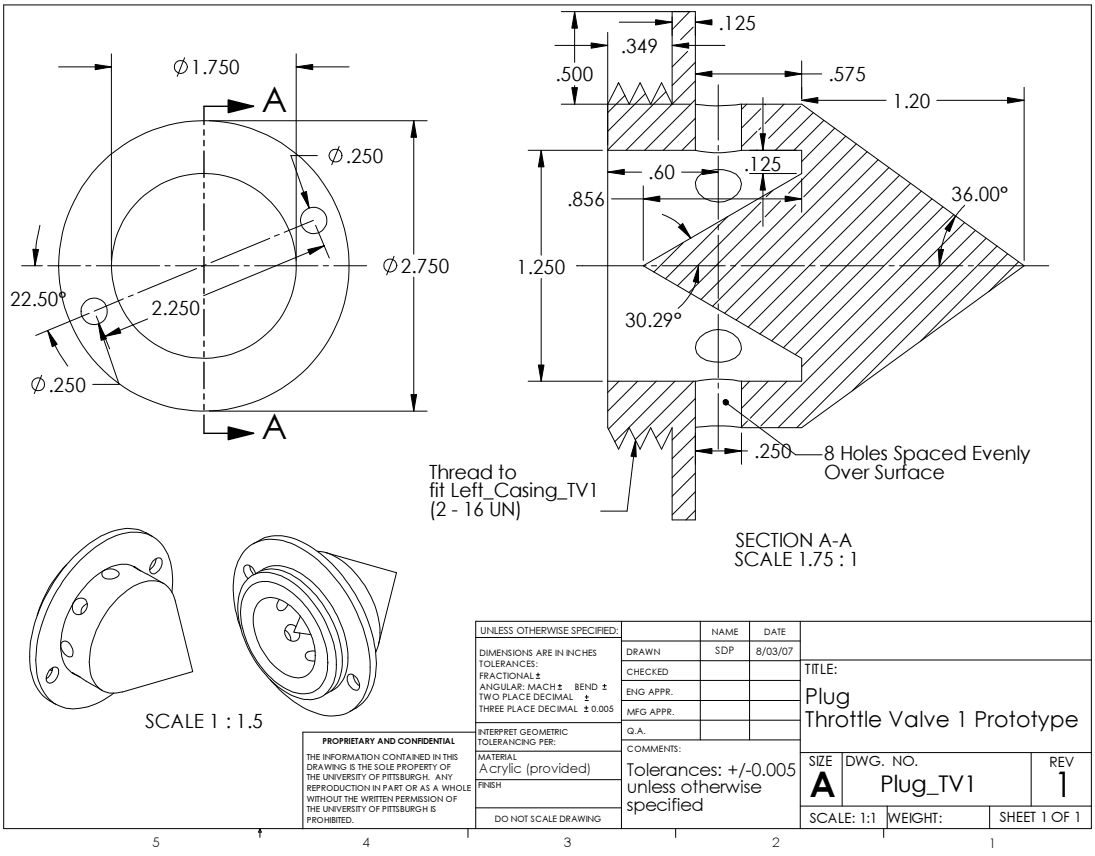

Figure 111: Barrel plug component drawing for barrel valve prototype (TV1).

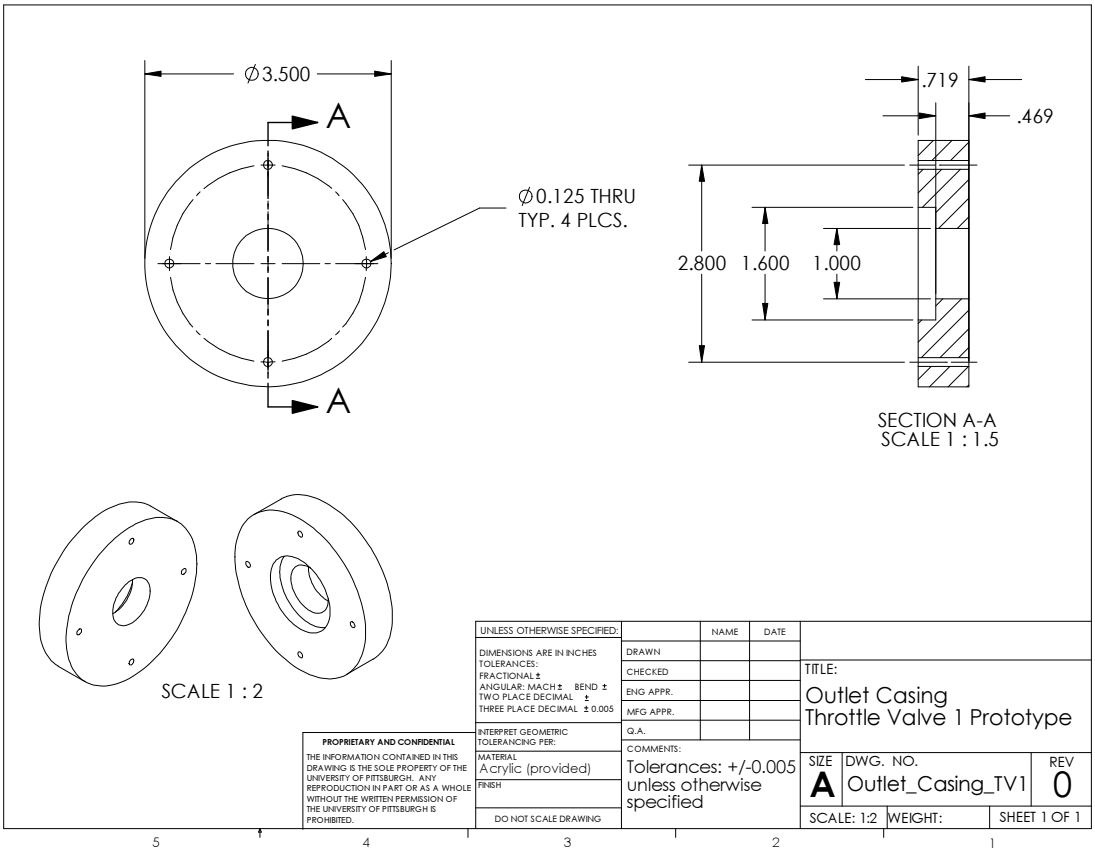

Figure 112: Outlet casing component drawing for barrel valve prototype (TV1).

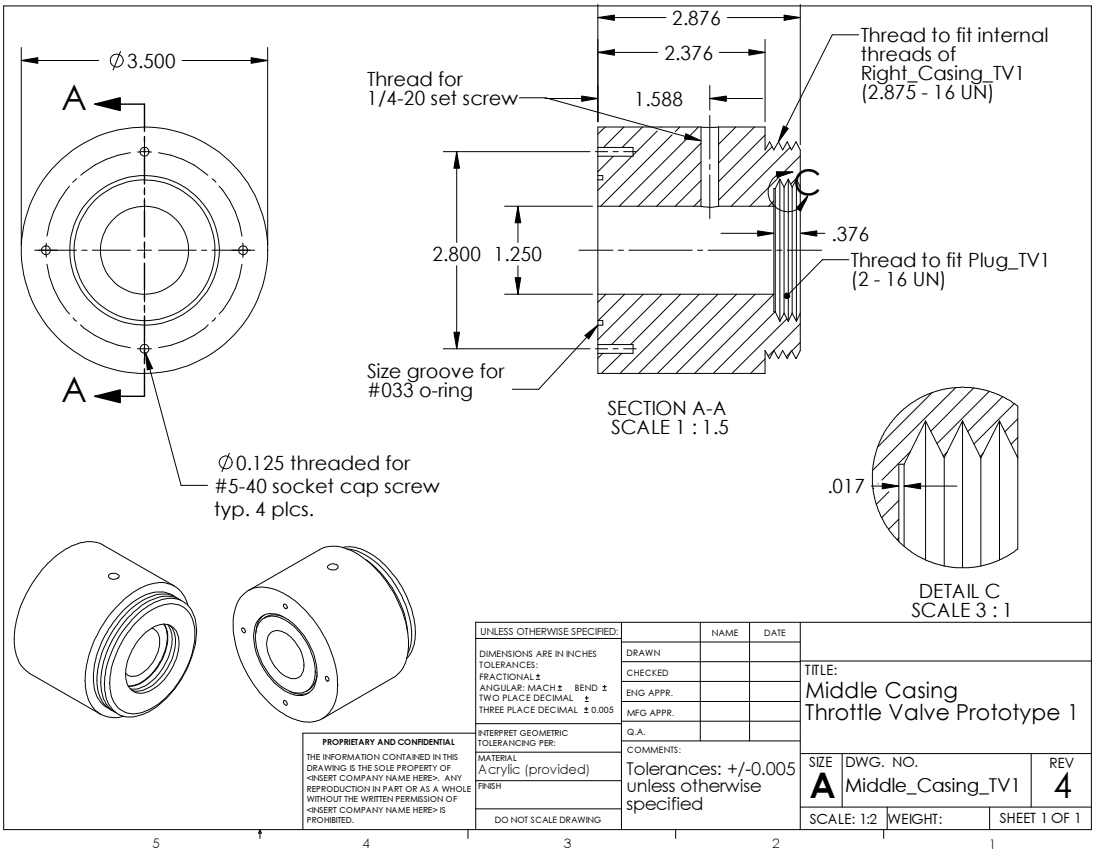

Figure 113: Middle casing component drawing for barrel valve prototype (TV1).

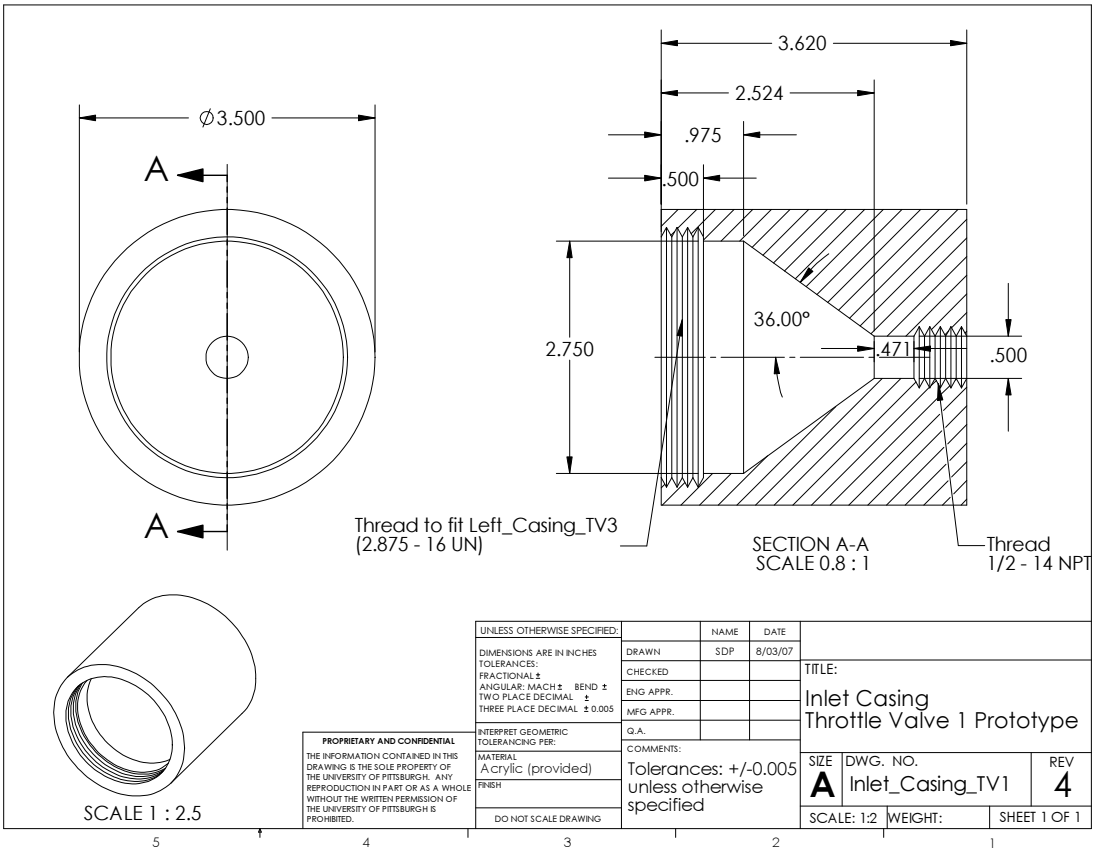

Figure 114: Inlet casing component drawing for barrel valve prototype (TV1).

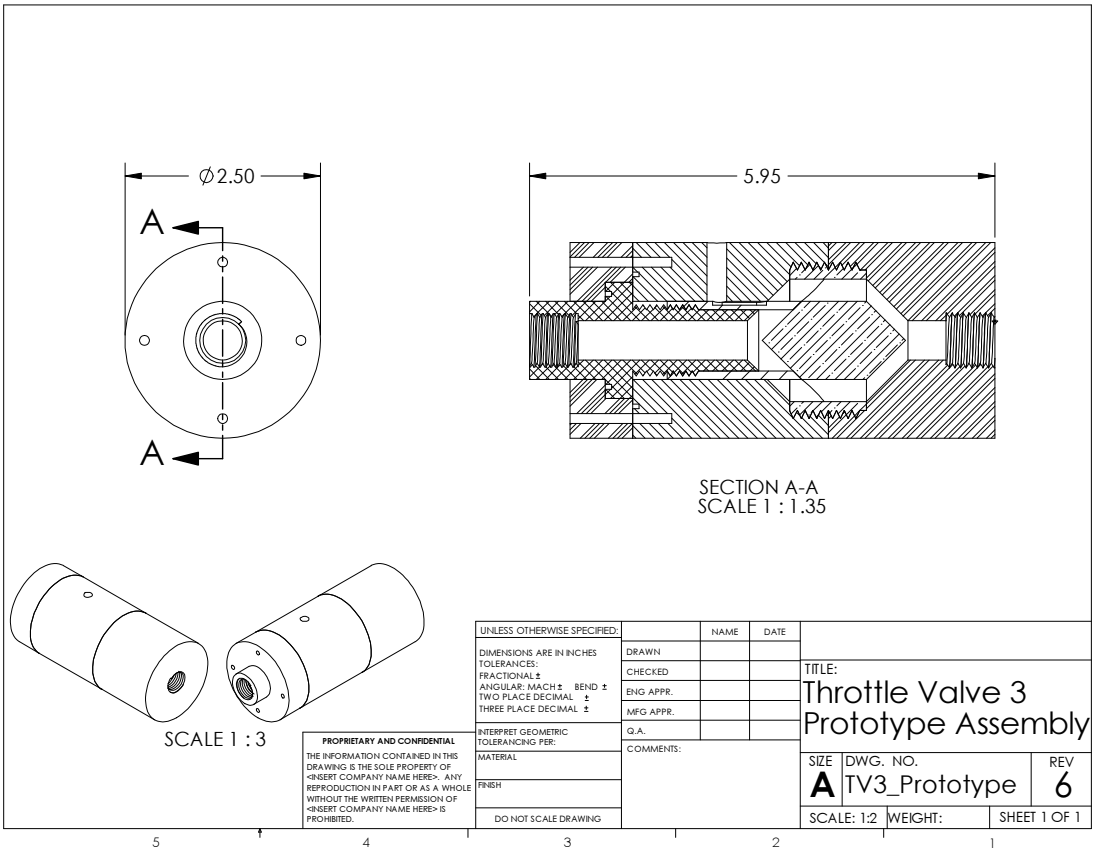

Figure 115: Assembly drawing for split-flow plug valve prototype (TV3).

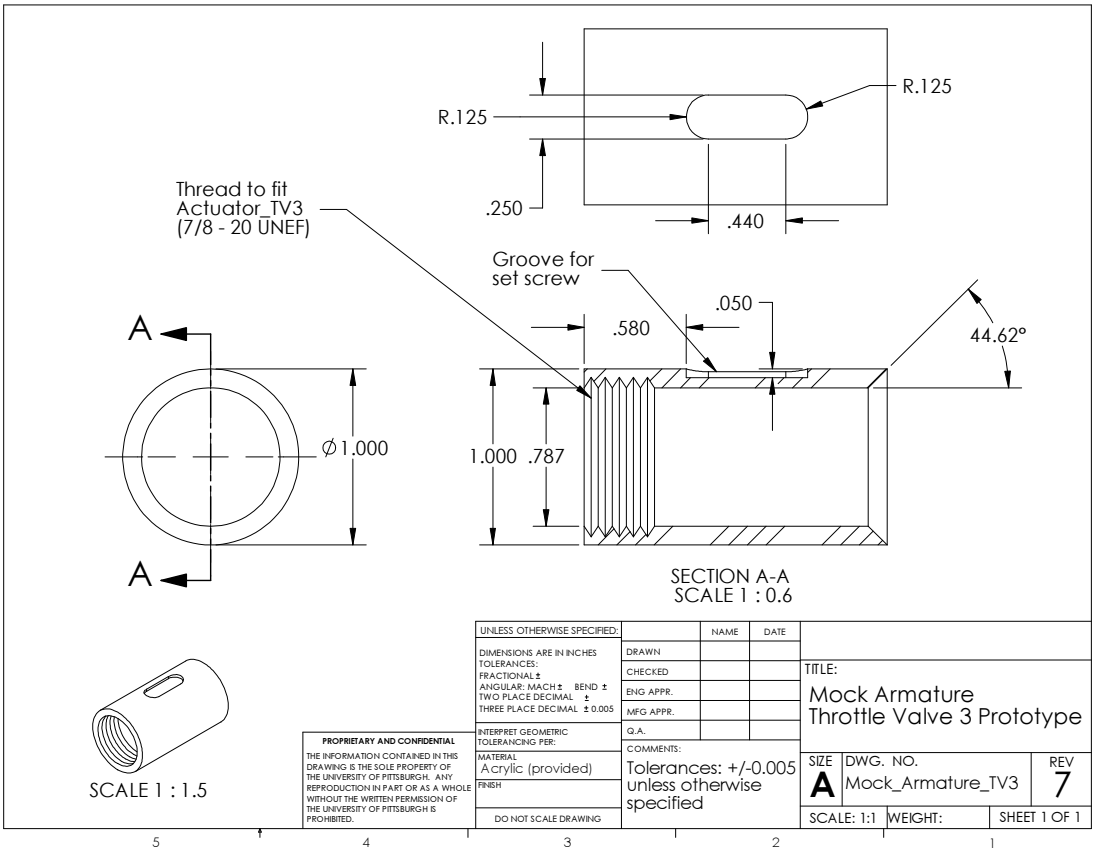

Figure 116: Mock armature component drawing for split-flow plug valve prototype (TV3).

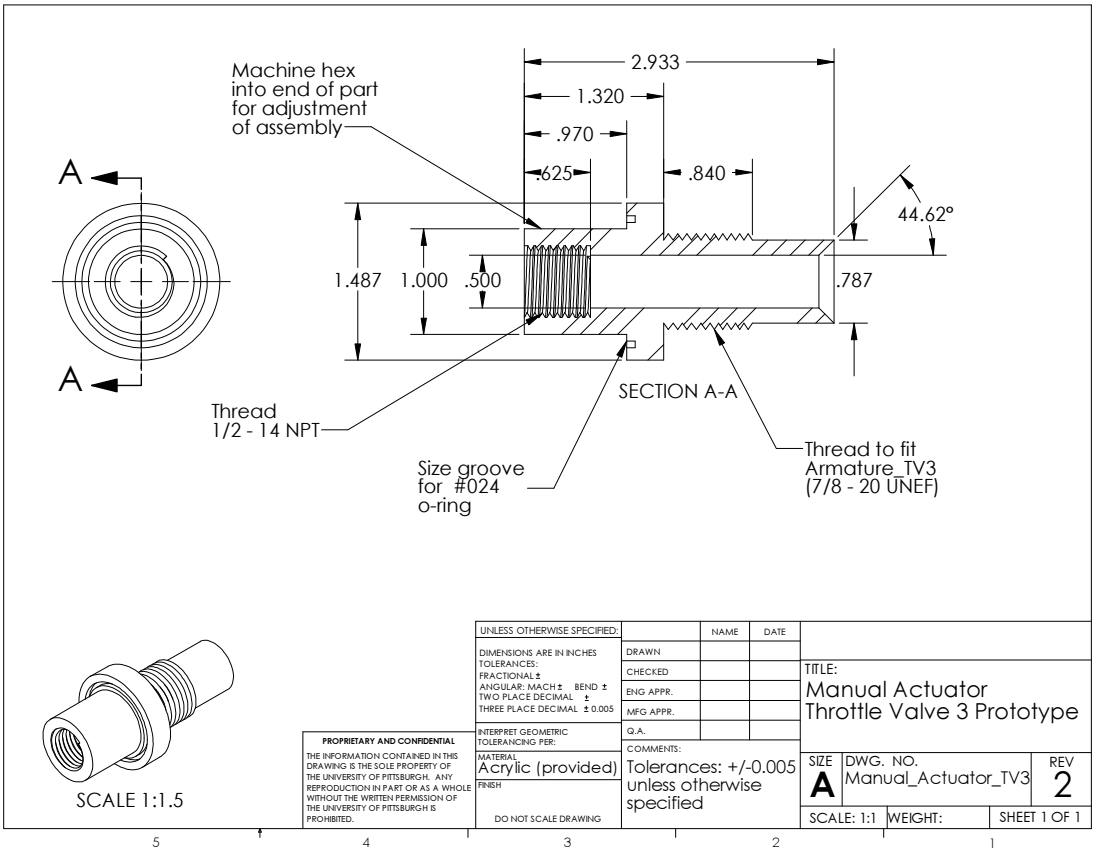

Figure 117: Manual actuator component drawing for split-flow plug valve prototype (TV3).

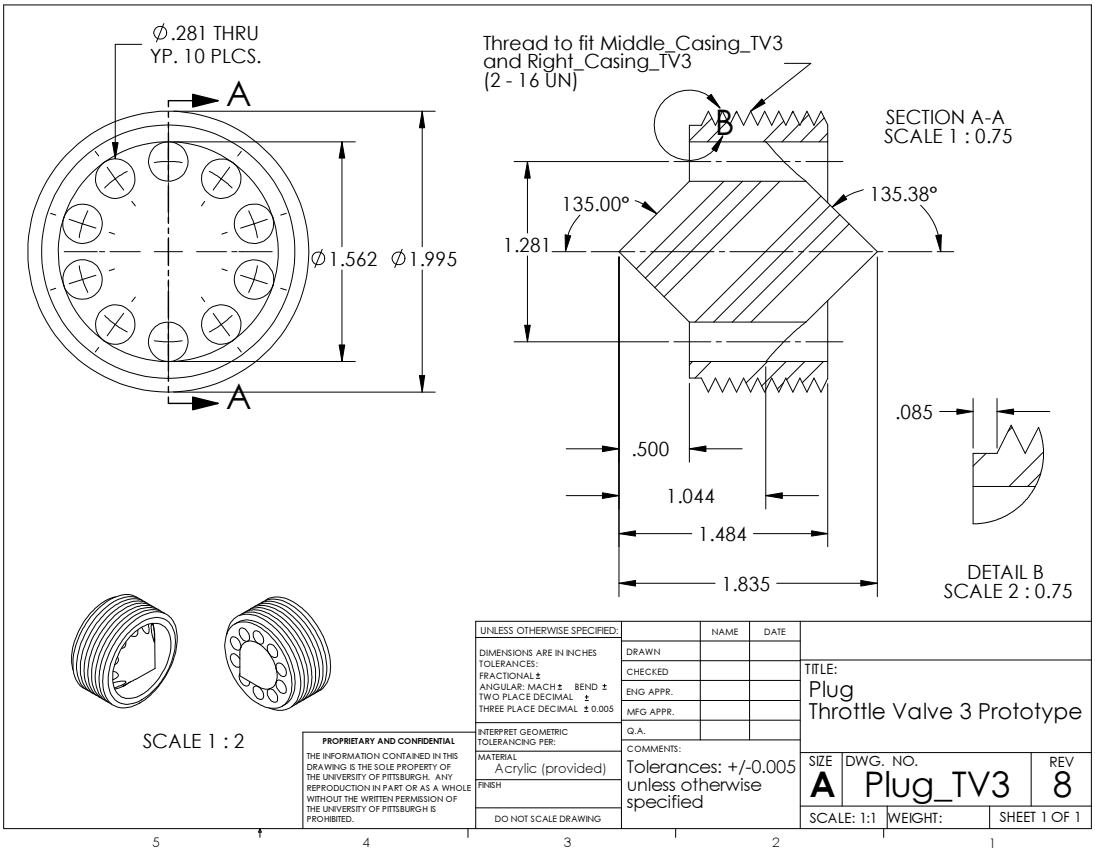

Figure 118: Barrel plug component drawing for split-flow plug valve prototype (TV3).

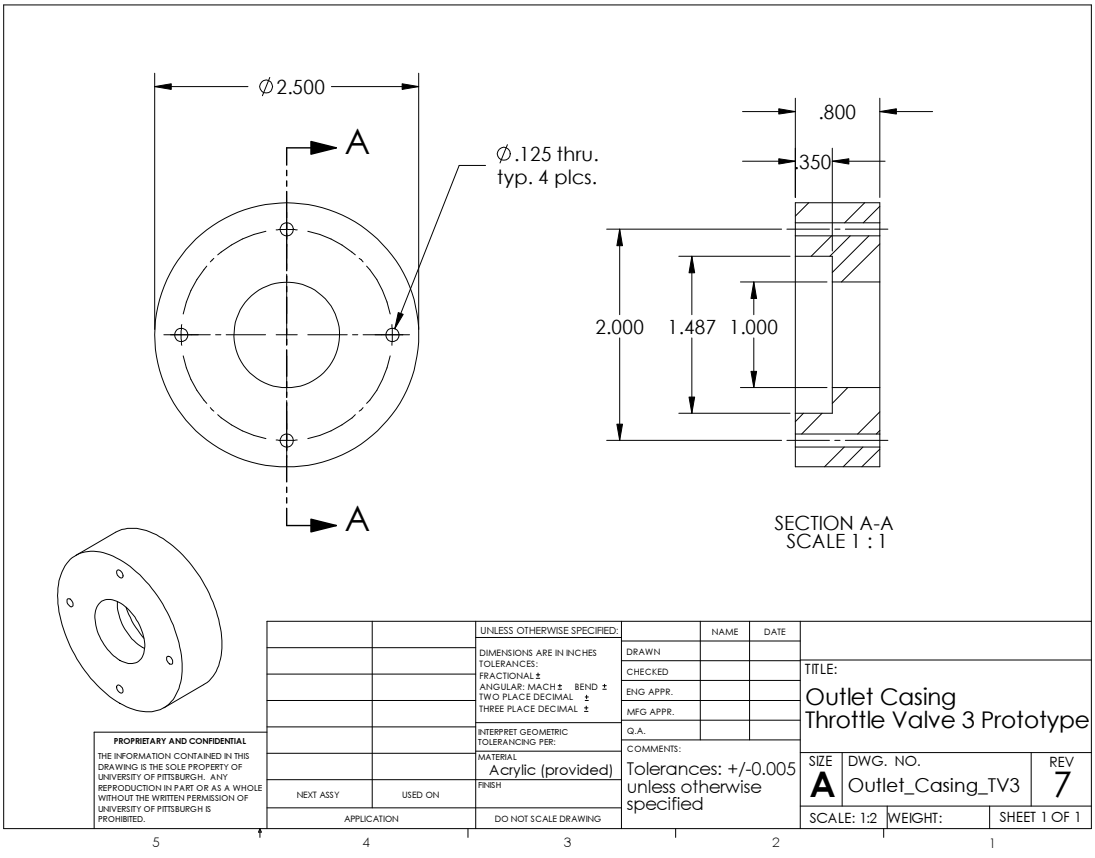

Figure 119: Outlet casing component drawing for split-flow plug valve prototype (TV3).

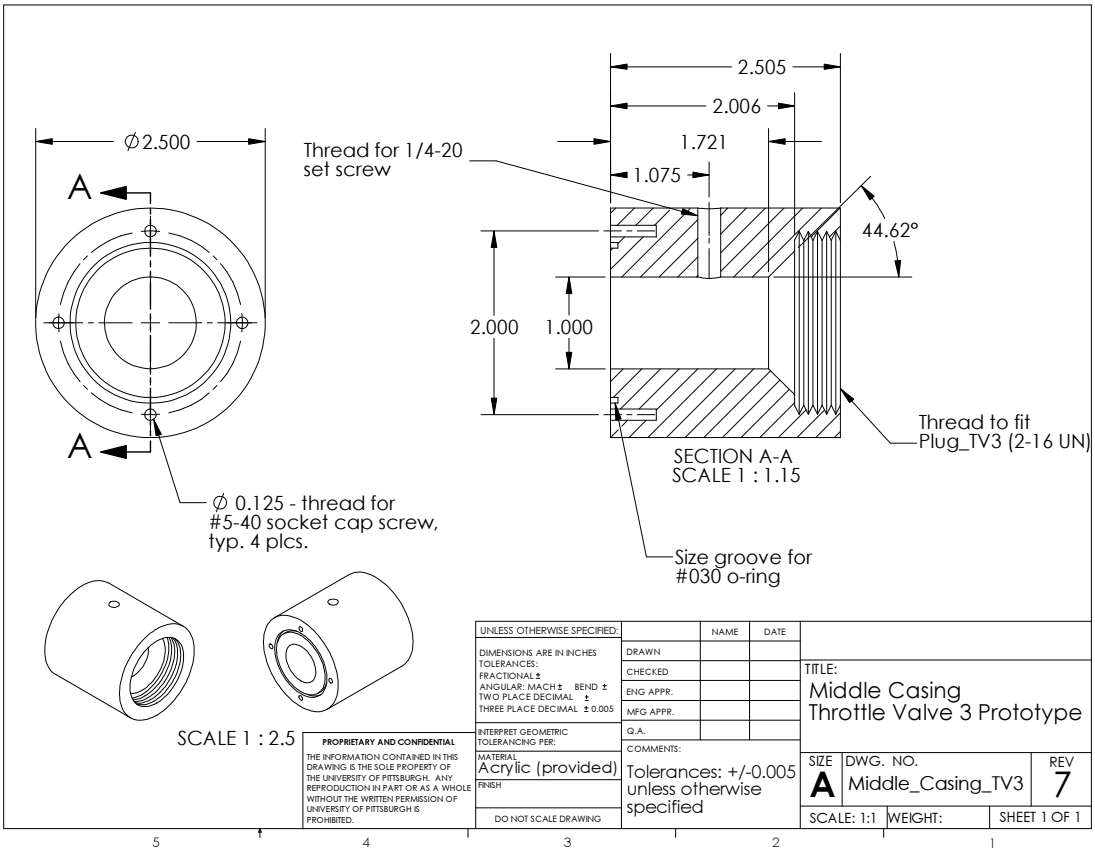

Figure 120: Middle casing component drawing for split-flow plug valve prototype (TV3).

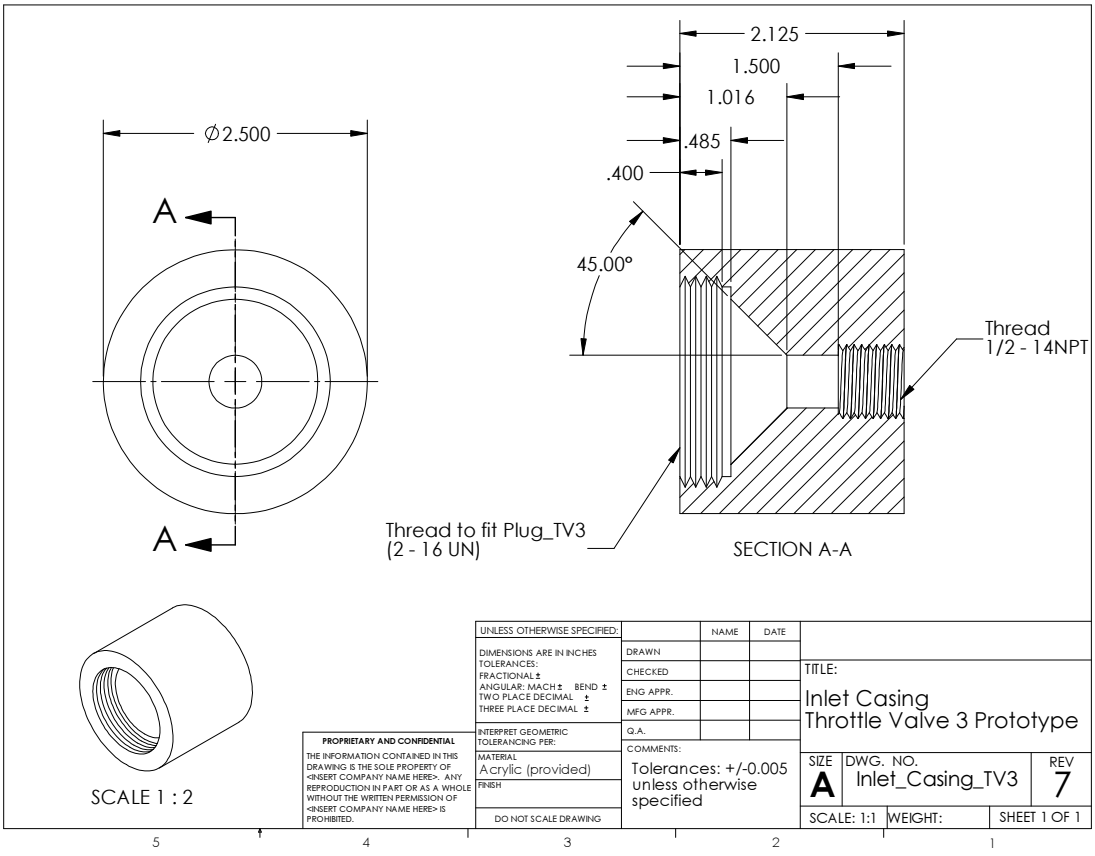

Figure 121: Inlet casing component drawing for split-flow plug valve prototype (TV3).

APPENDIX K

PRELIMINARY PROTOTYPE FLOW TESTING

The individual flow characteristics can be found in the following figures. All of the figures were created from data taken at the University of Pittsburgh using house supplied compressed air. As stated previously, both installed flow characteristic and the inherent flow characteristic of each valve indicate a linear region for a length of travel as well relatively quick opening. Also, TV3 is apparently a quicker opening valve than TV1 as seen in both types of flow characteristics. Ultimately, all of the figures shown indicate that both prototype valve designs are still viable options for the ACT valve.

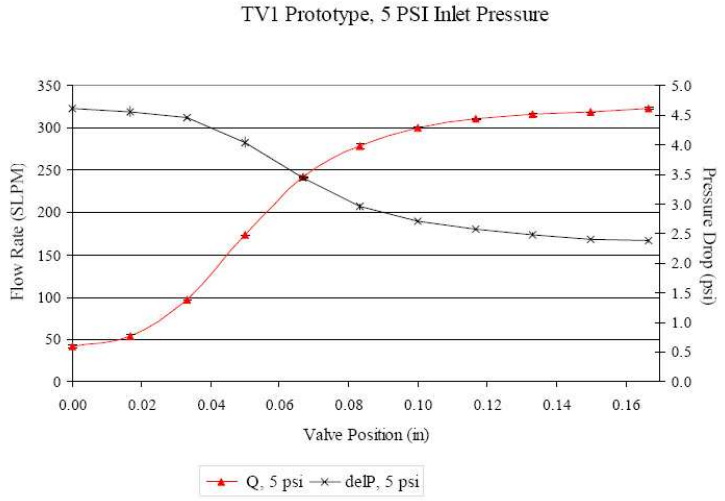

Figure 122: Installed flow characteristic for 5 psi inlet pressure for TV1 prototype valve.

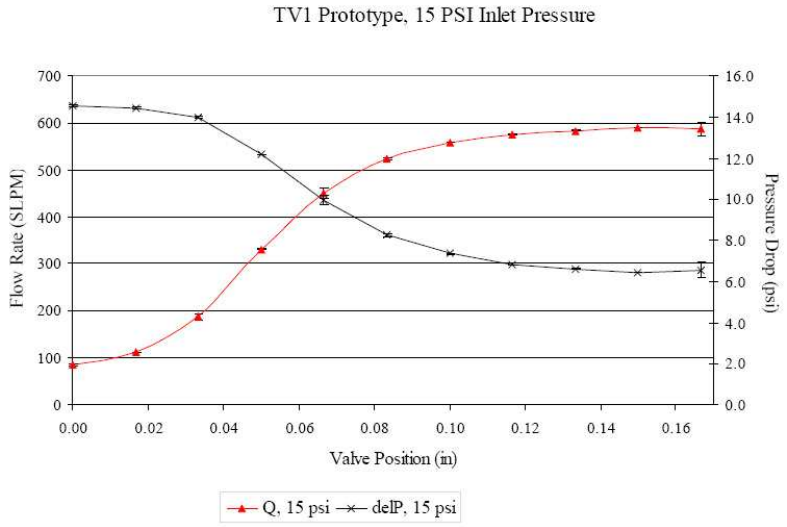

Figure 123: Installed flow characteristic for 15 psi inlet pressure for TV1 prototype valve.

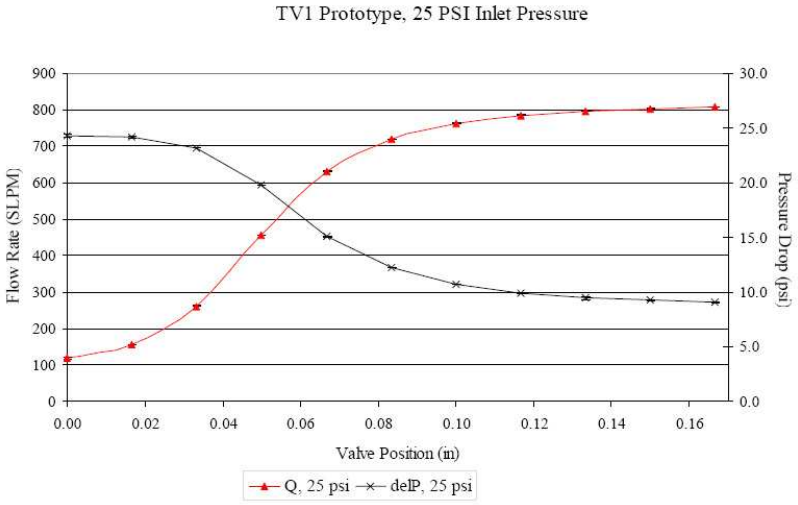

Figure 124: Installed flow characteristic for 25 psi inlet pressure for TV1 prototype valve.

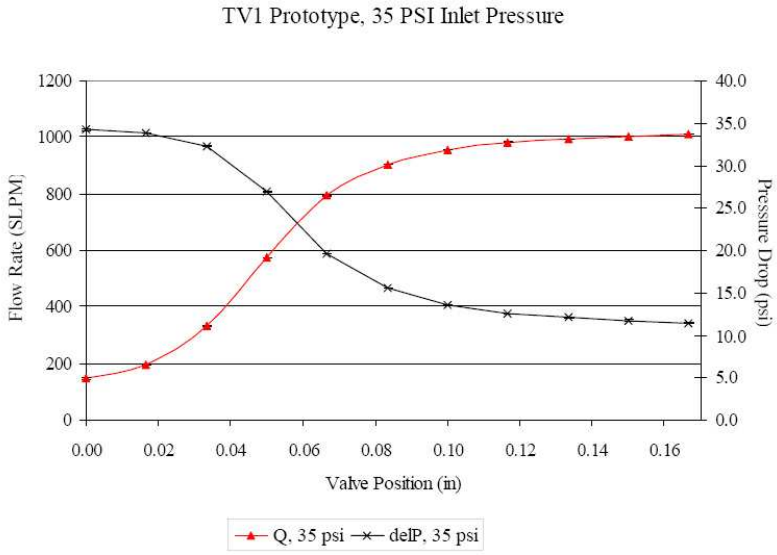

Figure 125: Installed flow characteristic for 35 psi inlet pressure for TV1 prototype valve.

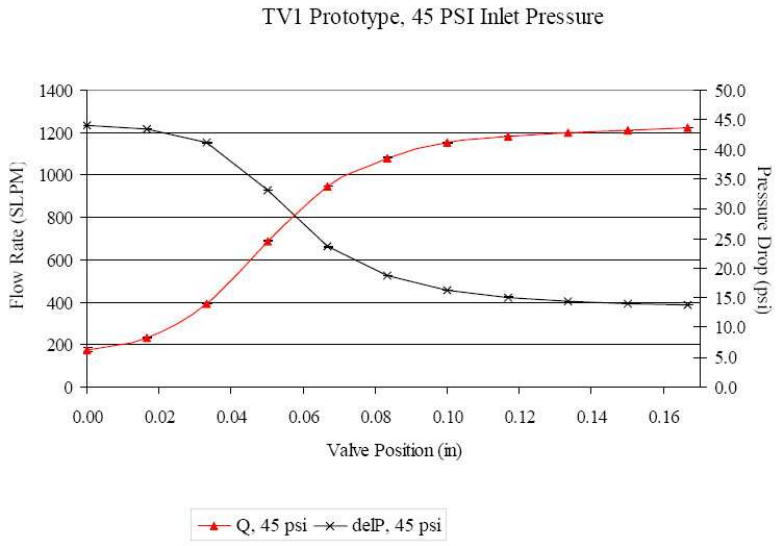

Figure 126: Installed flow characteristic for 45 psi inlet pressure for TV1 prototype valve.

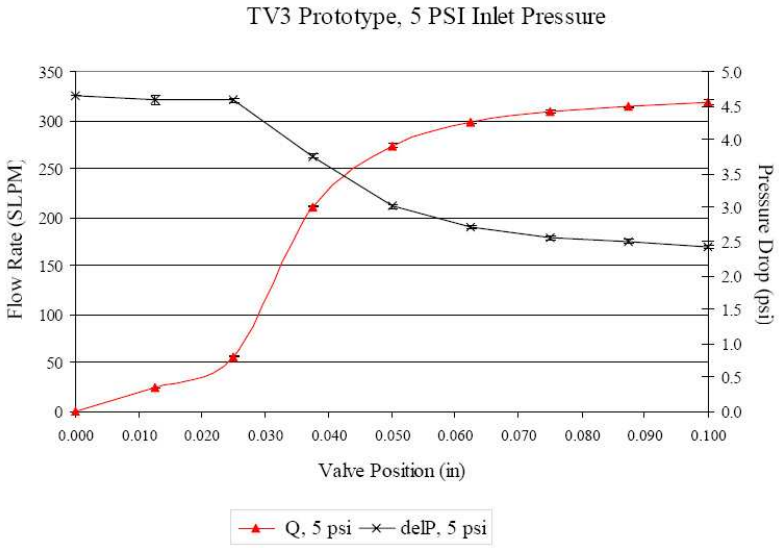

Figure 127: Installed flow characteristic for 5 psi inlet pressure for TV3 prototype valve.

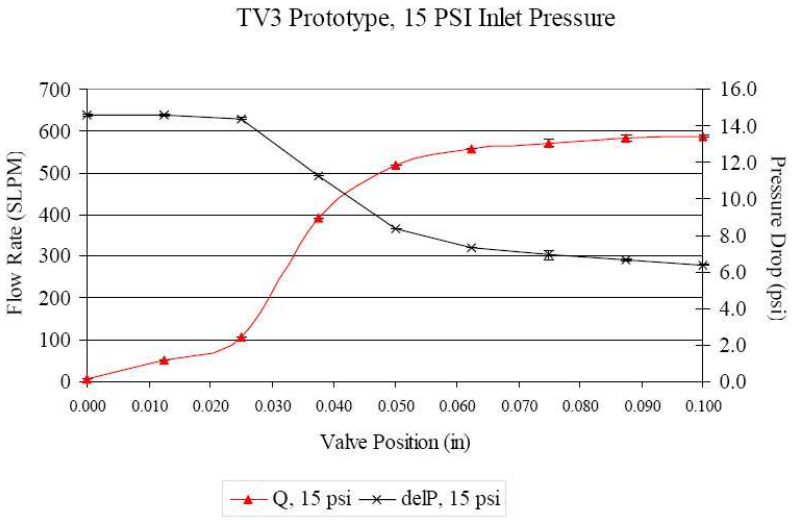

Figure 128: Installed flow characteristic for 15 psi inlet pressure for TV3 prototype valve.

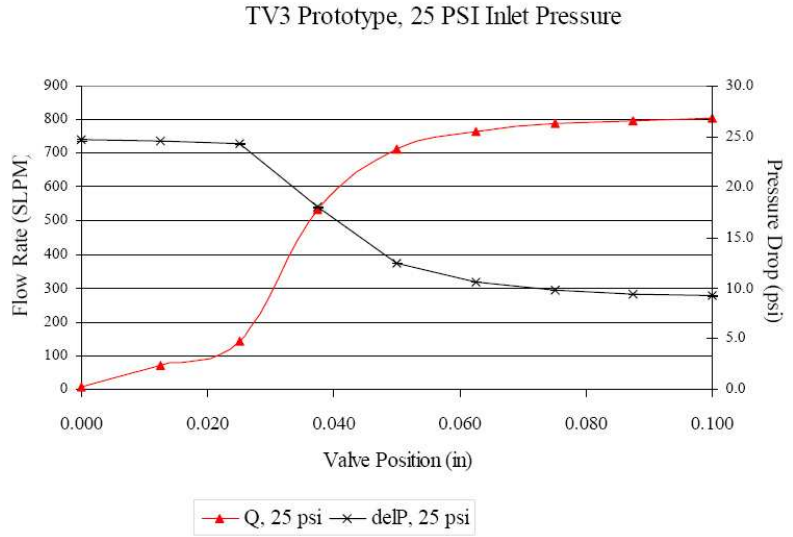

Figure 129: Installed flow characteristic for 25 psi inlet pressure for TV3 prototype valve.

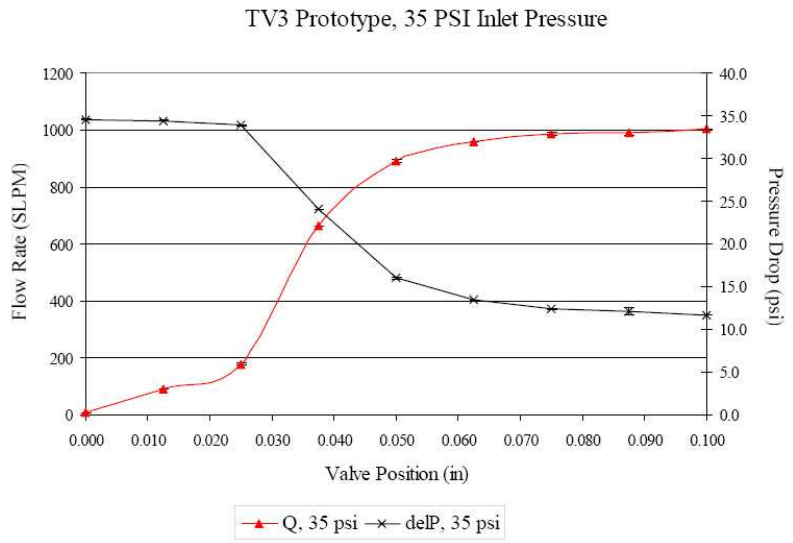

Figure 130: Installed flow characteristic for 35 psi inlet pressure for TV3 prototype valve.

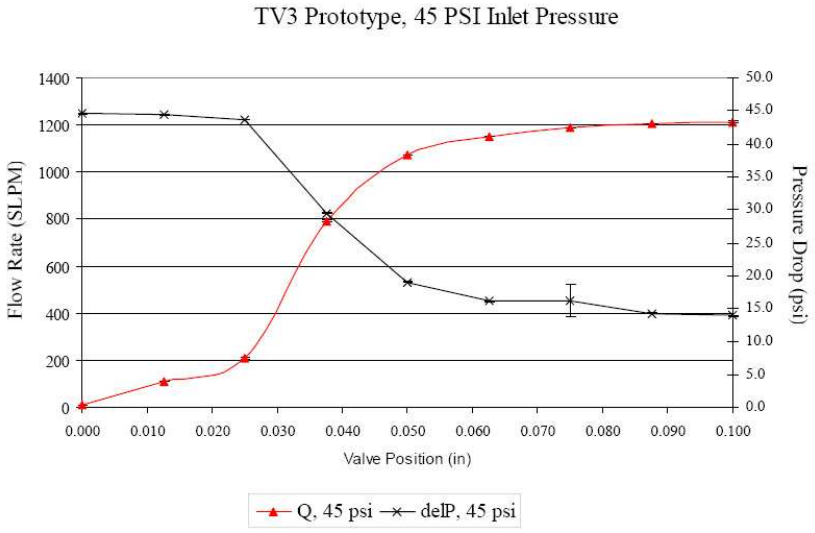

Figure 131: Installed flow characteristic for 45 psi inlet pressure for TV3 prototype valve.

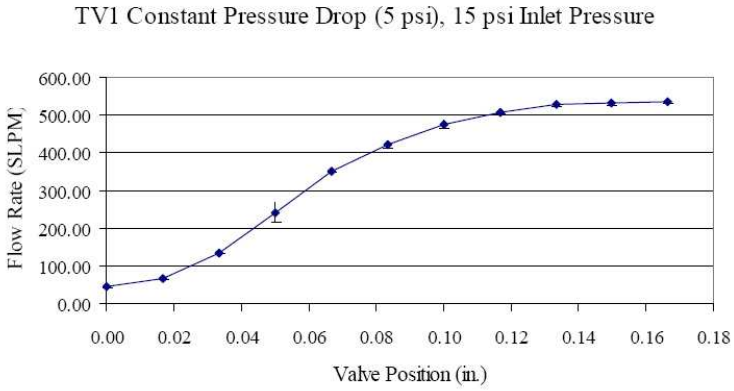

Figure 132: Inherent flow characteristic for 15 psi inlet pressure for TV1 prototype valve.

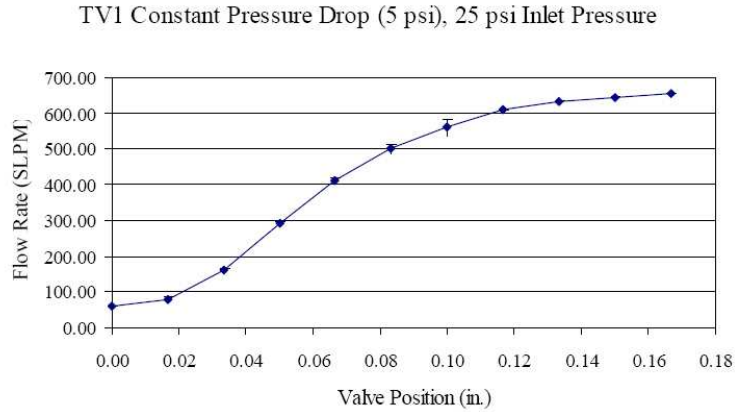

Figure 133: Inherent flow characteristic for 25 psi inlet pressure for TV1 prototype valve.

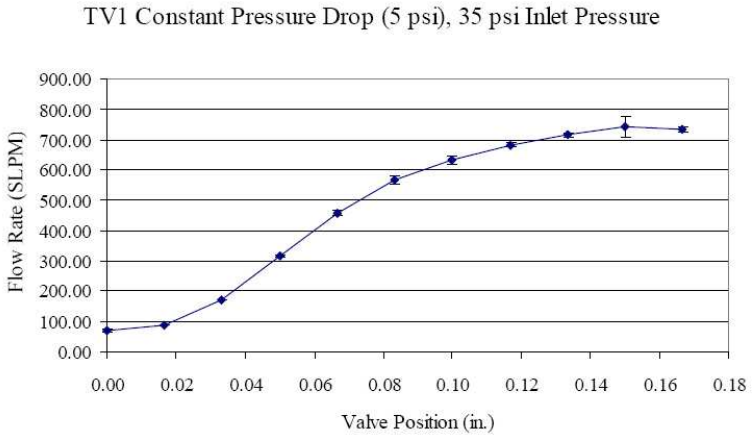

Figure 134: Inherent flow characteristic for 35 psi inlet pressure for TV1 prototype valve.

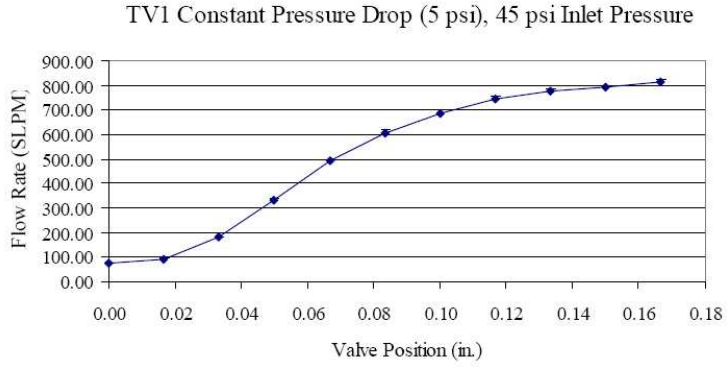

Figure 135: Inherent flow characteristic for 45 psi inlet pressure for TV1 prototype valve.

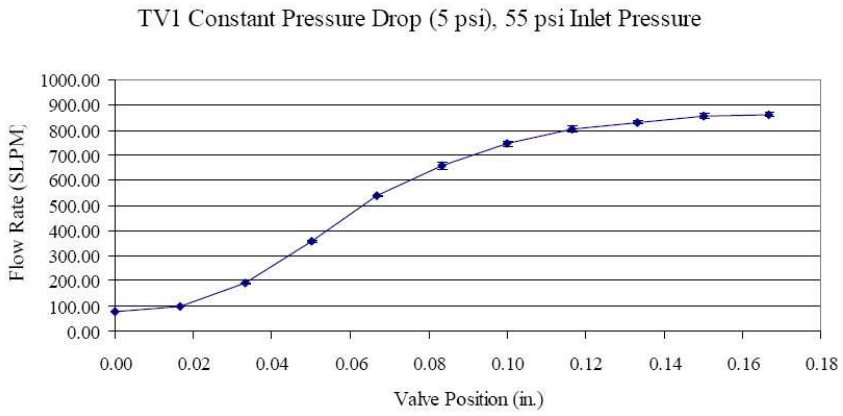

Figure 136: Inherent flow characteristic for 55 psi inlet pressure for TV1 prototype valve.

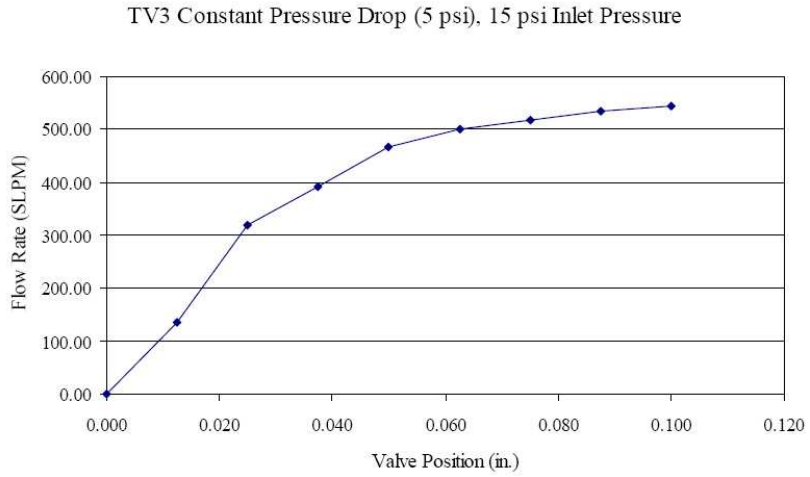

Figure 137: Inherent flow characteristic for 15 psi inlet pressure for TV3 prototype valve.

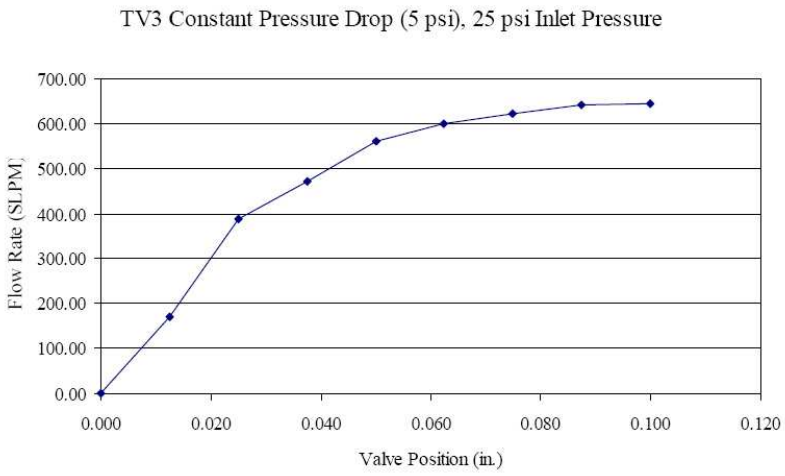

Figure 138: Inherent flow characteristic for 25 psi inlet pressure for TV3 prototype valve.

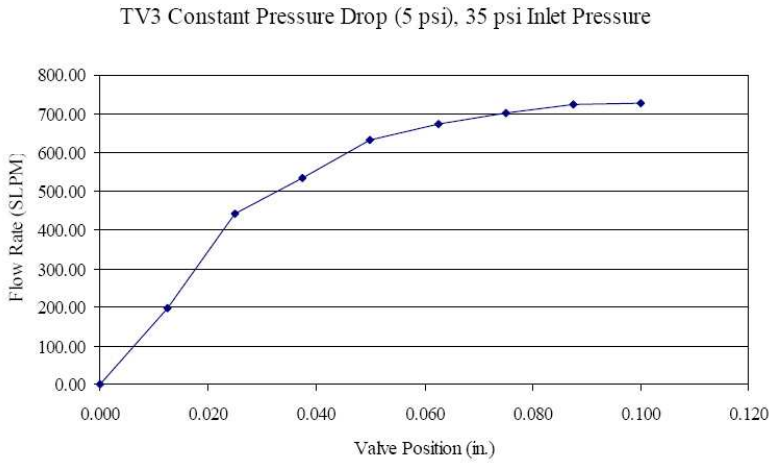

Figure 139: Inherent flow characteristic for 35 psi inlet pressure for TV3 prototype valve.

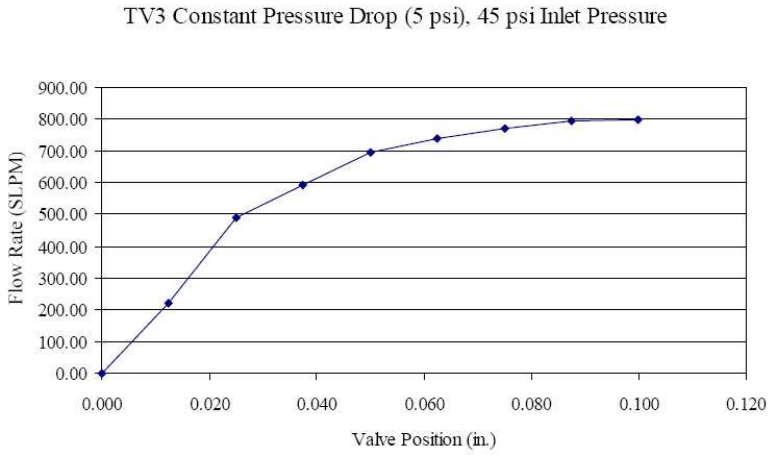

Figure 140: Inherent flow characteristic for 45 psi inlet pressure for TV3 prototype valve.

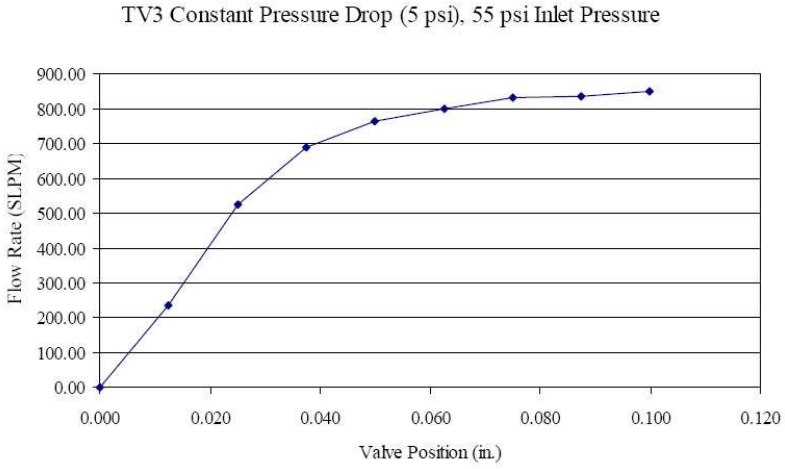

Figure 141: Inherent flow characteristic for 55 psi inlet pressure for TV3 prototype valve.

BIBLIOGRAPHY

[1] United States Department of Energy. FutureGen Initiative. Retrieved February 28, 2007 from http://www.fossil.energy.gov/programs/powersystems/futuregen/.

[2] K. McManus, T. Poinsot, and S. Candel. A review of active control of combustion instabilities. *Progress in Energy Combustion Science*, 19(11):1–29, 1993.

[3] J. Thornton, G. Richards, D. Straub, E. Liese, J. Trader Jr., and G. Fasching. Flashback Detection Sensor for Lean Premix Fuel Nozzles. U.S. Patent No. 6,429,020. Issued August 6, 2002.

[4] J. Thornton, G. Richards, D. Straub, K. Dodrill, and R. Nutter. Real-Time Combustion Control and Diagnostics Sensor. U.S. Patent No. 6,887,069 B1. Issued May 3, 2005.

[5] J. Thornton, G. Richards, and E. Robey. Detecting Flashback in Premix Combustion Systems. Presented at the American Flame Research Committee International Symposium, Newport Beach, California, September 17–21, 2000.

[6] J. Thornton, D. Straub, G. Richards, R. Nutter, and E. Robey. An In-Situ Monitoring Technique for Control and Diagnostics of Natural Gas Combustion Systems. Presented at the 2nd Joint Meeting of the U.S. Sections of the Combustion Institute, Oakland, California, March 25–28, 2001.

[7] J. Thornton, D. Straub, B. Chorpening, E. Huckaby, and K. Benson. A Combustion Control and Diagnostics Sensor for Gas Turbines. In *Proceedings of ASME/IGTI Turbo Expo Meeting*, Vienna, June 2004. ASME Paper GT2004-53392.

[8] B. Chorpening, J. Thornton, E. Huckaby, and K. Benson. Combustion Oscillation Monitoring Using Flame Ionization in a Turbulent Premixed Combustor. *ASME Journal of Engineering for Gas Turbines and Power*, 129:352–357, 2007.

[9] K. Benson, J. Thornton, D. Straub, E. Huckaby, and G. Richards. Flame Ionization Sensor Integrated into Gas Turbine Fuel Nozzle. *ASME Journal of Engineering for Gas Turbines and Power*, pages 42–48, 1997.

[10] W. Backé, S. Burzmann, H. Janocha, and A. Klein. *Actuators*. Springer-Verlag Berlin, Heidelberg, 2004.

[11] N. Sclater and N. Chironis. *Mechanisms and Mechanical Devices Sourcebook*. McGraw-Hill, New York, third edition, 2001. Retrieved July 19, 2007 from http://www.knovel.com.

[12] Phytron, Williston, Vermont. *VSS/VSH Extreme Environment Stepper Motors Data Sheet*. Retieved June 1, 2007 from ftp://ftp.phytron.de/datasheets/stepper_motors/vss-gb.pdf.

[13] Engineer's Edge. Hydraulic and Pneumatic Knowledge. Retrieved February 28, 2007 from http://www.engineersedge.com/hydraulic/hydraulic_actuator.htm.

[14] Engineer's Edge. Pneumatic Actuator Design and Operation. Retrieved February 28, 2007 from http://www.engineersedge.com/hydraulic/pneumatic_actuator.htm.

[15] M. Frankel. *Facility Piping Systems Handbook*. McGraw-Hill, New York, second edition, 2002.

[16] Engineer's Edge. Electric Solenoid Actuator. Retrieved February 28, 2007 from http://www.engineersedge.com/hydraulic/electric_solenoid_actuator.htm.

[17] Goodrich Engine Control Systems, Birmingham United Kingdom. *Thermiezo Data Sheet*. Retrieved June 1, 2007 from http://www.enginecontrols.goodrich.com/pdf/Thermiezo_Datasheet.pdf.

[18] W. Barvosa-Carter, C. Massey, G. McKnight, and P. Liu. Solid-state actuation based on reversible Li electroplating.

[19] Y. Koyama, T. Chin, U. Rhyner, R. Holman, S. Hall, and Y. Chiang. Harnessing the actuation potential of solid-state intercalation compounds. *Advanced Functional Materials*, 19:492–498, 2006.

[20] M. Schwartz. *Encyclopedia of Smart Materials*, volume 1 – 2. John Wiley & Sons, Hoboken, New Jersey, 2002.

[21] University of Birmingham. Magnetostriction. Retrieved February 28, 2007 from http://www.aacg.bham.ac.uk/magnetic_materials/other_mag_materials.htm.

[22] P. Skousen. *Valve Handbook*. McGraw-Hill, New York, 1998.

[23] G. Menges, W. Michaeli, and P. Mohren. *How To Make Injection Molds*. Hanser Publishers, Cincinnati, third edition, 2001.

[24] J. Vipperman. Active Combustion Throttle Valve Project Proposal, Energy Systems and Dynamics Proposal, March 2006. Presented at RDS/NETL in Morgantown, West Virginia.

[25] P. Smith and R. Zappe. *Valve Selection Handbook - Engineering Fundamentals for Selecting the Right Valve Design for Every Industrial Flow Application.* Elsevier, Amsterdam, 2004.

[26] W. Wijngaart, A. Thorsén, and G. Stemme. A seat microvalve nozzle for optimal gas-flow capacity at large-controlled pressure. *Journal of Microelectromechanical Systems*, 14(12):200–206, April 2005.

[27] J. Rodgers. Analysis and testing of a thunder^{TM}piezoelectric actuator as a prime mover in a gas flow control valve. Master's thesis, University of Pittsburgh, 2005.

[28] J. Vipperman. Active Combustion Throttles (ACT) Concepts Presentation, May 2005. Presented at NETL in Morgantown, West Virginia.

[29] J. Vipperman, W. Clark, J. Rodgers, B. Bucci, and N. Vickey. Project Status of VOAT, April 2004. Presented at NETL in Morgantown, West Virginia.

[30] J. Vipperman, D. Lambeth, W. Clark, N. Black, R. Hopkin, D. Gacek, and J. Pickel. Pitt/Lambeth Systems Progress Review Presentation, January 2007. Presented at NETL in Morgantown, West Virginia.

[31] B. Cullity. *Introduction to Magnetic Materials.* Addison-Wesley Publishing Company, Reading, Massachusetts, first edition, 1972.

[32] A. Boresi and R. Schmidt. *Advanced Mechanics of Materials.* John Wiley & Sons, Hoboken, New Jersey, sixth edition, 2003.

[33] W. Slaughter. *The Linearized Theory of Elasticity.* Birkhäuser, Boston, Massachusetts, first edition, 2002.

[34] R. Norton. *Machine Design: An Integrated Approach.* Prentice-Hall, Upper Saddle River, New Jersey, second edition, 2000.

[35] F. Incropera and D. DeWitt. *Introduction to Heat Transfer.* John Wiley & Sons, New York, fourth edition, 2002.

[36] D. Lambeth. Lambeth Systems. Pittsburgh, Pennsylvania.

[37] Ansoft Corporation, Pittsburgh, Pennsylvania, USA. *Maxwell® v12 3D/2D Electromagnetic Field Simulation.* Product datasheet. Retrieved March 26, 2008 from http://ansoft.com/products/em/maxwell/Maxwell.pdf.

[38] SolidWorks® Corporation, Concord, Massachusetts, USA. *SolidWorks® MCAD 3D Design Software.* Retrieved March 26, 2008 from http://www.solidworks.com/pages/products/3dmech.html.

[39] Ansoft Corporation, Pittsburgh, Pennsylvania, USA. *ePhysics^{TM}Coupled Thermal & Stress Analysis for EM Applications*. Product datasheet. Retrieved March 26, 2008 from http://ansoft.com/products/tools/ephysics/ePhysics060802.pdf.

[40] D. Lambeth. Personal communication, 2007.

[41] S. Heisler. *The Wiley Engineer's Desk Reference: A Concise Guide for the Professional Engineer*. Wiley, New York, second edition, 1998.

[42] J. Vipperman and N. Black. Survey of Actuation and Valve Technologies for Active Combustion Throttle (ACT) Project, fourth revision, August 2007. Report submitted to NETL Morgantown.